Annexure III

Raman Research Fellowships (RRF) for 2024-2025

Area	Research Topic	Name and Designation	Institute	Age (Yrs) as on July 31, 2024	Qualification & Res. Experience	Min. Period Required (2-6 months)	Remarks
Healthcare	NANOFERROBLOCK: DNA Origami Nanostructures Equipped with ssDNA Aptamers as DMT1 and ACSL4 Inhibitors for Combating Ferroptosis during Neuroinflammation	Dr. Sonia Verma; Scientist	CSIR-Central Drug Research Institute	**35 years**	Degree (Highest): Doctorate of Philosophy Institute: National Institute of Immunology Subject: Life Sciences Year: 2019 No. of year of Res. Experience (including Ph.D. period): 12 years	6 months	• Invitation enclosed from: • Prestigious Awards/ recognitions: N.A. • Publications in peer reviewed Journals: National:0 International: 4 • Proceeding: National:0 International:0 • Presentation: National:1 International: 0 • Patent: National: 0 International:0 • Last three years' foreign visits: 1 (Non-official visit) • Whether applied for RRF earlier: No

Publications List	
Research Articles	Impact factor
Verma S, Kumar A, Narang R, et al. Signature transcriptome analysis of stage specific atherosclerotic plaques of patients. **BMC Med Genomics. 2022**;15(1):99. https://doi.org/10.1186/s12920-022-01250-8	3.62
Kaushik N, Rastogi S, **Verma S**, et al. Transcriptome Analysis of Insulin Signaling-Associated Transcription Factors in C. elegans Reveal Their Genome-Wide Target Genes Specificity and Complexity. **Int J Mol Sci. 2021**;22(22). https://doi.org/10.3390/ijms222212462	5.6
Verma S, Jagtap U, Goyala A, et al. A novel gene-diet pair modulates C. elegans aging. **PLoS Genet. 2018**;14(8):e1007608. https://doi.org/10.1371/journal.pgen.1007608	5.10
Kumar N, Jain V, Singh A, Jagtap U, **Verma S**, Mukhopadhyay A. Genome-wide endogenous DAF-16/FOXO recruitment dynamics during lowered insulin signalling in C. elegans**. Oncotarget. 2015**;6(39):41418-41433. https://doi.org/10.18632/oncotarget.6282	2.54
Book Chapter	
Tripti Nair, **Sonia Verma**, and Arnab Mukhopadhyay. Diet-gene interactions that regulate longevity and diseases	

BMC Medical Genomics

RESEARCH

Open Access

Signature transcriptome analysis of stage specific atherosclerotic plaques of patients

Sonia Verma[1†], Abhay Kumar[2†], Rajiv Narang[3], Akshya K. Bisoi[4] and Dipendra K. Mitra[5*]

Abstract

Background: Inflammation plays an important role in all the stages of atherosclerotic plaque development. The current study aimed at assessing the altered expression of genes functioning in inflammation within the early stage (ES) and advanced stage (AS) atherosclerotic plaques obtained from patients undergoing coronary artery bypass grafting (CABG) surgery and identifying biomarker panel/s that may detect the status of plaque stages using peripheral blood samples.

Methods: A section of ES and AS plaques and normal left internal mammary arteries (LIMA) were obtained from 8 patients undergoing the CABG surgery. Total RNA isolated was analyzed for mRNA and miRNA expression profile by Affymetrix arrays. A significant number of mRNAs was found to be differentially expressed in ES and AS plaque tissues relative to LIMA. The pathway analysis of differentially expressed mRNAs in the two plaque stages was also performed using DAVID Bioinformatics Database.

Results: The mRNAs were found to be involved in critical inflammatory processes such as the toll-like receptor signaling pathway and cytokine-cytokine receptor interaction. Few miRNAs targeting these mRNAs were also altered in the two plaque conditions. QRT-PCR results showed a similar expression pattern of a few of the mRNAs and miRNAs in peripheral blood of the same patients relative to healthy controls.

Conclusion: Changes in mRNA and miRNA expression associated with various inflammatory processes occur in different atherosclerotic stage plaques as well as peripheral blood. Detection of such variations in patients' blood can be used as a possible prognostic tool to detect and/or predict the risk and stage of atherosclerosis.

Keywords: mRNA, miRNA, Atherosclerosis, Biomarker, Plaque stage

Background

Atherosclerotic vascular plaques are the major pathological basis for cardiovascular diseases (CVD) including ischemic heart disease (IHD), stroke, peripheral vascular disease, and renovascular hypertension. Inflammation is involved in the majority of atherosclerosis stages. The initial phase of atherosclerosis is mediated by the subendothelial accumulation of lipid molecules, including low-density lipoproteins (LDL), which later undergo oxidation by free radicals and oxidative enzymes [1, 2]. Accumulation of damaged mitochondrial DNA in circulation and immune cells is also one of the factors promoting inflammation during atherosclerosis [3, 4]. The expression of various chemokines and different adhesion molecules is stimulated with further recruitment, adhesion, and activation of circulating monocytes, other innate and adaptive immune cells as well as activated thrombocytes to the endothelium. VSMCs also migrate to the lesion site, transdifferentiate to plaque macrophages, express pro-inflammatory cytokines, and perform phagocytosis [5]. These cells along with circulating

*Correspondence: salilmitra2@gmail.com
†Sonia Verma and Abhay Kumar have contributed equally to this work.
[5] Department of Transplant Immunology and Immunogenetics, All India Institute of Medical Sciences (AIIMS), Room No-75, New Delhi 110029, India
Full list of author information is available at the end of the article

monocytes accumulate atherogenic modified LDL particles, such as oxidized LDL or desialylated LDL, and form foam cells, a characteristic feature of atherosclerotic plaques [1, 2].

At later stages of the development, the plaque is separated from the vessel lumen by a fibrous cap. At advanced stages, atherosclerosis is associated with prominent vascular wall thickening and calcification [6]. Both macrophages and VSMCs can release calcifying extracellular vesicles (EVs) [7]. The earliest calcifications also called microcalcifications (size < 50 μm), majorly originate from the lipid pool and early necrotic core, but can also be formed in the fibrous cap. Microcalcifications further exaggerate the inflammatory response [8]. The resulting pro-inflammatory response amplifies several processes related to microcalcification, triggering a battery of subsequent complications including rupture of the thrombotic plaque and/or blockade of vascular lumen leading to ischemic pathologies [9].

As the vascular plaque evolves, it converts from an early, lipid-rich atheroma to an advanced, fibro-calcified lesion [9]. Lipid-rich plaques with a thin fibrous cap are prone to rupture, precipitating in thrombus formation, leading to vascular occlusion causing acute ischemia and infarction of tissue. Methods to determine the nature of plaque are generally invasive and cumbersome. However, despite major advances in treatment, significant numbers of coronary artery disease (CAD) patients develop acute coronary syndromes and even have sudden cardiac death. Early detection of vulnerable plaque can identify patients at high risk for such events. Therefore it has become critical to develop improved molecular signature profiles for screening the plaque formation, preferably with stage specific signatures. Development of improved prognostics biomarker(s) and thus, novel therapeutic strategies for CVD, necessitates better understanding and identification of various key molecules and genetic pathways uniquely involved in various stages of atherosclerotic plaque formation.

Attempts toward the analysis of the gene expression profiles in atherosclerotic plaques are reported [10–14]. For comparative study, these reports used samples from different individuals, which may confound the results due to inter-individual genetic variation, tissue-specific differences in transcriptomes, and differences in systemic parameters. In CAD patients, distinct regions with ES or AS plaques may coexist within a single artery, hinting toward pathogenic attribute(s) leading to their sequential and/or differential evolution [15, 16]. Previous studies are mostly based on using autopsied specimens which may not truly represent the in vivo changes of the plaque. Therefore, to have better insights into the molecular profile of gene expression in the various stages of atherosclerotic plaques, we performed a microarray analysis of early stage (ES) and advanced stage (AS) plaques as well as healthy Left Internal Mammary Artery (LIMA) tissues obtained surgically from the same live individuals undergoing coronary artery bypass grafting (CABG) surgery.

We identified several inflammatory processes and pro-inflammatory cytokines associated with these plaques, evidencing a sustained inflammation and cytokine storm in the patients. Also, the miRNAs targeting these genes were found to be differentially expressed in the respective plaque stage. The expression levels of some of these genes were found to be following the same trend in patients' blood as observed in the plaques. Conclusively, our data provides for an early and faster prognostic tool for detecting and predicting the risk and stage of atherosclerosis.

Methods

Tissue collection

Patients' samples were obtained from 8 individuals (males-5, females-3), aged 55–80 years, undergoing CABG surgery at the apex tertiary referral center, All India Institute of Medical Sciences (AIIMS), New Delhi, India. Plaque tissues excised at the time of surgery as well as a 5–8 mm segment of LIMA were taken for analysis. The plaque tissue was divided into two parts depending upon the extent of calcification and lipid content. We used ES/lipid-rich plaque and AS/fibro-calcified plaque for further study. All these tissue fractions and LIMA segments were frozen immediately in QIAzol and stored at −80°C before RNA extraction. The study has been approved by the Institutional Ethics Committee, All India Institute of Medical Sciences, New Delhi, India, and all patients signed informed written consent.

RNA isolation

RNA was extracted from tissues using Qiagen miRNeasy Mini Kit. The tissues were placed in a 2 ml sterile Eppendorf tube containing RLT lysis buffer (Qiagen®). Samples were then homogenized individually on ice with a mechanical tissue homogenizer turned to the maximum position (3000 rpm) in short pulses of 15 seconds each for 10 cycles. The homogenates were separated into aqueous and organic phases by centrifugation after adding chloroform. The upper, aqueous phases containing RNA were extracted. After adding ethanol, the samples were applied to the RNeasy Mini spin column for total RNA binding to the membrane. Following washes, total RNAs were eluted in RNase-free water. The concentrations of the RNA were determined using NanoDrop 2000 (Thermo Scientific, USA). RNA from peripheral blood was also isolated using the same kit.

Microarray analysis

For microarray analysis, RNA from tissues with the similar condition of 4 patients was pooled to make one batch for sequencing. RNA pooling as a strategy before performing microarray experiments has been widely reported to optimize both the cost of data generation as well as the statistical power for differential gene expression analysis [17–19]. The biggest advantage of pooling occurs when the biological variability is large [17]. Two batches, each having 3 different samples, representing ES, AS and LIMA were sent for sequencing to Imperialls Life Sciences (P) Limited, India. In brief, for mRNA, cDNA synthesis, amplification, and gene expression profiling were done with the GeneChip WT PLUS Reagent Kit (Affymetrix) and labeled with the Genechip hybridization wash and stain kit (Affymetrix). Samples were hybridized with Gene Chip Human Transcriptome Array (HTA) 2.0 (Affymetrix) following the manufacturer's protocol. For miRNA, total RNA was labeled with Biotin using the AffymetrixFlashTag™ Biotin HSR kit following the manufacturer's protocol. Labeled extracts were hybridized to the GeneChip miRNA 4.0 Arrays overnight and subsequently processed using GeneChip Hybridization Wash and Stain kit (Affymetrix) according to the manufacturer's instructions.

Differential gene expression analysis

Transcriptome Analysis Console [TAC] 3.1 software [Affymetrix, CA, USA] provided by the Affymetrix Corporation was used to analyse significantly differentially expressed genes [fold change > 2 or fold change < −2] using a default algorithm one-way between-subject ANOVA [unpaired] and a filter criteria ANOVA p-value [Condition pair] < 0.05.

Functional enrichment of genes

The online tool, DAVID Bioinformatics Resources analyses was used to conduct the Kyoto Encyclopedia of Genes and Genomes (KEGG) pathway enrichment analysis of statistically significant, differentially-expressed mRNAs [20–22]. The *p*-value< 0.05 was set as the cut-off for selecting significantly over-represented pathways.

miRNAs targeting differentially expressed mRNAs

Differentially expressed mRNAs were subjected to the online database miRWalk (http://mirwalk.uni-hd.de/), where correlations between miRNAs and their target genes have been experimentally confirmed. In the database, three algorithms including targetScan, miRDB, and miRTarBase are used to predict miRNAs targeting the gene of interest. Any miRNA predicted for a given mRNA by all the three algorithms was considered to be targeting that gene.

MiRNA-target genes correlation

The reverse correlation between mRNAs and the miRNAs targeting these genes was screened by overlapping the predicted miRNAs of up-regulated mRNAs with the identified down-regulated miRNAs and vice-versa for the respective plaque tissue relative to LIMA.

QRT-PCR

1µg of RNA isolated from peripheral blood was reverse transcribed and used for miRNA quantification using Mir-X™ miRNA First-Strand Synthesis and TB Green qRT-PCR kit (Takara Bio Inc.). U6 was used as an internal control. For mRNA quantification, about 1µg of RNA isolated from peripheral blood was converted to cDNA with the cDNA Reverse Transcription Kit (Applied Biosystems, USA). Quantitative RT-PCR (qRT-PCR) was carried out on RealPlex PCR system (Eppendorf, USA) with SYBR Premix Ex Taq™ (TaKaRa Bio Inc.). GAPDH was used as the internal control. Statistical analysis was performed using GraphPad 7.0. The primers used are enlisted in Additional file 1.

Results

Differential gene expression profiling in ES and AS plaque

To investigate the variation in the expression of genes in human ES and AS atherosclerotic plaques, microarray sequencing and analysis of total RNA isolated from both the plaque tissues as well as LIMA was carried out. For ES plaques, 518 genes were significantly up-regulated and 497 genes were significantly down-regulated relative to LIMA (Fig. 1a). In AS plaque samples, we found more genes to be differentially expressed, i.e. 846 up-regulated genes while 1338 down-regulated genes as compared to LIMA (Fig. 1a). Interestingly, in both the plaques 279 and 358 common genes were up and down-regulated, respectively (Fig. 1a). The list of the top 50 differentially expressed mRNAs is provided in Additional file 2. Some of these genes such asSPP1, TGFB, and AKT3 have been associated with atherosclerosis in previous studies on mice and human samples, thus supporting our findings [23–28]. The topmost 10 up-regulated and down-regulated mRNAs are presented in Fig. 1b and c. In summary, the microarray data indicates that atherosclerotic plaques are associated with alterations in gene expression which may further differ among various plaque stages.

ES Plaques are associated with the up-regulation of inflammatory mediators

Inflammation plays an important role in atherosclerosis. Elevated levels of inflammatory cytokines and chemokines have been observed in various studies on affected cardiac tissues [10–14]. In the current study, we delineated the genes involved in the inflammation of ES and AS plaques

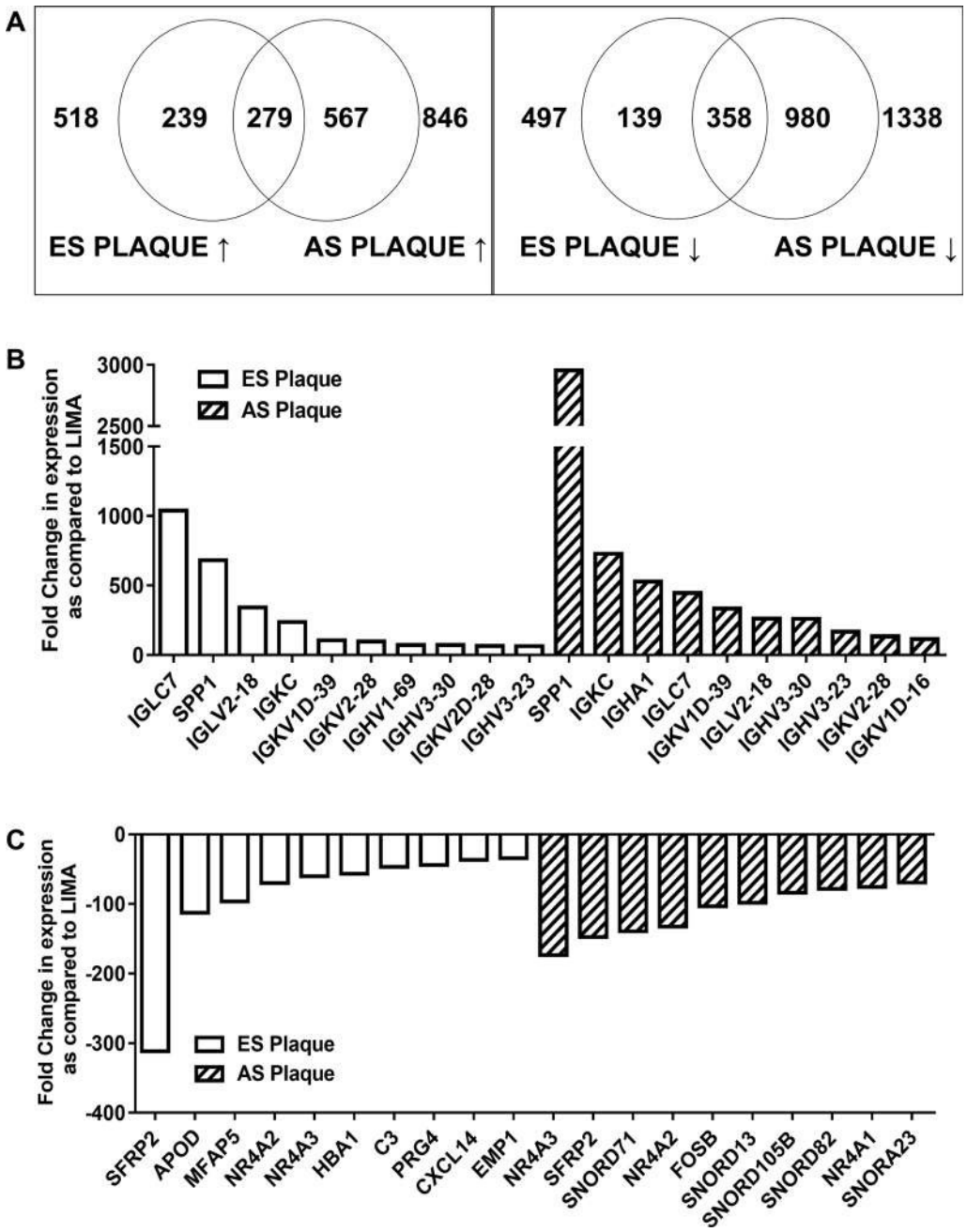

Fig. 1 Microarray analysis reveals alterations in gene expression associated with atherosclerotic plaques. **a** Venn diagram of differentially expressed genes in early (ES) and advanced stage (AS) atherosclerotic plaque as compared to Left Internal Mammary Artery (LIMA) (↑—up-regulated; ↓—down-regulated). **b** Bar graph of top 10 mRNAs significantly up-regulated as compared to LIMA in microarray analysis. **c** Bar graph of top 10 mRNAs significantly down-regulated as compared to LIMA in microarray analysis. n = 2 (each with sample pooled from 4 patients); $p < 0.05$

(See figure on next page.)

Fig. 2 The differentially expressed genes in the plaques are associated with inflammation. **a** Bar graph showing significantly-enriched inflammation associated KEGG pathways of differentially expressed genes in early stage (ES) atherosclerotic plaques. The KEGG pathway analysis was done using an online database, DAVID. **b** List of differentially expressed genes functioning in inflammation pathways mentioned in A and C. **c** Bar graph showing significantly-enriched inflammation associated KEGG pathways of differentially expressed genes in advanced stage (AS) atherosclerotic plaques. n = 2 (each with sample pooled from 4 patients); $p < 0.05$

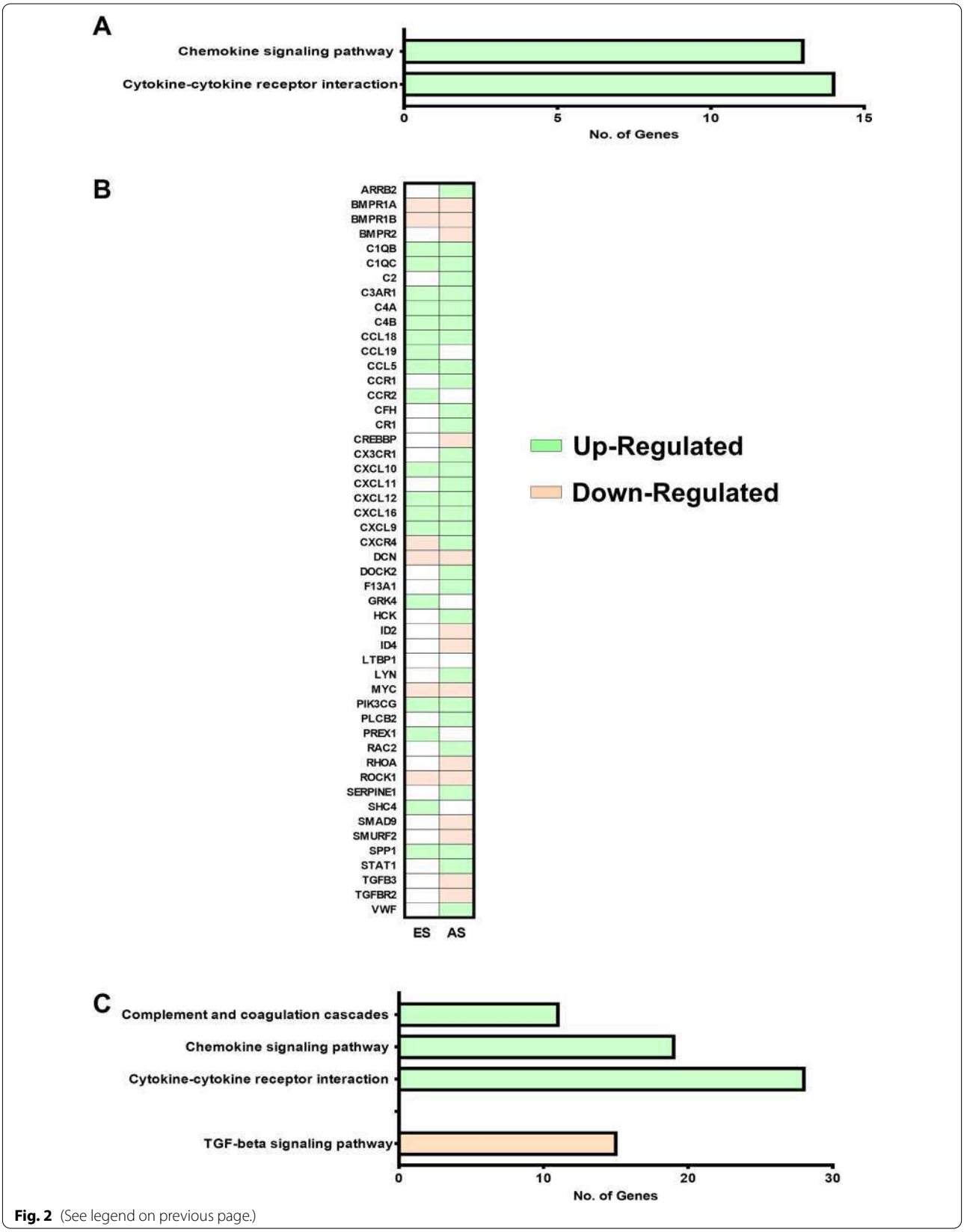

Fig. 2 (See legend on previous page.)

by KEGG pathway analysis of differentially expressed genes using DAVID. In ES plaques, 19up-regulated genes were related to the chemokine signaling pathway and cytokine-cytokine receptor interaction (Fig. 2a, Additional file 3). Interestingly, most of these pro-inflammatory genes like CCL5, CXCL10, CXCL9, CTSK, and CD14 have been previously reported to be elevated in the serum of patients with coronary artery diseases [13, 14, 29–32]. The list of differentially expressed genes functioning in inflammation pathways is shown in Fig. 2b.

Few of these 19 genes were also found to be up-regulated in AS plaques while the expression of remaining genes was found only in ES plaque; for example, PREX1, SHC4, and CCR2 (Fig. 3a and b). These ES plaque-specific genes function in regulating the signaling pathways for chemotaxis and migration of various immune cells. Since these genes show plaque-specific up-regulation, they can be used as biomarkers to indicate the presence of ES plaque in patients.

AS plaques are also associated with the up-regulation of inflammatory mediators

Upon pathway analysis for up-regulated genes in AS plaques, 48 of these genes were found to be involved in complement and coagulation cascades along with chemokine signaling pathway and cytokine-cytokine receptor interaction (Fig. 2c, b, Additional file 3). Among the genes functioning in the chemokine signaling pathway and cytokine-cytokine receptor interaction, 23 were found to be up-regulated specifically in AS plaque (Fig. 3a and b). We also observed that the few genes functioning in the chemokine signaling pathway and cytokine-cytokine receptor interaction, whose expression was enhanced in both ES and AS plaque, showed higher fold change in the later stage (Fig. 3a and b). Among these genes are SPP1, CXCL9, CXCL12, and CCL5.

The up-regulated genes involved in Complement and Coagulation Cascade include C1QB, C1QC, CFH, and C2 (Fig. 2b and c, Additional file 3). These genes function in the classical complement pathway which is activated not only during bacterial infections but also in the absence of proper immune regulatory mechanisms. Therefore, in AS plaque, the activation of this system might be involved in the clearance of damaged cells. In summary, the AS plaque is not only associated with a greater number of highly expressed genes but also shows a higher fold change of commonly up-regulated genes as compared to ES plaques. Examining the expression levels of such genes in peripheral blood of patients would suggest the prevalence of plaque stage and support the clinicians in further management of the disease.

AS plaques are associated with down-regulation of anti-inflammatory mediators

The inflammatory response must be actively terminated when no longer needed to prevent unnecessary "bystander" damage to tissues. Failure to do so results in chronic inflammation, and cellular destruction. We found a similar observation in AS plaques; 15 down-regulated genes were involved in the anti-inflammatory-TGF-beta signaling pathway (Fig. 2c, Additional file 3). The loss of expression of some of these genes like BMPRII (receptor of the TGF-beta) and DCN (cellular matrix proteoglycan that binds to TGF-beta) has been reported in human coronary arteries with advanced atherosclerotic lesions further supporting our observations and also suggesting an unchecked hyper-inflammatory condition in AS plaques [33]. Few of these genes like BMPR1B, ROCK1, and DCN were also found to be down-regulated in ES plaque as well and their fold change difference was similar to that found in AS plaque (Fig. 3d).

Distinct miRNA profiles in ES and AS plaque

The expression levels of 132 miRNAs differed in the two plaque tissues relative to LIMA. However, the variation in the expression of these miRNAs was insignificant in our data. This might be due to the small sample size. Of these miRNAs, 38 were up-regulated and 62 were down-regulated in the ES plaques when compared to LIMA (Fig. 4a and b). In AS plaques, 40 miRNAs were up-regulated and 30 miRNAs were down-regulated as compared to LIMA (Fig. 4a and b). Also, 5 miRNAs were up-regulated and 29 miRNAs were down-regulated in both the plaques (Fig. 4a and b). The full list of differentially expressed miRNAs is provided in Additional file 4. Recently, the down-regulation of miR-143 has been observed in advanced coronary atherosclerotic plaques [34]. Mir-143 is thought to be involved in cardiac morphogenesis and cancer [35]. In human aortic aneurysms, the expression of mir-143 has also been found to be significantly decreased when compared to

(See figure on next page.)

Fig. 3 Expression of various inflammatory pathways-associated genes is altered in atherosclerotic plaques. Graphs showing microarray-analysis-based fold change in expression of genes in early stage (ES) and advanced stage (AS) atherosclerotic plaques as compared to (Left Internal Mammary Artery) LIMA. Using an online database DAVID the genes were found to be involved in chemokine signaling pathway (**a**), Cytokine-cytokine receptor interaction (**b**), Complement and coagulation cascades (**c**), and TGF-beta signaling pathway (**d**). n = 2 (each with sample pooled from 4 patients); $p < 0.05$

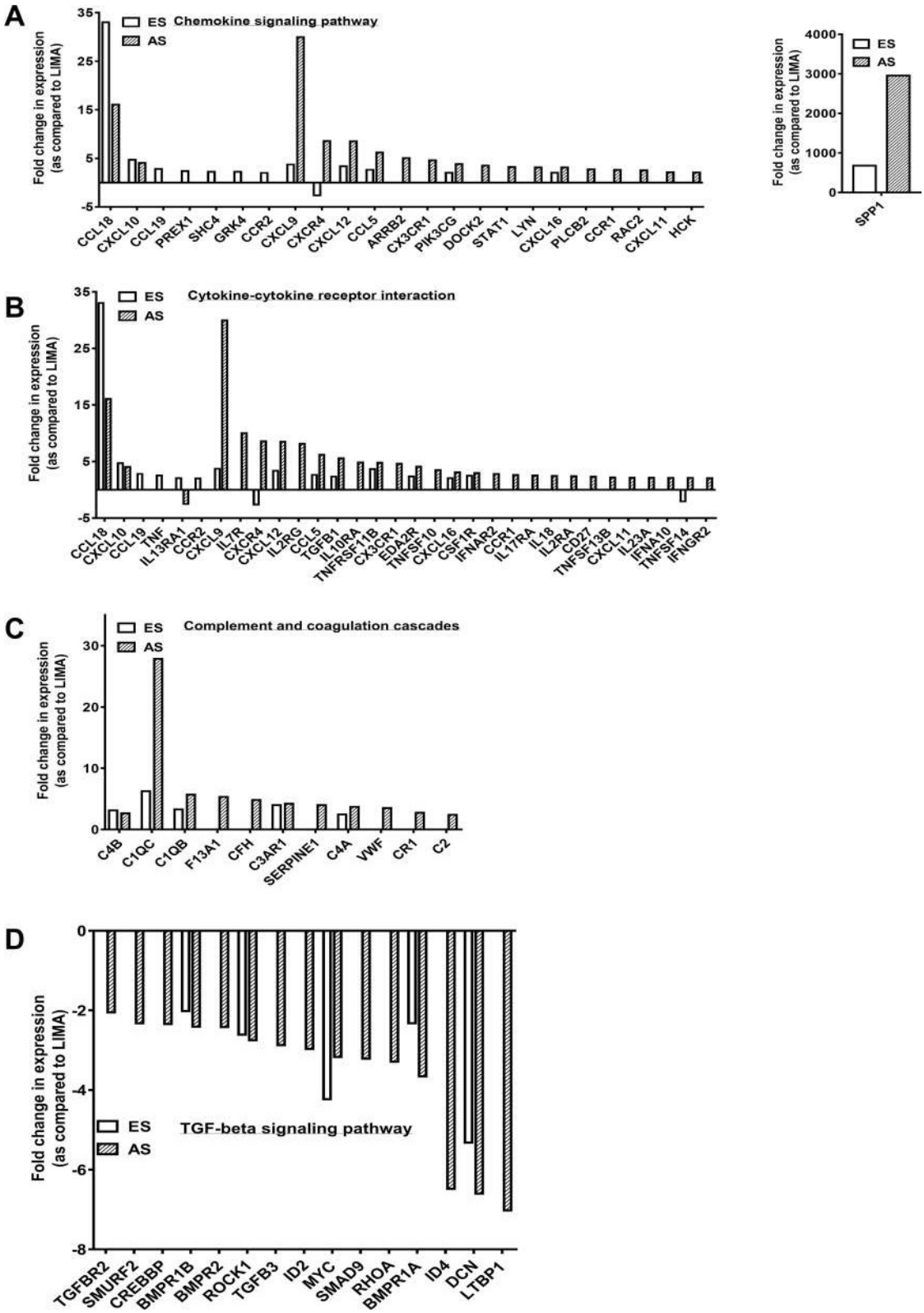

Fig. 3 (See legend on previous page.)

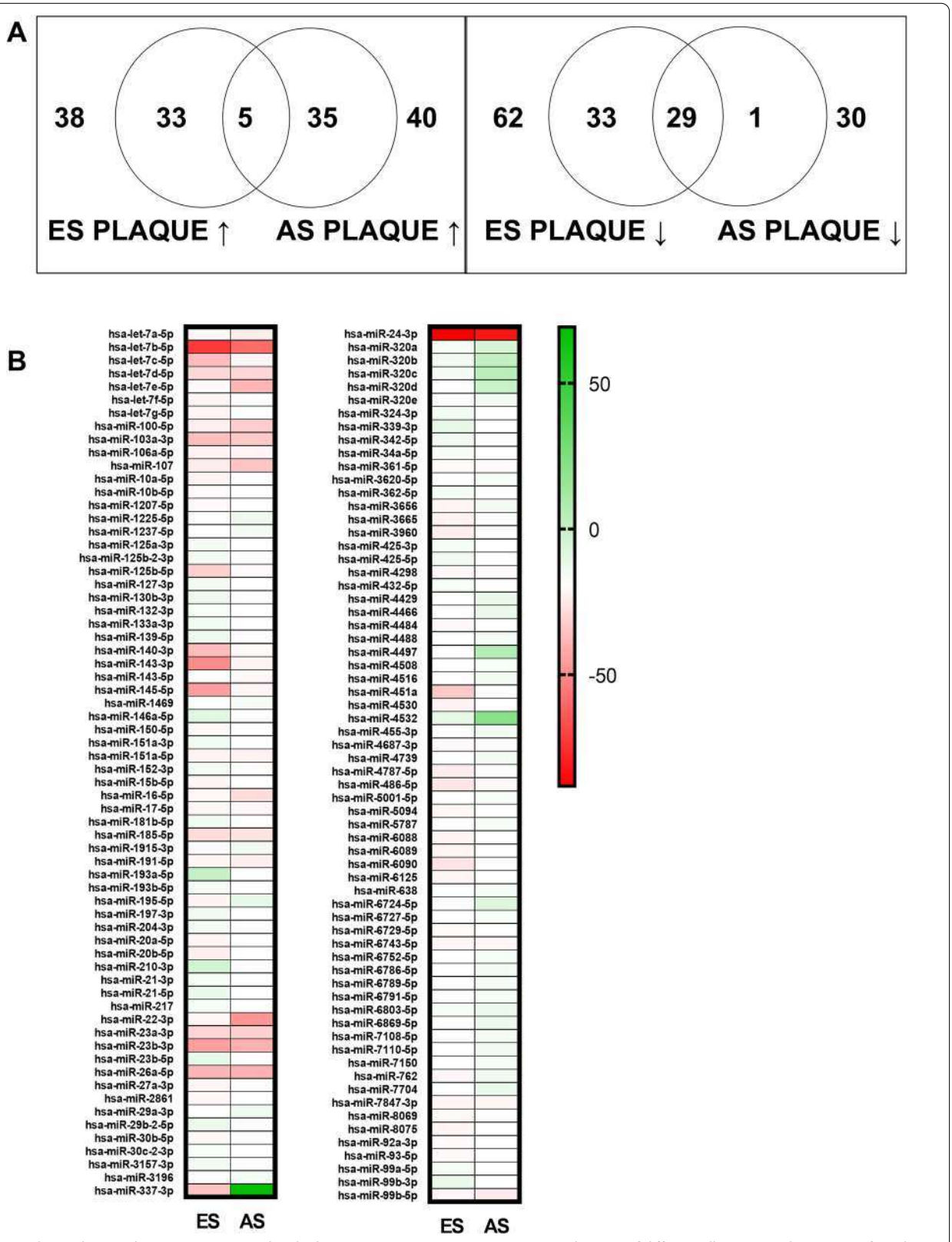

Fig. 4 Atherosclerotic plaques are associated with alterations in miRNA expression. **a** Venn diagram of differentially expressed miRNAs as found in microarray analysis in early (ES) and advanced stage (AS) atherosclerotic plaques as compared to Left Internal Mammary Artery (LIMA)**. b** Heat-map of miRNAs differentially expressed in the two plaques. n = 2 (each with sample pooled from 4 patients)

controls [36]. In our study, we report down-regulation of this miRNA not only in AS plaque but also in ES plaque. Interestingly the fold change was much lower in ES plaque (−40) than AS plaque (−4), suggesting its possible role in altering vascular smooth muscle cells morphology early during atherosclerosis.

The two miRNAs that were up-regulated in ES showed down-regulation in AS plaque. Of these, miR-22 is reduced in human arteries from arteriosclerosis obliterans [37]. The down-regulation of miR-22 increases the expression of pro-inflammatory cytokines and therefore suggests the creation of an unfavorable pro-inflammatory situation that promotes plaque formation [38]. We also found 4 miRNAs, down-regulated in ES plaque, to be up-regulated in AS plaque. In summary, the miRNA expression analysis shows an association of atherosclerotic plaques with variable expression of different miRNAs, and the presence of a similar trend of expression of these miRNAs in ES and As plaques can be used as a potential biomarker.

Negative correlation between miRNAs and mRNAs profile in atherosclerotic plaque

The small non-coding RNAs-miRNAs are known to regulate the expression of various genes by inhibiting their translation. To understand the role of miRNAs in atherosclerosis-associated inflammation, using the miRWalk database we first predicted the miRNAs for the inflammatory mediators that were up-regulated in ES and AS plaque as compared to LIMA. Next, these miRNAs were then overlapped with the miRNAs that were found to be down-regulated in the microarray analysis of respective tissue. A Similar methodology was employed for down-regulated inflammatory mediators and the miRNAs targeting them. In this manner, miRNA-target gene interaction pairs of reverse association in the two plaque tissues were obtained. We found 3 such interacting pairs with up-regulated mRNAs and down-regulated miRNAs (Table 1). 2 of these pairs included miRNAs (hsa-miR-125b-5p and hsa-miR-23a-3p) down-regulated in AS plaque. Interestingly, the target gene of hsa-miR-125b-5p and hsa-miR-23a-3p- TNFAIP3 was also found to be up-regulated in the AS plaque. The remaining interaction pair included miRNA, hsa-miR-22-3p, and its target CSF1R. In both the plaques, this miRNA was down-regulated while its target gene was up-regulated (Table 1). The opposite trend of expression of the above-mentioned miRNAs and mRNAs in patients' blood can further support the diagnosis of plaque stage.

Distinct mRNA/miRNA profiles are detected in patients' blood

In an effort to use the identified mRNAs as biomarkers for the detection of the atherosclerotic condition, we quantified the levels of a few mRNAs in patients'

Table 2 The panel of genes proposed in the study to be used as biomarker for diagnosis of plaque stage

	ES	AS
Chemokine signalling pathway and cytokine-cytokine receptor interaction		
SPP1	↑*	↑↑
CCL18	↑↑	↑
CXCL9	↑	↑↑
CXCL12	↑	↑↑
IL13RA1	↑	↓†
TNFSF14	↓	↑
CXCR4	↓	↑
CCL19	↑	
TNF	↑	
IL7R		↑
IL2RG		↑
ARRB2		↑
IL10RA		↑
Complement and coagulation cascades		
C1QC	↑	↑↑
C1QB	↑	↑↑
F13A1		↑
CFH		↑
SERPINE1		↑
TGF-beta signaling pathway		
BMPR2		↓
TGFB3		↓
TGFBR2		↓

*Up-regulated, †down-regulated

Table 1 miRNA-target gene interaction pairs of reverse association in the two plaque tissues

	miRNA	Fold change vs LIMA	Target mRNA	Fold change vs LIMA
ADVANCED STAGE	hsa-miR-125b-5p	− 2.26	TNFAIP3	4.88
	hsa-miR-23a-3p	− 15.88	TNFAIP3	4.88
EARLY STAGE	hsa-miR-22-3p	− 3.32	CSF1R	2.49
ADVANCED STAGE	hsa-miR-22-3p	− 36.7	CSF1R	2.95

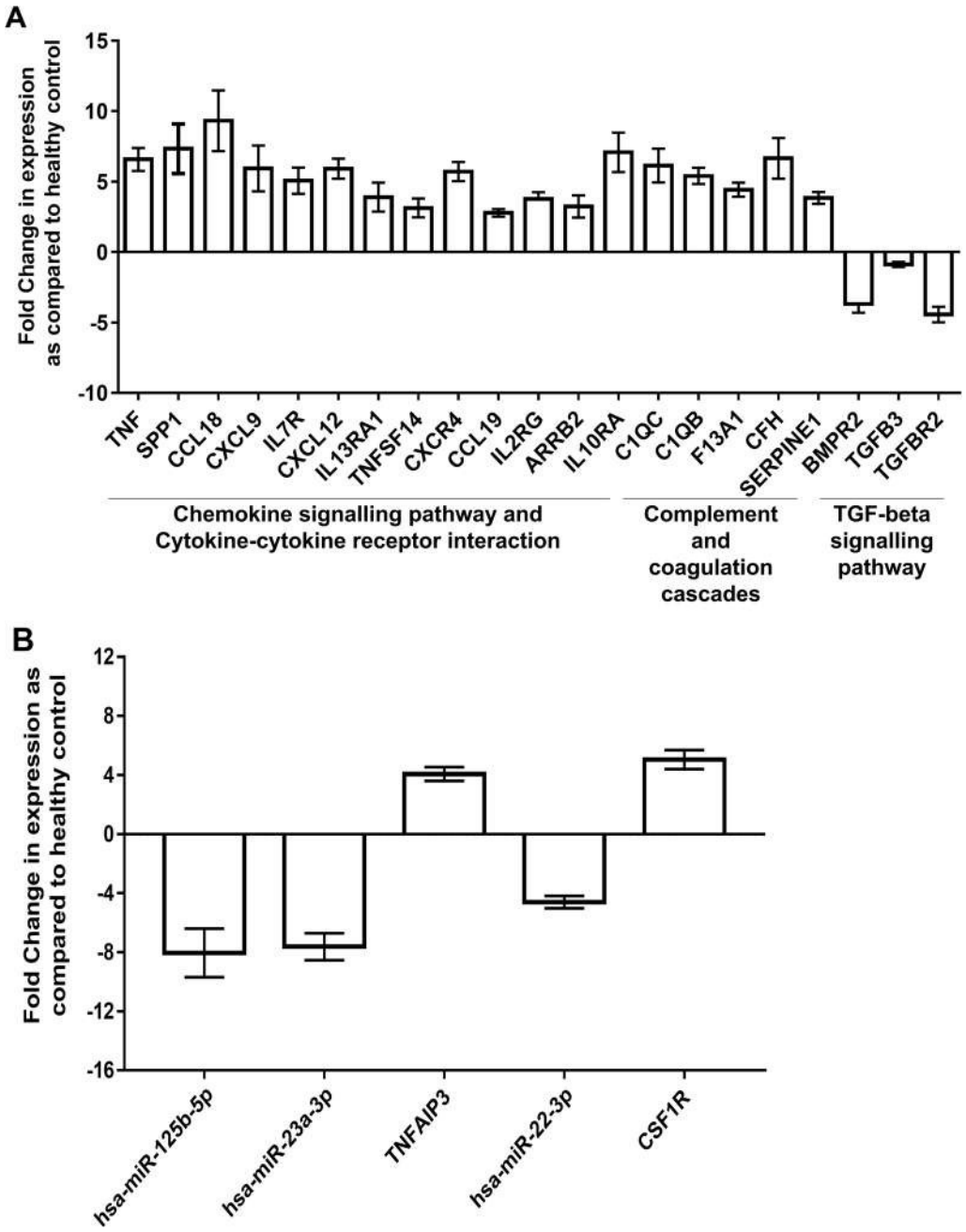

Fig. 5 The Expression of mRNA/miRNA is also altered in the peripheral blood of patients. **a** QRT-PCR based quantification of mRNAs of a proposed biomarker panel in peripheral blood of patients and comparison with healthy control. **b** QRT-PCR based quantification of identified miRNA-mRNA interaction pairs in peripheral blood of patients and comparison with healthy control. GAPDH mRNA was used for normalization. n = 13 (8 patients; 5 healthy control); Error bar indicates standard error mean. The student's t-test was performed independently for each gene between healthy peripheral blood samples and patients' peripheral blood samples. *p* = non-significant

blood by qRT-PCR and compared them with that of healthy blood samples. The panel included the mRNAs that showed altered expression in both the plaques and specifically in ES or AS plaques (Table 2). The qRT-PCR result showed up-regulation of genes that were involved in the chemokine signaling pathway, cytokine-cytokine receptor interaction, and complement and coagulation cascades while the expression of genes that were functioning in the TGF-beta signaling pathway was found to be lowered as compared to healthy controls (Fig. 5). We

also performed QRT-PCR for the miRNA-mRNA pairs found in our study (Table 1). An Expression pattern similar to the microarray analysis was found. However, the mRNAs and miRNAs showed a non-significant *p*-value. Increasing the sample size may improve the significance of our result. These results support the presence of differentially expressed miRNA and mRNA in patients' blood and their use as potential biomarkers for assessing the stage and risk of atherosclerosis.

Discussion

Atherosclerosis is a chronic inflammatory condition of the arteries. Various effector immune mechanisms and signaling networks are involved in the pathology of atherosclerotic plaque formation [39–44]. Elevated levels of inflammatory cytokines and chemokines have been observed in various studies on affected cardiac tissues [45–47]. However, studies on differential expression of immune/ inflammatory genes in plaques of early versus advanced stages remain scant. Volger et al, 2007, studied gene expression profiles of endothelium from human large arteries having focal atherosclerosis of the ES or AS [32]. The transcriptomes of the lesional arteries were compared with the transcriptomes of their unaffected sides, thus limiting genetic and external confounders. The authors, however, collected samples post-mortem after the disease. Post-mortem tissues undergo significant changes in their physical and chemical compositions possibly altering the profile of mRNA stability retrieval and amplification required for transcriptome profiling [48]. Therefore, we performed a microarray analysis of ES and AS plaque as well as healthy LIMA tissue obtained surgically from the same live individuals undergoing CABG Surgery.

Here, we attempted to understand the differential expression profiles of immune response-related genes in early versus advanced atherosclerotic plaques. We found that the ES and AS plaques are associated with differential expression of various mRNAs and miRNAs, suggesting that the transcriptional regulations and responses in the initial stage of plaque formation may contribute to the subsequent pathophysiology of atherosclerosis (Fig. 6). In both the plaques, significant numbers of genes were found to be involved in more than one arm of the immune system. Interestingly, few of these genes have already been reported to be involved in atherosclerosis pathology, supporting the validity of our data. Examples of such genes are SPP1, CXCL9, CCL18, FcγRIIIA, etc. [23–28]. The higher expression patterns of common genes in AS versus ES plaques suggest that atherosclerosis involves an array of processes where alterations in their profiles shift the balance from ES to AS stage evolution. A prominent example of such a common gene is SPP1, required for macrophage chemotaxis, critical in lipid peroxidation, and a pathological landmark of atherosclerosis [49, 50]. Our results also unravel the differentially expressed genes in plaque in stage specific manner, and definitive profiles marking the dominance of early and/or advanced atherosclerotic changes in patients. For example, the chemokine CCL19 was up-regulated only in ES plaque, which might be involved in the trafficking of various inflammatory cells at the plaque site. On the other hand, AS plaques showed up-regulation of genes involved in stronger inflammation (e.g.- C1QC, C1QB, TYROBP, etc.).

The over-expression of genes functioning in the chemokine signaling pathway in ES plaques suggests the initiation of various immune cells recruitment at the affected tissue. For example, CCL18 for naïve T cells, CCL19 for T and B cell migration, and CCL5 for blood monocytes, memory T helper cells, and eosinophils [51–53]. The genes (like CCL5, TNF, CXCL10) which are involved in cytokine-cytokine signaling stimulate these incoming immune cells to release various other signaling and pro-inflammatory molecules; for instance, activation of eosinophils by CCL5 and stimulation of monocytes by CXCL10 [53]. Therefore, chemotaxis and activation of a diverse immune cell population in ES plaque suggest an onset of inflammation in the affected vascular tissue. The up-regulation of genes coding for different cytokine receptors like IL7R, IL2RG, IFNGR2, and IL17RA only in AS plaque and the absence of expression of their respective cytokines in microarray analysis indicates a compensatory phenomenon in which cells attempt to enhance the probability of binding to the scarce cytokines. Also, the suppression of the genes required for TGF-beta signaling in AS plaque and ES plaque suggests a failure of immune-regulatory mechanisms to check the on-going inflammation.

In an attempt to understand the regulation of differentially expressed mRNAs at the post-transcriptional level, microarray analysis against miRNAs for both plaques was carried out, followed by the identification of miRNA-mRNA interaction pairs for the corresponding plaques. Few of the resulting miRNAs like hsa-miR-17, hsa-miR-16, hsa-miR-195, hsa-miR-27a, hsa-miR-20b, etc. have already been reported in other studies to be associated with coronary artery disease [54–56]. We found three miRNA-mRNA pairs associated with atherosclerosis. Among them, one pair included hsa-miR-125b and its target TNFAIP3. Hsa-miR-125b act as a negative regulator of inflammatory genes and TNFAIP3 is involved in the cytokine-mediated immune and inflammatory responses [57]. Therefore, the involvement of hsa-miR-125b in inflammation during atherosclerosis can also be proposed via TNFAIP3. The second interaction pair

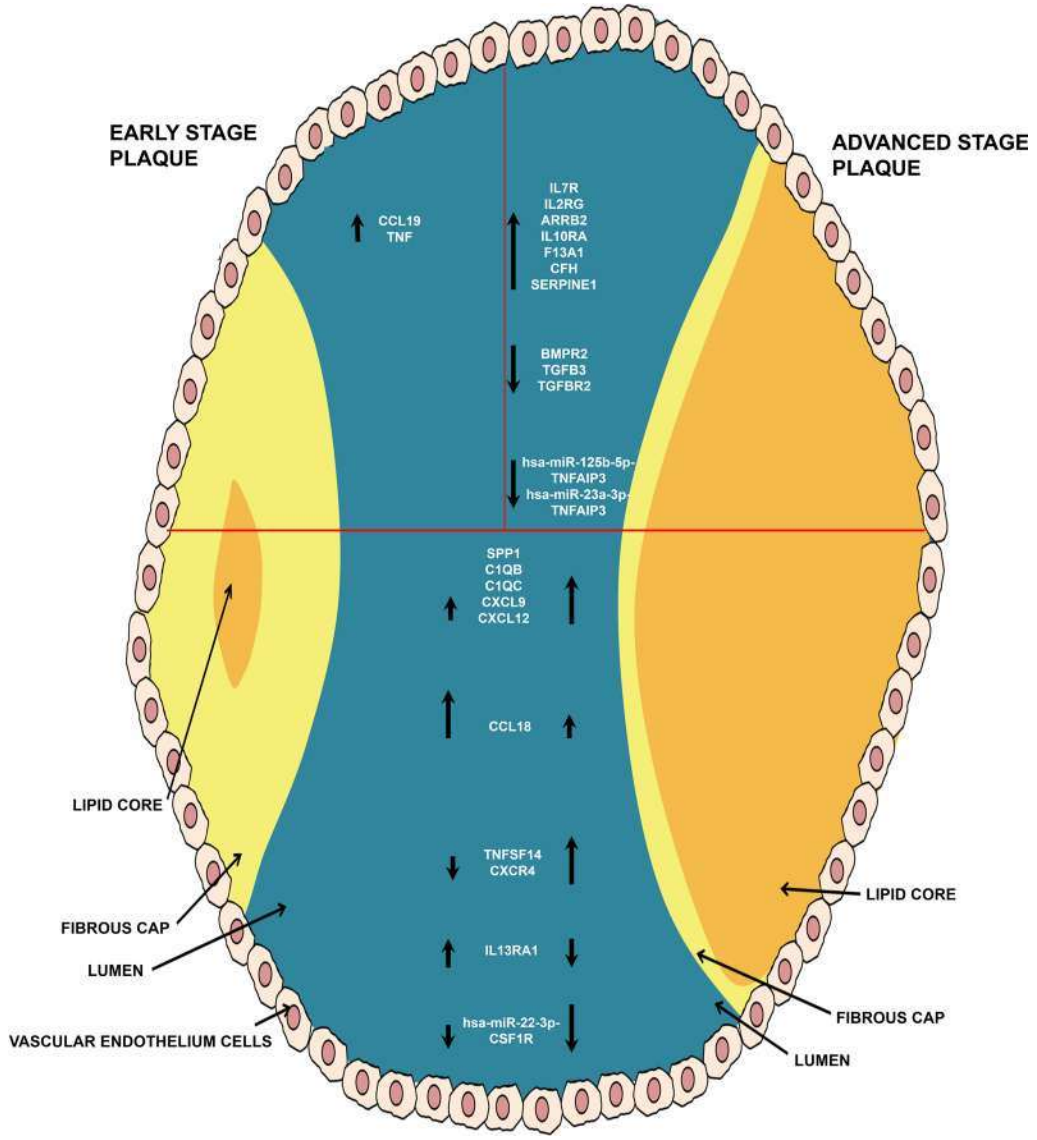

Fig. 6 Summary of mRNA and miRNA expression analysis in atherosclerotic plaques as compared to LIMA. The upper left panel represents the differentially expressed in early stage plaques only. The upper right panel represents the differentially expressed mRNA and miRNA along with miRNA-mRNA pairs in advanced stage plaques only. The lower panel shows mRNA, miRNA, and miRNA-mRNA pairs differentially expressed in both the plaques

included hsa-miR-22-3p and its target CSF1R. Since CSF1R promotes the release of pro-inflammatory chemokines, the finding that this gene is up-regulated while the miRNA targeting it is down-regulated in ES and AS plaques suggest the role of this miRNA-mRNA pair in atherosclerosis associated inflammation.

Identifying microarray-based biomarkers may complement and help in circumventing the invasive techniques for clinical evaluation of the stage of atherosclerotic pathophysiology and its implication in patient prognosis and healthcare. Circulating mRNAs and miRNAs are being investigated as possible biomarkers for the early detection and progression of various diseases [58–60]. Moreno et al. (2009) reported that the plasma level of CD163-TWEAK (tumor necrosis factor-like weak inducer of apoptosis) is a potential biomarker of atherosclerosis [61]. Therefore, differentially expressed mRNAs and miRNAs profiles identified in the present study may reveal a fingerprint of the presence and/or the dominance of ES and AS plaques. We correlated the same in the peripheral blood of the patients intending to identify the significant changes in their blood. The pattern

of expression difference was similar to that reported in microarray analysis, supporting the hypothesis that the expression levels of common and stage specific mRNA and miRNAs in the blood samples of patients can be used as a biomarker for early detection and monitoring of progression and/or regression of coronary atherosclerosis and thus possibly to evaluate the effectiveness of anti-atherosclerotic therapies on a larger scale. However, we need a proper scoring system for the expression of these stage specific genes so that weightage to ES or AS could be given. Although we cannot know the frequency of the particular plaque stage in the patient, the ratio of the expression of stage specific genes can tell us the condition of more prevalent plaque.

Conclusions

From our results, two distinct mRNA-miRNA pair profiles are evident:

Panel 1—SPP1↑, CCL18↑↑, CXCL9↑, CXCL12↑, IL13AR1↑, TNFSF14↓, CXCR4↓, CCL19↑, TNF↑, C1QC↑, C1QB↑
Panel 2–SPP1↑↑, CCL18↑, CXCL9↑↑, CXCL12↑↑, IL13AR1↓, TNFSF14↑, CXCR4↑, IL7R↑, IL2RG↑, ARRB2↑, IL10RA↑, C1QC↑↑, C1QB↑↑

The former has a high correlation with ES plaque and later with AS plaque. Such profiles are also reflected in the peripheral blood. Therefore, we propose that ratios of these profiles may signature the proportion of advanced pathology in patients. This might supplement the imaging analysis of atherosclerotic plaques and enable clinicians to better assess the disease state and plan for clinical management accordingly.

Abbreviations

CVD: Cardiovascular diseases; IHD: Ischemic heart disease; CAD: Coronary artery disease; ES: Early stage; AS: Advanced stage; LIMA: Left internal mammary artery; CABG: Coronary artery bypass grafting; KEGG: Kyoto encyclopaedia of genes and genomes.

Supplementary Information

The online version contains supplementary material available at https://doi.org/10.1186/s12920-022-01250-8.

Additional file 1. The list of primers used for qRT-PCR.

Additional file 2. Significantly-enriched inflammation associated KEGG pathways of differentially expressed genes in early stage and advanced stage atherosclerotic plaque.

Additional file 3. Differentially expressed mRNAs.

Additional file 4. Differentially expressed miRNAs.

Acknowledgements

Not applicable

Author contributions

DKM has contributed in the conceptualization, data interpretation, and manuscript preparation. SV and AK have performed the experiments, analyzed data, and prepared the manuscript. RN has contributed by selecting and recruiting patients and reviewing the manuscript. AKB has provided the tissue samples and helped in improving the manuscript. All authors read and approved the final manuscript.

Funding

Not applicable.

Availability of data and materials

The datasets generated and/or analyzed during the current study are available in the European Bioinformatics Institute Array Express repository, (accession number-E-MTAB-10052 (mRNA data); E-MTAB-10051 (miRNA data)).

Declarations

Ethics approval and consent to participate

This study was performed in accordance with the Declaration of Helsinki and had been approved by the Institutional Ethics Committee, All India Institute of Medical Sciences, New Delhi, India, and all patients signed informed written consent.

Consent for publication

Not applicable

Competing interests

The authors declare that they have no competing interests.

Author details

[1]Division of Neuroscience and Ageing Biology, CSIR-Central Drug Research Institute, Lucknow, Uttar Pradesh, India. [2]Department of Microbiology, Indira Gandhi Institute of Medical Sciences, Patna, India. [3]Department of Cardiology, All India Institute of Medical Sciences, New Delhi, India. [4]Department of Cardiothoracic and Vascular Surgery, Cardio, and Neurosciences Center, AIIMS, New Delhi, India. [5]Department of Transplant Immunology and Immunogenetics, All India Institute of Medical Sciences (AIIMS), Room No-75, New Delhi 110029, India.

Received: 29 November 2021 Accepted: 4 April 2022
Published online: 29 April 2022

References

1. Poznyak AV, Nikiforov NG, Markin AM, Kashirskikh DA, Myasoedova VA, Gerasimova EV, et al. Overview of OxLDL and its impact on cardiovascular health: focus on atherosclerosis. Front Pharmacol. 2021;11(11): 613780.
2. Orekhov AN, Ivanova EA, Melnichenko AA, Sobenin IA. Circulating desialylated low density lipoprotein. Cor Vasa. 2017;59(2):e149–56.
3. Bezsonov E, Sobenin I, Orekhov A. Immunopathology of atherosclerosis and related diseases: focus on molecular biology. IJMS. 2021;22(8):4080.
4. Sobenin I, Chistiakov D, Bobryshev Y, Postnov A, Orekhov A. Mitochondrial mutations in atherosclerosis: new solutions in research and possible clinical applications. CPD. 2013;19(33):5942–53.
5. Grootaert MOJ, Bennett MR. Vascular smooth muscle cells in atherosclerosis: time for a re-assessment. Cardiovasc Res. 2021;117(11):2326–39.
6. Durham AL, Speer MY, Scatena M, Giachelli CM, Shanahan CM. Role of smooth muscle cells in vascular calcification: implications in atherosclerosis and arterial stiffness. Cardiovasc Res. 2018;114(4):590–600.
7. Chistiakov DA, Myasoedova VA, Melnichenko AA, Grechko AV, Orekhov AN. Calcifying matrix vesicles and atherosclerosis. Biomed Res Int. 2017;2017:1–7.
8. Shi X, Gao J, Lv Q, Cai H, Wang F, Ye R, et al. Calcification in atherosclerotic plaque vulnerability: friend or foe? Front Physiol. 2020;5(11):56.
9. Bentzon JF, Otsuka F, Virmani R, Falk E. Mechanisms of plaque formation and rupture. Circ Res. 2014;114(12):1852–66.
10. Shen Y, Xu L, Tang X, Lin C, Yan D, Xue S, et al. Identification of potential therapeutic targets for atherosclerosis by analysing the gene signature

related to different immune cells and immune regulators in atheromatous plaques. BMC Med Genomics. 2021;14(1):145.
11. Sivapalaratnam S, Farrugia R, Nieuwdorp M, Langford CF, van Beem RT, Maiwald S, et al. Identification of candidate genes linking systemic inflammation to atherosclerosis; results of a human in vivoLPS infusion study. BMC Med Genomics. 2011;4(1):64.
12. Albright J, Quizon PM, Lusis AJ, Bennett BJ. Genetic network identifies novel pathways contributing to atherosclerosis susceptibility in the innominate artery. BMC Med Genomics. 2014;7(1):51.
13. Maracle CX, Agca R, Helder B, Meeuwsen JAL, Niessen HWM, Biessen EAL, et al. Noncanonical NF-κB signaling in microvessels of atherosclerotic lesions is associated with inflammation, atheromatous plaque morphology and myocardial infarction. Atherosclerosis. 2018;270:33–41.
14. Arslan S, Berkan Ö, Lalem T, Özbilüm N, Göksel S, Korkmaz Ö, et al. Long non-coding RNAs in the atherosclerotic plaque. Atherosclerosis. 2017;266:176–81.
15. Lehoux S, Castier Y, Tedgui A. Molecular mechanisms of the vascular responses to haemodynamic forces. J Intern Med. 2006;259(4):381–92.
16. Cheng C, Tempel D, van Haperen R, van der Baan A, Grosveld F, Daemen MJAP, et al. Atherosclerotic lesion size and vulnerability are determined by patterns of fluid shear stress. Circulation. 2006;113(23):2744–53.
17. Kendziorski C, Irizarry RA, Chen K-S, Haag JD, Gould MN. On the utility of pooling biological samples in microarray experiments. Proc Natl Acad Sci. 2005;102(12):4252–7.
18. Shih JH, Michalowska AM, Dobbin K, Ye Y, Qiu TH, Green JE. Effects of pooling mRNA in microarray class comparisons. Bioinformatics. 2004;20(18):3318–25.
19. Peng X, Wood CL, Blalock EM, Chen KC, Landfield PW, Stromberg AJ. Statistical implications of pooling RNA samples for microarray experiments. BMC Bioinformatics. 2003;9.
20. Kanehisa M, Goto S. KEGG: Kyoto encyclopedia of genes and genomes. :4.
21. Kanehisa M, Furumichi M, Sato Y, Ishiguro-Watanabe M, Tanabe M. KEGG: integrating viruses and cellular organisms. Nucleic Acids Res. 2021;49(D1):D545–51.
22. Kanehisa M. Toward understanding the origin and evolution of cellular organisms. Protein Sci. 2019;28(11):1947–51.
23. Chmielewski S, Olejnik A, Sikorski K, Pelisek J, Błaszczyk K, Aoqui C, et al. STAT1-dependent signal integration between IFNγ and TLR4 in vascular cells reflect pro-atherogenic responses in human atherosclerosis. Dhillon NK, editor. PLoS ONE. 2014 Dec 5;9(12):e113318.
24. Sikorski K, Wesoly J, Bluyssen HAR. Data mining of atherosclerotic plaque transcriptomes predicts STAT1-dependent inflammatory signal integration in vascular disease. Int J Mol Sci. 2014;15(8):14313–31.
25. Aquila G, Fortini C, Pannuti A, Delbue S, Pannella M, Morelli MB, et al. Distinct gene expression profiles associated with Notch ligands Delta-like 4 and Jagged1 in plaque material from peripheral artery disease patients: A pilot study. J Transl Med. 2017;15(1):1–14.
26. Rohlena J, Volger OL, Van Buul JD, Hekking LHP, Van Gils JM, Bonta PI, et al. Endothelial CD81 is a marker of early human atherosclerotic plaques and facilitates monocyte adhesion. Cardiovasc Res. 2009;81(1):187–96.
27. Huang Y, Yin H, Wang J, Ma X, Zhang Y, Chen K. The significant increase of FcγRIIIA (CD16), a sensitive marker, in patients with coronary heart disease. Gene. 2012;504(2):284–7.
28. Huang Y, Yin H, Wang J, Liu Q, Wu C, Chen K. Aberrant expression of FcγRIIIA (CD16) contributes to the development of atherosclerosis. Gene. 2012;498(1):91–5.
29. Xu Z, Han Y, Liu J, Jiang F, Hu H, Wang Y, et al. MiR-135b-5p and MiR-499a-3p promote cell proliferation and migration in atherosclerosis by directly targeting MEF2C. Sci Rep. 2015;5(1):12276.
30. Sen SK, Boelte KC, Barb JJ, Joehanes R, Zhao X, Cheng Q, et al. Integrative DNA, RNA, and protein evidence connects TREML4 to coronary artery calcification. Am J Hum Genet. 2014;95(1):66–76.
31. Nührenberg TG, Langwieser N, Binder H, Kurz T, Stratz C, Kienzle R-P, et al. Transcriptome analysis in patients with progressive coronary artery disease: identification of differential gene expression in peripheral blood. J of Cardiovasc Trans Res. 2013;6(1):81–93.
32. Volger OL, Fledderus JO, Kisters N, Fontijn RD, Moerland PD, Kuiper J, et al. Distinctive expression of chemokines and transforming growth factor-β signaling in human arterial endothelium during atherosclerosis. Am J Pathol. 2007;171(1):326–37.
33. Kim CW, Song H, Kumar S, Nam D, Kwon HS, Chang KH, et al. Anti-inflammatory and antiatherogenic role of bmp receptor ii in endothelial cells. Arterioscler Thromb Vasc Biol. 2013;33(6):1350–9.
34. Fu X, Guo L, Jiang Z-M, Zhao L-S, Xu A-G. An miR-143 promoter variant associated with essential hypertension. 5.
35. Kitade Y, Akao Y. MicroRNAs and their therapeutic potential for human diseases: MicroRNAs, miR-143 and -145, function as anti-oncomirs and the application of chemically modified mir-143 as an anti-cancer drug. J Pharmacol Sci. 2010;114:276–80.
36. Elia L, Quintavalle M, Zhang J, Contu R, Cossu L, Latronico MVG, et al. The knockout of miR-143 and -145 alters smooth muscle cell maintenance and vascular homeostasis in mice: correlates with human disease. Cell Death Differ. 2009;16(12):1590–8.
37. Huang S, Wang M, Wu W, Wang R, Cui J, Li W, et al. Mir-22-3p inhibits arterial smooth muscle cell proliferation and migration and neointimal hyperplasia by targeting HMGB1 in arteriosclerosis obliterans. Cell Physiol Biochem. 2017;42(6):2492–506.
38. Youn GS, Park JK, Lee CY, Jang JH, Yun SH, Kwon HY, et al. MicroRNA-22 negatively regulates LPS-induced inflammatory responses by targeting HDAC6 in macrophages. BMB Rep. 2020;53(4):223–8.
39. Homma S. Histopathological modifications of early atherosclerotic lesions by risk factors—findings in PDAY subjects. Atherosclerosis. 2001;156(2):389–99.
40. Kolodgie FD, Narula J, Burke AP, Haider N, Farb A, Hui-Liang Y, et al. Localization of apoptotic macrophages at the site of plaque rupture in sudden coronary death. Am J Pathol. 2000;157(4):1259–68.
41. Yan Z, Hansson GK. Innate immunity, macrophage activation, and atherosclerosis. Immunol Rev. 2007;219(1):187–203.
42. Binderup T, Duivenvoorden R, Fay F, van Leent MMT, Malkus J, Baxter S, et al. Imaging-assisted nanoimmunotherapy for atherosclerosis in multiple species. Sci Transl Med. 2019;11(506):eaaw7736.
43. Pirillo A, Bonacina F, Norata GD, Catapano AL. The interplay of lipids, lipoproteins, and immunity in atherosclerosis. Curr Atheroscler Rep. 2018;20(3):12.
44. Tabas I, Lichtman AH. Monocyte-macrophages and T cells in atherosclerosis. Immunity. 2017;47(4):621–34.
45. Galkina E, Ley K. Immune and inflammatory mechanisms of atherosclerosis. Annu Rev Immunol. 2009;27(1):165–97.
46. Singh RB, Mengi SA, Xu Y-J, Arneja AS, Dhalla NS. Pathogenesis of atherosclerosis: A multifactorial process. 2002;7(1):14.
47. Rafieian-Kopaei M, Setorki M, Doudi M, Baradaran A, Nasri H. Atherosclerosis: process, indicators, risk factors and new hopes. Int J Prev Med. 2014;5(8):20.
48. Zhu Y, Wang L, Yin Y, Yang E. Systematic analysis of gene expression patterns associated with postmortem interval in human tissues. Sci Rep. 2017;7(1):5435.
49. Singh RP, Patarca R, Schwartz J, Singh P, Cantor H. Definition of a specific interaction between the early T lymphocyte activation 1 (Eta-1) protein and murine macrophages in vitro and its effect upon macrophages in vivo. J Exp Med. 1990;171(6):1931–42.
50. Giachelli CM, Lombardi D, Johnson RJ, Almeida M. Evidence for a Role of osteopontin in macrophage infiltration in response to pathological stimuli in vivo. 6.
51. Adema GJ, Hartgers F, Verstraten R, de Vries E, Marland G, Menon S, et al. A dendritic-cell-derived C-C chemokine that preferentially attracts naive T cells. Nature. 1997;387(6634):713–7.
52. Thelen M, Uguccioni M. Function of chemokines and their receptors in immunity. In: Encyclopedia of Immunobiology [Internet]. Elsevier; 2016 [cited 2022 Jan 20]. p. 572–8. https://linkinghub.elsevier.com/retrieve/pii/B9780123742797100086
53. Dembic Z. Cytokines of the immune system. In: The cytokines of the immune system [Internet]. Elsevier; 2015 [cited 2022 Jan 20]. p. 241–62. https://linkinghub.elsevier.com/retrieve/pii/B9780124199989000079
54. Stather PW, Sylvius N, Wild JB, Choke E, Sayers RD, Bown MJ. Differential microrna expression profiles in peripheral arterial disease. 8.
55. Fichtlscherer S, De Rosa S, Fox H, Schwietz T, Fischer A, Liebetrau C, et al. Circulating MicroRNAs in patients with coronary artery disease. Circ Res. 2010;107(5):677–84.
56. Ren J, Zhang J, Xu N, Han G, Geng Q, Song J, et al. Signature of Circulating MicroRNAs as Potential Biomarkers in Vulnerable Coronary Artery Disease. Beltrami AP, editor. PLoS ONE. 2013;8(12):e80738.

57. Valmiki S, Ahuja V, Puri N, Paul J. miR-125b and miR-223 contribute to inflammation by targeting the key molecules of NFκB pathway. Front Med. 2020;6.
58. Condrat CE, Thompson DC, Barbu MG, Bugnar OL, Boboc A, Cretoiu D, et al. miRNAs as biomarkers in disease: latest findings regarding their role in diagnosis and prognosis. Cells. 2020;9(2):276.
59. Mori MA, Ludwig RG, Garcia-Martin R, Brandão BB, Kahn CR. Extracellular miRNAs: from biomarkers to mediators of physiology and disease. Cell Metab. 2019;30(4):656–73.
60. Terrinoni A, Calabrese C, Basso D, Aita A, Caporali S, Plebani M, et al. The circulating miRNAs as diagnostic and prognostic markers. Clin Chem Lab Med (CCLM). 2019;57(7):932–53.
61. Moreno JA, Muñoz-García B, Martín-Ventura JL, Madrigal-Matute J, Orbe J, Páramo JA, et al. The CD163-expressing macrophages recognize and internalize TWEAK. Potential Conseq Atherosclerosis Atherosclerosis. 2009;207(1):103–10.

Publisher's Note

International Journal of
Molecular Sciences

MDPI

Article

Transcriptome Analysis of Insulin Signaling-Associated Transcription Factors in *C. elegans* Reveal Their Genome-Wide Target Genes Specificity and Complexity

Neha Kaushik [1], Soumya Rastogi [1], Sonia Verma [2], Deepak Pandey [1], Ashutosh Halder [1], Arnab Mukhopadhyay [3] and Neeraj Kumar [1,*]

[1] Department of Reproductive Biology, All India Institute of Medical Sciences, Ansari Nagar, New Delhi 110029, India; neha1993kaushik@gmail.com (N.K.); soumya.rastogi05@gmail.com (S.R.); deepakpandey@aiims.edu (D.P.); ashutoshhalder@gmail.com (A.H.)
[2] Division of Neuroscience and Ageing Biology, CSIR-Central Drug Research Institute, Lucknow 226031, India; sonia.verma1@cdri.res.in
[3] Molecular Aging Laboratory, National Institute of Immunology, Aruna Asaf Ali Marg, New Delhi 110067, India; arnab@nii.ac.in
* Correspondence: drnknirwal@aiims.edu; Tel.: +91-11-26593945

Abstract: Insulin/IGF-1-like signaling (IIS) plays a crucial, conserved role in development, growth, reproduction, stress tolerance, and longevity. In *Caenorhabditis elegans*, the enhanced longevity under reduced insulin signaling (rIIS) is primarily regulated by the transcription factors (TFs) DAF-16/FOXO, SKN-1/Nrf-1, and HSF1/HSF-1. The specific and coordinated regulation of gene expression by these TFs under rIIS has not been comprehensively elucidated. Here, using RNA-sequencing analysis, we report a systematic study of the complexity of TF-dependent target gene interactions during rIIS under analogous genetic and experimental conditions. We found that DAF-16 regulates only a fraction of the *C. elegans* transcriptome but controls a large set of genes under rIIS; SKN-1 and HSF-1 show the opposite trend. Both of the latter TFs function as activators and repressors to a similar extent, while DAF-16 is predominantly an activator. For expression of the genes commonly regulated by TFs under rIIS conditions, DAF-16 is the principal determining factor, dominating over the other two TFs, irrespective of whether they activate or repress these genes. The functional annotations and regulatory networks presented in this study provide novel insights into the complexity of the gene regulatory networks downstream of the IIS pathway that controls diverse phenotypes, including longevity.

Keywords: FOXO/DAF-16; NRF-2/SKN-1; HSF1/HSF-1; insulin-IGF-1 signaling; *daf-2*; *C. elegans*; transcriptomics; RNAi

Citation: Kaushik, N.; Rastogi, S.; Verma, S.; Pandey, D.; Halder, A.; Mukhopadhyay, A.; Kumar, N. Transcriptome Analysis of Insulin Signaling-Associated Transcription Factors in *C. elegans* Reveal Their Genome-Wide Target Genes Specificity and Complexity. *Int. J. Mol. Sci.* **2021**, *22*, 12462. https://doi.org/10.3390/ijms222212462

Academic Editor: Alexey Moskalev

Received: 12 October 2021
Accepted: 9 November 2021
Published: 18 November 2021

1. Introduction

The evolutionarily conserved insulin/insulin-like growth factor (IGF)-1 signaling (IIS) pathway is among the best-characterized genetic network that regulates aging and a host of other biological functions in various organisms ranging from simple invertebrates to mammals [1]. In *C. elegans*, the reduced IIS condition (rIIS) exhibited by *daf-2* receptor mutants controls these processes at the transcriptional level primarily by its three TFs, namely, DAF-16/FOXO, SKN-1/Nrf (NF-E2-related factor), and HSF-1 (heat shock transcription factor 1) [2–4]. Under optimal conditions, IIS sequesters the two prominent transcription factors (TFs), DAF-16 and SKN-1, within the cytoplasm in their inactive forms through a series of well-organized phosphorylation events. These events do, however, cease in reduced IIS receptor signaling (rIIS), leading to the reversal of cytoplasmic sequestration and translocation of the TFs into the nucleus, where they engage in transcriptional regulation [2,3]. However, HSF-activation appears to be a tightly controlled multistep process that includes oligomerization, posttranslational modifications, nuclear localization, and acquisition of

DNA binding activity [5,6]. In *C. elegans*, many of these HSF-1 activation processes are negatively regulated by insulin signaling by the formation of a DDL-1-containing HSF-1 inhibitory complex (DHIC) that seems to reduce the pool of HSF-1 susceptible to heat stress stimulation. Reduced IIS activity promotes DDL-1 phosphorylation and disrupts DHIC formation, and consequently, increases HSF-1 activity under heat-stressed and unstressed conditions [7].

The leading output of rIIS, DAF-16, belongs to the FoxO family of Forkhead transcription factors, which are known to regulate differentiation, metabolism, proliferation, and survival [8]. In *C. elegans*, DAF-16 is also responsible for a dramatic increase in life span, stress tolerance, higher fat stores, and has a proclivity to arrest at an alternate developmental stage called dauer on rIIS [9–11]. Various DAF-16/FOXO targets in the rIIS condition were identified by multiple approaches such as bioinformatics predictions [12], microarrays [13–16], serial analysis of gene expression (SAGE) [17], protein mass spectrometry [18], DamID [19], RNA-Seq, and ChIP-Seq [20,21], although precise regulation and function of numerous other genes remain to be explored.

SKN-1, best known as a regulator of antioxidant and xenobiotic defense, is an ortholog of the Nrf (NF-E2-related factor)/CNC family of transcription regulators [3,22]. During the earliest embryonic stages, it initiates the development of the feeding and digestive system, but in the post-embryonic period, its role shifts towards controlling normal lifespan and stress resistance [3,23,24]. SKN-1 promotes lifespan by maintaining protein homeostasis through the regulation of the proteasome machinery [25–27]. Constitutive nuclear overexpression of SKN-1 also extends lifespan in a DAF-16/FOXO-independent manner [3]. Under rIIS, it extends longevity parallel to DAF-16 but in a genetically distinct scenario from the dauer pathway [28]. Genome-wide binding sites of SKN-1 were revealed by the modENCODE consortium using ChIP-Seq in *C. elegans* larval stages [29]. SKN-1 expression profiling under the rIIS condition in *C. elegans* has been reported by a single study using microarray, which is based on predefined transcripts/genes [28,30]. Therefore, the full spectrum of genome-wide targets needs to be revealed by using highly specific and sensitive probe-independent alternative technologies.

HSF-1, another important TF, acting downstream of IIS, is implicated in processes, including stress resistance, development, metabolism, and longevity [4,7,31–35]. Shortening and extension of lifespan were reported to be dependent on genetic ablation and overexpression of *hsf-1*, respectively [7,31,36,37]. The knockdown of *hsf-1* also suppressed the enhanced longevity phenotype of the *daf-2(e1370)* strain [4]. Genome-wide binding sites of HSF-1 in *C. elegans* were reported in L2 larval stages by ChIP-Seq [38]. The role of HSF-1 in the regulation of gene expression was reported through RNA-Seq in wild-type adults [39], L2 larvae [38], and overexpressed *hsf-1* young adult *C. elegans* animals [40]; however, HSF-1 genome-wide transcriptional targets under rIIS condition still need to be explored.

Here, we elucidate the genome-wide transcriptional complexity of the principal TFs under rIIS using RNA-Seq in a comparable genetic and experimental setting. Our study provides a comprehensive framework to understand the transcriptional interplay by IIS-associated TFs under analogous conditions.

2. Results

2.1. Characteristics Concurrently Modulated by TFs under rIIS

To select comparable genetic and experimental conditions, *C. elegans'* strain, temperature, and developmental stages were considered, which represent the effects of all TFs on the well-discerned longevity phenotype. We examined two widely used *daf-2* alleles with moderate (e1368, class 1) or strong (e1370, class 2) phenotypes [41]. The studies on double mutant *daf-2(e1370)* and *hsf-1(sy441)* were avoided as *hsf-1* mutant has an egg-laying and temperature-sensitive developmental arrest phenotype [33]. The longevity phenotype of the class II allele, *daf-2(e1370)*, has been reported to be mainly dependent on DAF-16 and HSF-1 [4,15]. On the other hand, the longevity of the class I allele, *daf-2(e1368)*, pri-

marily depends on DAF-16 and SKN-1 [3,41]. We observed that all TFs included in this study regulate the longevity phenotype in e1368 (class1) but not in the e1370 (class 2) allele (Figures 1A and A2A). Therefore, the class I allele *daf-2(e1368)* was used for further revelation of the underlying gene complexity. To knock down the specific TFs efficiently, RNAi hypersensitive double mutant strain *rrf-3(pk1426);daf-2(e1368)* was opted for [42]. TF-specific RNAi clones in each biological replicate were found to be efficient at knocking down their target expression (Figure A1A).

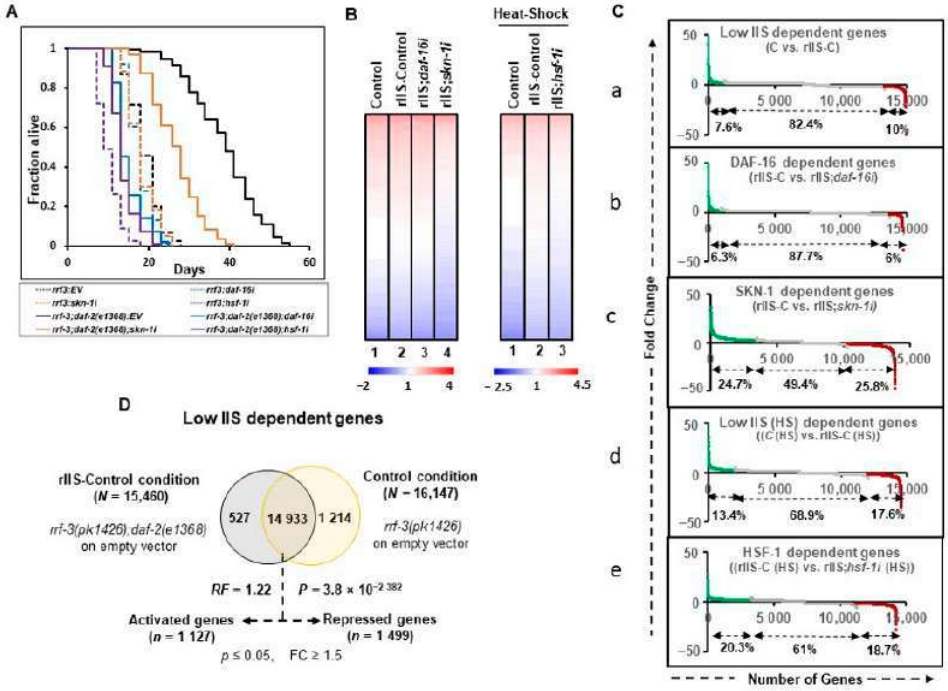

Figure 1. Global transcriptional outputs of transcription factors affecting class 1 rIIS receptor mutant longevity. (**A**) Lifespans of mutants *rrf-3(pk1426)* and *rrf-3(pk1426);daf-2(e1368)* on empty vector (EV), *daf-16, skn-1,* and *hsf-1* RNAi. Strains of *rrf-3(−)* and *rrf-3(−);daf-2(−)* on the empty vector (EV) were marked as "control (C)" and 'rIIS-Control (rIIS-C)", respectively. The knockdown of *daf-16* and *hsf-1* genes reverts the lifespans of rIIS mutant (*rrf-3(−);daf-2(−)*) close to control levels, while it partially depends on *skn-1* RNAi. (**B**) DAF-16, SKN-1 and HSF-1dependent genes were identified by feeding *rrf-3(−);daf-2(−)* animals on *daf-16, skn-1* and *hsf-1* RNAi, respectively. Heat-map representation of the total gene expression by RNA-Seq ($\log_{10}$ RPKM values) contributing to (left panel) control: lane 1, rIIS: lane 2, DAF-16 dependent genes: lane 3, and SKN-1 dependent genes: lane 4, (right panel) control (HS): lane 1, rIIS (HS) dependent genes: lane 2, and HSF-1 (HS) dependent genes: lane 3. Strong knockdown of TFs by the RNAi represented by the lowered expression values in TFs knockdown conditions compared to rIIS. (**C**) Significant fold change, (**a**) rIIS vs. control at 20 °C, (**b**,**c**) rIIS vs. rIIS mutant on *daf-16, skn-1* RNAi, (**d**) rIIS (HS) vs. control (HS) at 33 °C for 2 h, and (**e**) rIIS (HS) vs. rIIS (HS) on *hsf-1* RNAi. At the genome-wide level, differentially expressed genes due to DAF-16 are less than that of SKN-1 and HSF-1. Activated and repressed genes were shown by green and red colors, respectively. (**D**) Venn diagram shows the overlap among genes that are differentially expressed during low IIS conditions. Genes selected with $p \leq 0.05$ and fold change $\geq$1.5. P: Hypergeometric *p*-value, HS: heat-shock, RF: representation factor, FC: fold change.

For transcriptomics analysis, samples were collected at L4/Day-1 adult stage after growing the worms at 20 °C on control or TF RNAi, except for *hsf-1* RNAi *(hsf-1i).* Under normal temperature, HSF-1 exists in a monomeric form that, under heat stress, trimerizes and gets transcriptionally activated [43,44]. *C. elegans* can be temperature-stressed by being grown at 32–40 °C [33,45–47]. To activate HSF-1, we chose to provide acute heat shock at 33 °C for 2 h, and the animals were harvested immediately. This provides enough time for the induction of the heat-responsive genes without affecting the health of the thermotolerant *daf-2* allele used in the study.

2.2. DAF-16 Regulates a Relatively Small Fraction of the Genome-Wide Transcriptional Output

To gain insight into the regulatory functions of the TFs downstream of rIIS, we performed RNA-seq of two independent biological replicates of L4/ young adult (YA) worms after TF-specific RNAi knockdown, starting at the L1 larval stage (Table S1). Principal components analysis (PCA) and unsupervised hierarchical clustering tree analysis that grouped all the biological replicates under the same branch indicate a high degree of reproducibility with similar gene expression between biological replicates (Figure A1B, C). We refer to the *rrf-3(pk1426)* strain on the empty vector (EV) as "Control (C)" and *rrf-3(pk1426);daf-2(e1368)* double mutant on EV as "rIIS-Control (rIIS-C)" conditions. The heat-stressed samples of the same genetic background are referred to as "C (HS)" and "rIIS-C (HS)".

Visualization of the comprehensive transcriptomic data ($\log_{10}$ RPKM values) indicates that only a small fraction of the total genes changes their expression at normal temperatures (20 °C) between control and rIIS conditions, as compared to that of heat-shock conditions (Figure 1B left and right panels: lane-1and lane-2). However, these gene expression patterns appear to revert to the control conditions on *daf-16i* (Figure 1B, left panel: lane 1–3). On *skn-1* and *hsf-1* RNAi, a large proportion of the genes appear to change their expression pattern compared to their respective rIIS conditions (Figure 1B left panel: lane 2 and 4 and right panel: lane 2 and 3). This data indicates that the RNAi of the TFs worked efficiently to bring down the expression levels of most of the genes close to that of the control conditions.

Common genes among different conditions were compared for further analysis and the exclusive genes specific to a single condition were discarded as most of them had low read counts (RPKM < 10). We identified 14,933 (96.6%, RF = 1.22, $P = 3.8 \times 10^{-2382}$) common genes under rIIS condition (rIIS-C vs. C), 14,552 (94.9%, RF = 1.24, $P = 5.0 \times 10^{-2272}$) in rIIS (HS) condition [rIIS-C (HS) vs. C (HS)], 14,698 (94.25%, RF = 1.25, $P = 5.1 \times 10^{-2605}$) in *daf16i* (rIIS-C vs. rIIS;*daf-16i*), 13,881 (96.3%, RF = 1.15, $P = 3.6 \times 10^{-855}$) in *skn-1i* (rIIS-C vs. rIIS;*skn-1i*) and 14,278 (95.7%, RF = 1.28, $P = 9.2 \times 10^{-2701}$) in *hsf-1i* [rIIS (HS) vs. rIIS;*hsf-1i* (HS)] condition (Figure 1C, D and Figure A2B–E). Then, differentially expressed genes ($p \leq 0.05$) with fold change (FC ≥ 1.5) were considered among these common pools of genes (Table S2). In this study, all comparisons were made in such a way that up- and down-regulated genes are termed "activated" and "repressed" genes, respectively. A total of 1127 (7.6%) and 1960 (13.4%) activated, and 1499 (10%) and 2568 (17.6%) repressed, genes were identified specific to rIIS and rIIS (HS) conditions, respectively (Figure 1Ca, D, Cd and Figure A2B). Similarly, DAF-16, SKN-1, and HSF-1 were found to activate 932 (6.3%), 3424 (24.7%), and 2902 (20.3%), and repress 878 (6%), 3586 (25.8%), and 2663 (18.7%) genes, respectively (Figures 1C and A2C–E). This data indicates that DAF-16 regulates a smaller set of the total transcriptional output of the *C. elegans* genome than SKN-1 and HSF-1, hinting towards a more diverse but important role of SKN-1 and HSF-1, compared to DAF-16. These TF-specific genes also showed significant overlap with the previously published literature using stronger class-I allele *daf-2(e1370)* that further strengthens our confidence in our experimental strategy (Figure A3).

2.3. DAF-16 Alone or with SKN-1 Regulates the Majority of Genes under rIIS

To validate our data, we specifically compared the expression levels of well-known targets (identified in the stronger allele of *daf-2*) in our data sets (Figure 2A). Activation of *sod-3* and repression of *dod-24* genes under rIIS condition was found to be entirely dependent on DAF-16 (Figure 2A, upper panel) as reported earlier [15,48]. Similarly, the targets of SKN-1 (*gst-4* and *lys-4*) [3,28]) and HSF-1 (*pgp-9* and *daf-7*) [39,49] were found to be mainly dependent on their respective TFs (Figure 2A, middle and lower panels). Quantitative analysis of these genes further confirmed their dependence on their respective TFs under the rIIS condition (Figure A4A). The above observation suggests that in the moderate *daf-2* allele, TFs regulate transcriptional output, which can be reliably extrapolated to the other rIIS strains.

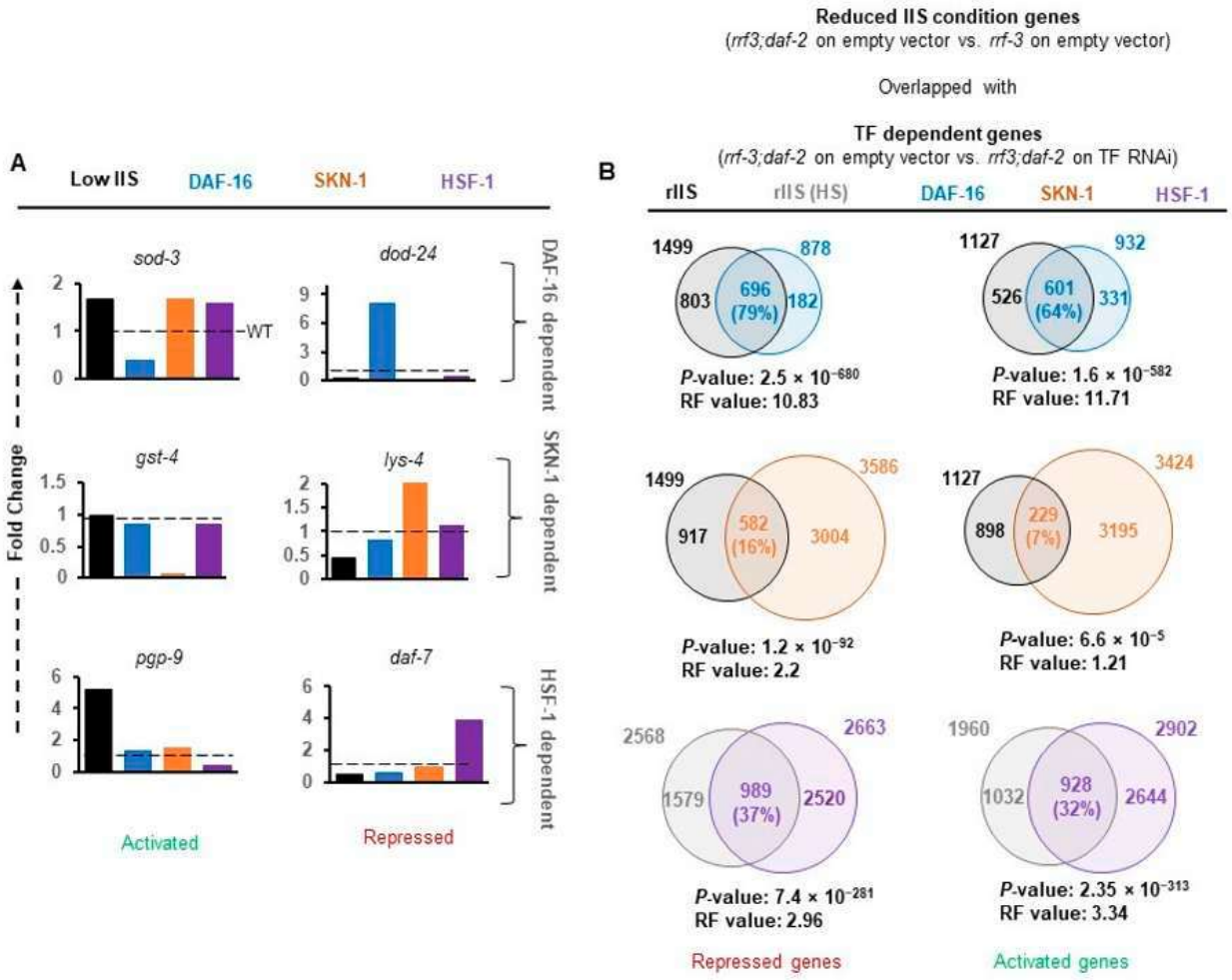

Figure 2. The major proportion of genes under reduced insulin signaling is controlled by DAF-16. (**A**) RNA expression of TFs' well-established targets. Expression of the genes *sod-3*, *gst-4*, and *pgp-9* activated by DAF-16, SKN-1, and HSF-1. *lys-4*, and *daf-7* repressed by DAF-16, SKN-1, and HSF-1, respectively, increased without their regulators. (**B**) Venn diagrams represent the number of genes regulated by TFs, specifically under reduced insulin signaling. Major fractions of rIIS-dependent activated (N = 601, 64%,) or repressed (N = 696, 79%) genes are controlled by DAF-16, followed by HSF-1 (928, 32%) and (989, 37%). Contrarily, a small fraction of SKN-1-regulated genes were either activated (N = 229, 7%) or repressed (N = 582, 16%). Genes selected with $p \leq 0.05$ and fold change $\geq$1.5. P: Hypergeometric p-value, HS: heat-shock, RF: representation factor, FC: fold change.

TF-dependent differential gene expression (rIIS-C vs. rIIS;TF RNAi-referred as TF-regulated genes) reflects the cumulative gene response. To delineate the rIIS-specific contribution, genes changing expression on rIIS condition were compared with TF-regulated genes (Figure 2B). We observed that most DAF-16-regulated genes were either activated (N = 601, 64%, RF = 11.71, $P = 1.6 \times 10^{-582}$) or repressed (N = 696, 79%, RF = 10.83, $P = 2.5 \times 10^{-680}$) under rIIS conditions (Figures 2B and A4B top panels). Contrarily, a small fraction of SKN-1 regulated genes were either activated (N = 229, 7%, RF = 1.21, $P = 6.6 \times 10^{-5}$) or repressed (N = 582, 16%, RF = 2.2, $P = 1.2 \times 10^{-32}$; Figures 2B and A4B middle panels). In the case of HSF-1, nearly 1/3 of the genes were found to be activated (928, 32%, RF = 1.01, P = 0.42) and repressed (989, 37%, RF = 1.66, $P = 2.0 \times 10^{-13}$) under rIIS condition (Figures 2B and A4B lowest panels). Even from the rIIS point of view, 49.4% ((696 + 601)/(1499 + 1127))of rIIS-dependent genes were found to be regulated by DAF-16, 42.3% ((989 + 928)/(2568 + 1960)) by HSF-1, and 31.2% ((582 + 229)/(1499 + 1127)) by SKN-1 (Figure 2B).

To further gain insight into the TF interactions for the regulation of their targets, each cluster of the TF-dependent differentially expressed genes were considered together. We identified activated and repressed genes for each transcription factor knockdown compared to their controls, resulting in a total of 14,385 differentially expressed genes for all transcription factors that correspond to 9034 non-redundant genes (Figure A5A,C). It shows that 4344 (48%) differentially expressed genes were specific to a single TF, 4031 (44.6%) were shared by at least two TFs, and 659 (7.3%) were identified in all TF knockdown conditions (Figure A5C). Under rIIS conditions, these genes fall into 1589 activated and 1816 repressed from the total of 4025 genes (Figure A5B,D), which corresponds to 3297 non-redundant genes (Figure A6D). Further, 2646 (80%) genes were found to be specific for a single TF, 547 (17.4%) by any two TFs, and a very small fraction (77 genes, 2.3%) by all TFs (Figure A6D). This implies that only a small number of genes are regulated jointly by all three TFs, and most of them are regulated independently by a single TF under rIIS condition (Figure A5C,D). Despite a smaller set of genes regulated by SKN-1 under the rIIS condition, it regulates the major set (N-355) of common genes with DAF-16 (Figure A5D), but at the genome-wide level, SKN-1 and HSF-1 were found to regulate the largest set (N-3423) of non-redundant genes (Figure A5C). Together, our data suggest that DAF-16 independently or jointly with SKN-1 regulates the largest fraction of rIIS-dependent genes.

2.4. Distinct Activator and Repressor Activities of TFs under rIIS

To comprehend the accurate nature of these transcription factors, we further investigated how effectively TF knockdown can bring the rIIS-dependent differential gene expression close to the control condition. This approach appears to be a more suitable and reliable predictor to understand the exact function of these transcription factors, as it is based on a larger inclusion of datasets that we might have overlooked in our overlap analysis (Figure 2B) owing to stringent and independent comparisons based on fold change. With this approach, we found that RNAi knockdown of DAF-16 extensively reversed the gene expression of rIIS to control levels (78% of activated and 50% of rIIS repressed genes) as reported earlier in the class-2 mutant strain [20] (Figure 3, left panels).

Similarly, SKN-1 and HSF-1 TF data analysis with similar parameters revealed that they significantly reversed almost equal fractions, i.e., 1/3 (36% of activated and 32% of rIIS repressed genes) and 1/2 (53% of activated and 48% of rIIS repressed genes) of differential gene expressions of rIIS, respectively (Figure 3, middle and right panels) indicating that both of them acts as a transcriptional activator and repressor to the same extent, which is in contrast to the above observation. This suggests that DAF-16 controls the majority of the rIIS genes predominantly by acting as a transcriptional activator, as reported earlier [20]. While SKN-1 and HSF-1 both act as transcriptional activators as well as repressors almost to the same extent.

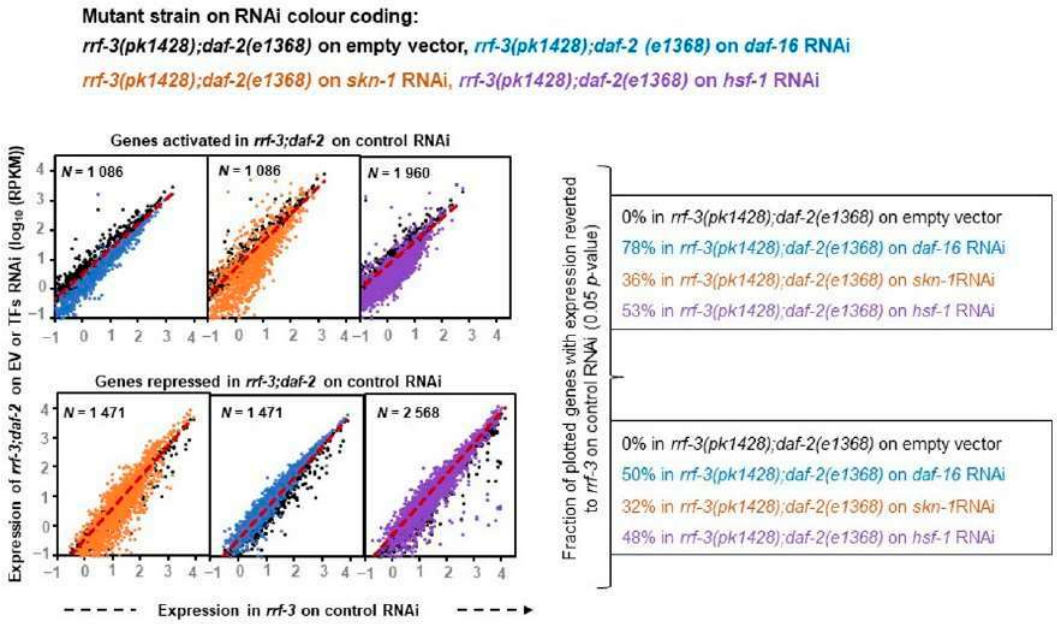

Figure 3. Distinct activator and repressor activities of TFs downstream of insulin signaling. Scatter-plots comparing gene expression ($\log_{10}$ RPKM) in control (*rrf-3* mutant on empty vector) with rIIS condition (*rrf-3;daf-2*) double mutant on empty vector) and TF knock-down conditions (*rrf-3;daf-2*) double mutant on *daf-16/skn-1/hsf-1* RNAi). Genes expressed with RPKM $\geq$ 10 in all comparing conditions either significantly activated (top panel) or repressed (down panel) by *rrf-3(pk1426);daf-2(e1368)* were considered. Colors indicate the strains on RNAi in which the gene expression was analyzed. Gene expression away from the plots' diagonals represents significantly activated or repressed genes in the rIIS condition compared to control (black dots). The shift of genes near to the plots' diagonals due to *rrf-3;daf-2* on TFs RNAi represents the fraction of genes with expression reverted to the "control" condition. Mutant *rrf-3;daf-2* on *daf-16* RNAi extensively, *rrf-3;daf-2* on *skn-1* RNAi partially and *rrf-3;daf-2* on *hsf-1* RNAi marginally reverted the rIIS expression near to control levels. As indicated by the large fraction of DAF-16-dependent activation of genes suggests its predominant role as an activator, while SKN-1/HSF-1 shows a similar extent of activation and repression activities.

2.5. Shared Genes under rIIS Condition Are Predominantly Governed by DAF-16

To understand the exact mode of individual TF regulation, all commonly differentiated genes between "rIIS-C" (when all TFs get localized within the nucleus) and knockdown of each TF under rIIS conditions were considered, which in turn, provided four sets of overlapping genes (Figure A6A–C). Quadrant plot of these genes (1311 of DAF-16, 1390 of SKN-1, and 2264 of HSF-1 dependent) revealed that 99% of DAF-16 and 85% of HSF-1-dependent genes are regulated in the same manner as that of the "rIIS-C" condition (Figure 4A,C, quadrant 1 and 3). Surprisingly, genes regulated by these TFs show similar expression patterns under the rIIS condition, despite their slight target overlap (Figure A5D). While in the case of SKN-1, 40% of its genes exhibit a reverse pattern under "rIIS-C" (Figure 4B, quadrant 2 and 4). Such gene expression regulation seems to be dominated by other factors under the rIIS condition.

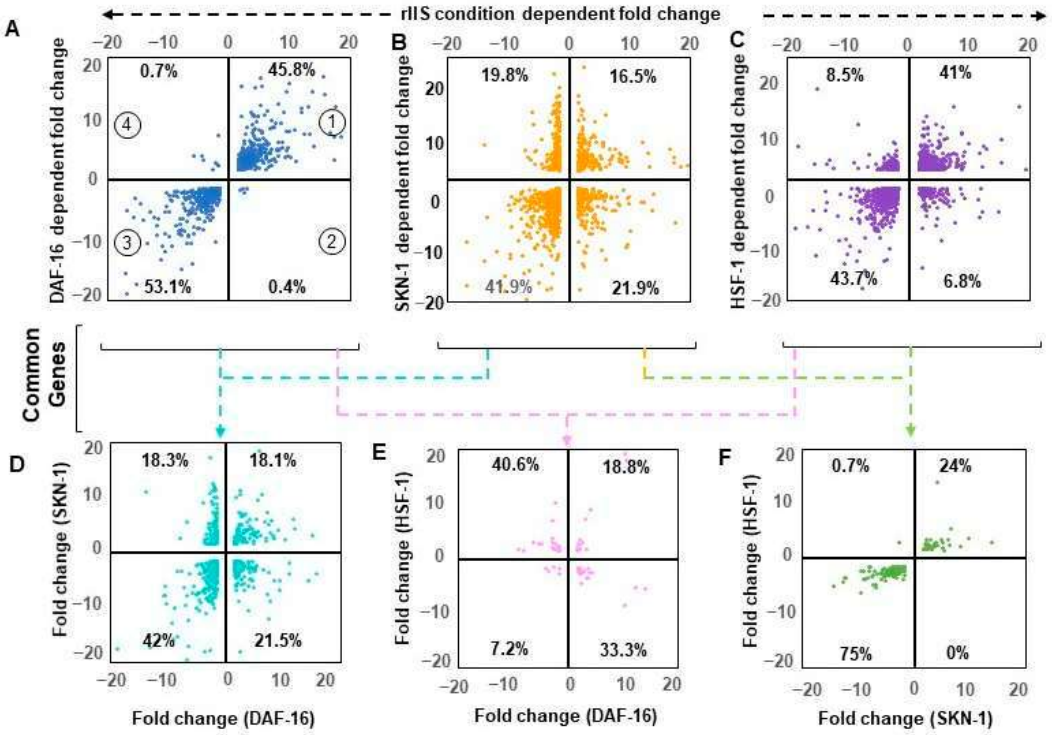

Figure 4. A combinatorial pattern of gene regulation. Quadrant scatter plot depicts all four possible combinations between fold change of activated and repressed genes in two different conditions. Only common genes were considered for analysis. Percentage in each quarter represents the fraction of the total common genes between compared conditions. The upper panel represents a pattern of transcription factor-regulated genes with reduced insulin signaling. Almost all DAF-16 regulated genes partner together with rIIS-dependent genes (**A**). Similarly, most of the HSF-1-regulated genes also aligned with the rIIS condition (**C**), but the SKN-1-regulated genes indicated a mixed pattern (**B**). In the lower panel, common genes between transcription factors under rIIS were considered for analysis (please refer to Figure A6 for detailed analysis). The majority (60%, quarter 1 and 3) of the SKN-1-dependent genes partner together with DAF-16 (**D**), while most of the HSF-1-regulated genes (74%, quarter 2 and 4) behave oppositely to DAF-16 (**E**). SKN-1 and HSF-1 regulate most of their common genes (99%) in the same manner (**F**).

To penetratingly examine if another TF under this study is dominating in the regulation of genes that behave against the nature of their respective TF under rIIS condition, common targets between any two and all three TFs were further compared (Figure A6D). First, we considered the genes shared by any two TFs under the "rIIS condition" (Figure 4D–F and Figure A6E–G). The distribution of genes regulated by DAF-16 and SKN-1 shows that both these TFs regulate around 60% of their shared genes similarly (Figure 4C, quarter 1 and 3), and the remaining behaves differently (Figure 4C, quarter 2 and 4) while DAF-16 and HSF-1 regulate most of their common targets (74%) inversely (Figure 4E, quarter 2 and 4). However, almost all (99%) of the common genes between SKN-1 and HSF-1 are regulated in a similar manner (Figure 4F, quarter 1 and 3). Nevertheless, this comparative gene expression pattern does not reveal how they behave when all TFs sequester in the nucleus, i.e., under the rIIS condition. Therefore, further expression was considered in the rIIS condition (Figure 5A). Genes commonly regulated by DAF-16 with SKN-1 or HSF-1 under the rIIS condition (Figure 5A, serial no. 1–8) revealed that other TF regulatory capacity is undermined in the presence of DAF-16. DAF-16-independent genes regulated by SKN-1 and HSF-1 (Figure 4F) were expected to behave in a similar manner under the rIIS condition. Surprisingly, 57% and 20% of their shared target genes get repressed and activated differently under the rIIS condition (Figure 5A, serial no. 9–12). As the expression of these genes was not DAF-16-dependent, it hints at the involvement of some other factor

under the rIIS condition whose actions may be strong enough to determine the direction of these genes' expressions.

A

S. No	Combinations		Total Genes (N)	Low IIS (Activated (%)	Low IIS (Repressed (%)
1	D	S	102	99	1
2	D	S	121	98	2
3	D	S	103	1	99
4	D	S	236	0	100
5	D	H	13	100	0
6	D	H	23	100	0
7	D	H	28	3	97
8	D	H	5	0	100
9	S	H	35	43	57
10	S	H	0	NA	NA
11	S	H	1	0	100
12	S	H	110	20	80

B

S. No	Combinations			Total Genes (N)	Low IIS (Activated (%)	Low IIS (Repressed (%)
1	D	S	H	24	100	0
2	D	S	H	2	100	0
3	D	S	H	6	100	0
4	D	S	H	69	97	3
5	D	S	H	63	1	99
6	D	S	H	4	25	75
7	D	S	H	1	0	100
8	D	S	H	57	0	100

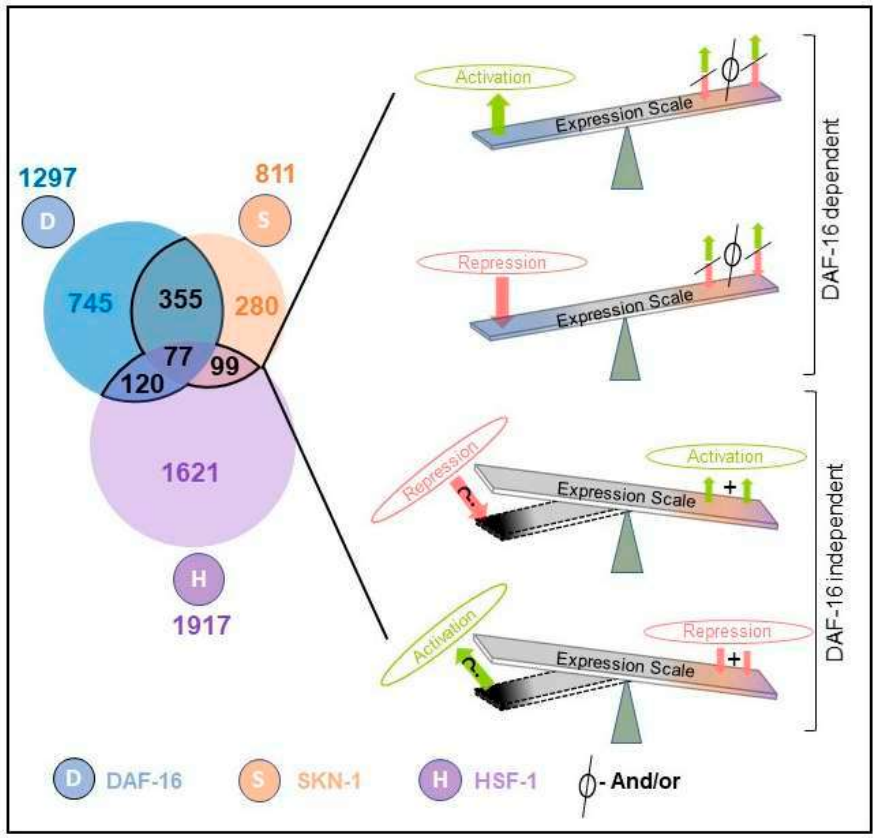

Figure 5. DAF-16 is a key determining factor for the combinatorial regulation of genes. (**A**) Genes are shared by any two TFs. Serial No. 1–8: Differential expression of most genes under rIIS condition (last two columns) are the same as controlled by DAF-16 (first column). Serial No. 9–12: DAF-16-independent genes jointly regulated by SKN-1 and HSF-1. Several genes (57% and 20 %) expressed under the rIIS condition were found to be opposite to the SKN-1 and HSF-1 nature of regulation. (**B**) Genes shared by all three TFs. It shows the dominant nature of DAF-16 under the rIIS condition to determine the direction of expression of the commonly regulated gene by all three TFs. Green and red color boxes indicate activated and repressed genes, respectively. Dotted oval shaped circles represent most of the genes either activated or repressed jointly by any two (**A**) or all three TFs (**B**) under rIIS condition. (**C**) Model for common genes targeted by any two or all three TFs. The relative contribution of TFs is incorporated to provide a nuanced portrayal of the multiple possibilities that cause the expression of gene targets under the rIIS condition. In this view, the effect of TFs on the right side is shown with a seesaw. In the above two panels, overweighted seesaw side indicates DAF-16 dominance irrespective of the contribution made by the other two TFs under the rIIS condition. However, the majority of DAF-16-independent genes are either activated or repressed by SKN-1 or HSF-1 synergistically, but few others behave differently, as indicated by the overweighted dark color side. The result is that wherever DAF-16 is involved, it masks the effect of other TFs.

Next, we considered the commonly regulated genes by all three TFs under the rIIS condition (Figure A6D). Further, the grouping and association of these genes (N-226) with all possible combinations of TFs indicate that the direction of expression of these genes under the rIIS condition is determined by DAF-16, irrespective of the contribution made by SKN-1 and HSF-1 TFs (Figure 5B). This means that even the combined strength of SKN-1 and HSF-1 is not sufficient to change the direction of expression of these genes if DAF-16 sets to command them (Figure 5B, serial no. 4 and 5). This hints at the fact that it is the DAF-16 that controls the expression of common genes, and no other TF plays a significant role if the direction of expression is determined by DAF-16. Alternatively, it also implies

that under the rIIS condition, if genes are majorly governed by SKN-1 or HSF-1, then DAF-16 may cooperate with them analogously; but for the genes that behave opposite to the nature of these TFs, DAF-16 leads and determines the direction of most of these genes. Together, our data suggest a sophisticated mechanism for balancing the expression of rIIS-dependent genes through these TFs (Figure 5C).

2.6. Molecular and Gene Regulatory Signatures of the TFs Targets Downstream of rIIS

It is well established that longevity and its associated characteristics are multifactorial and involve complex interactions of different signaling mechanisms. To explore how the various molecular signatures involved are guided by these TFs, we built regulatory networks of genes regulated by rIIS downstream TFs (Figure 2B). To visualize the molecular interplay of each TF on different biological processes, individual TF-specific networks based on their target genes differential expression were created. We selected only significantly enriched clusters regulated by individual TFs (Figures 6 and 7).

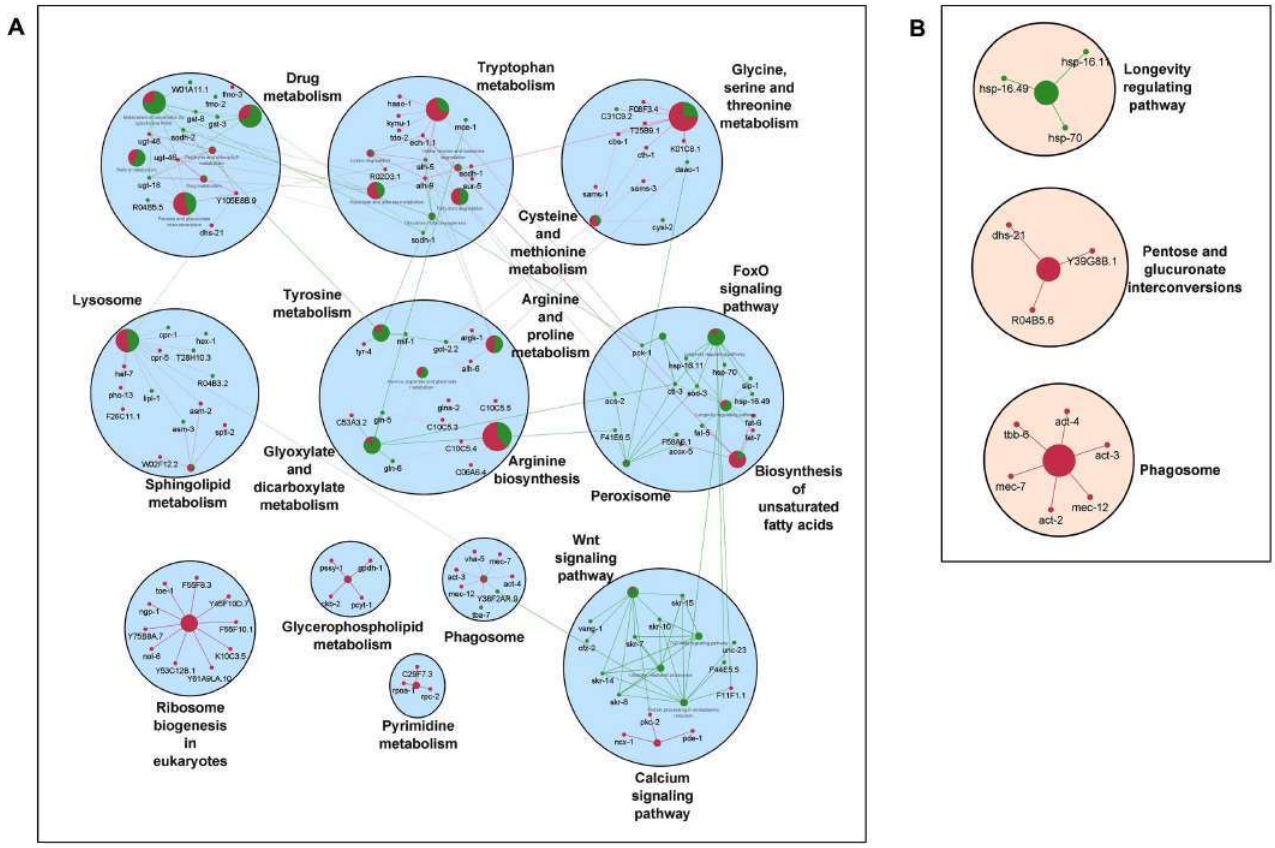

Figure 6. Gene networks of DAF-16 and SKN-1-regulated genes under rIIS conditions. (**A**) DAF-16-dependent pathway network. Most of the genes are activated in FoxO and calcium signaling, while ribosome biogenesis, pyrimidine metabolism, phagosome, and glycerophospholipids-related genes were found to be in a repressed condition. (**B**) SKN-1-dependent pathway network. Longevity regulating genes are activated while phagosome, pentose, and glucuronate interconversion genes remain repressed. Activated and repressed genes are shown by green and red colors, respectively.

For ease of understanding, these clusters were again re-grouped under more general terms, such as carbohydrate metabolism, lipid metabolism, amino-acid metabolism, RNA processing, etc. (Figure A7). We observed the maximum pathways/gene clusters to be regulated by HSF-1, followed by DAF-16, and a few by SKN-1 (Figures 6 and 7). As expected, the genes involved in longevity were found to be regulated by all three TFs with maximum contribution by DAF-16 followed by SKN-1 and HSF-1 (Figure A7), as reported earlier [3,4,15].

Similarly, the role of these TFs in lifespan remodeling through autophagy and carbohydrate metabolism is well evident, also reflected in our study (Figures 6 and 7). Genes controlling carbohydrate and lipid metabolic pathways were found to be dependent on DAF-16 and HSF-1. However, most of the amino-acid metabolism-regulating genes were DAF-16 dependent, except the branched-chain amino acid (valine, leucine, and isoleucine), and the conserved regulator of physiological aging was found to be primarily activated by both DAF-16 and HSF-1, as reported earlier [50]. DAF-16 activation is known to slow down the turnover of most proteins, which points towards the decreased abundance of the translational machinery [51]. Our data suggest that the genes required for translational machinery are also repressed at the transcription level by DAF-16 (Figure 6A). Moreover, many of these ribosomal genes were also found to be repressed by HSF-1 under rIIS (Figure 7).

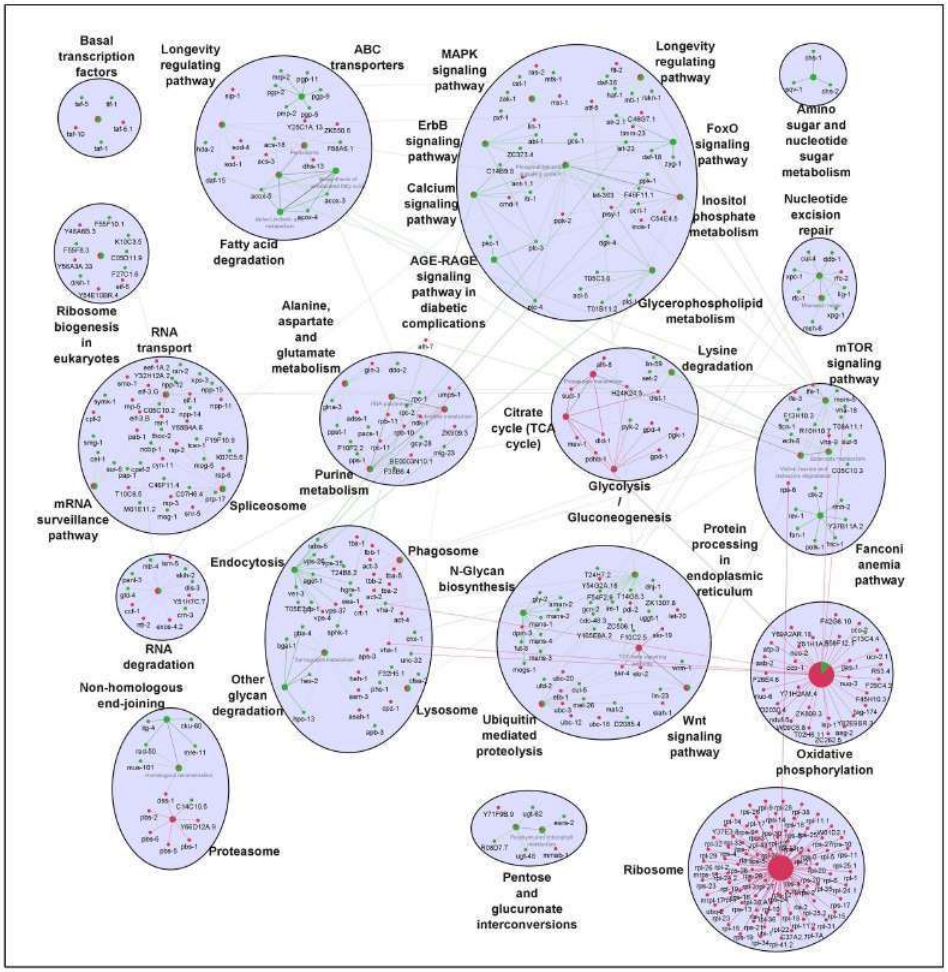

Figure 7. Gene network of HSF-1-regulated genes downstream of the rIIS condition. HSF-1 regulates multiple diverse pathways. Several pathways, including longevity, amino sugar, nucleotide sugar, ABC transporters, non-homologous end-joining, and mTOR signaling, mainly involve gene activation. Meanwhile, ribosome, proteosome, glycolysis, TCA cycle, and oxidative phosphorylation-related genes were found to be repressed by HSF-1. Activated and repressed genes are shown by green and red colors, respectively.

To further evaluate these networks, a comparison among the proportion of gene associations per cluster was made where both contrasting and similar patterns of gene expression were observed for the regulation of different biological processes. We found that these TFs regulate many similar, as well as distinct, pathways. For instance, pentose and glucuronate interconversion and phagosomes are regulated by all TFs. Carbohydrate, lipid, and amino-

acid metabolism, etc., are regulated both by DAF-16 and HSF-1. Specifically, glyoxylate and dicarboxylate metabolism, arginine, proline, glycine, serine, threonine, vitamins, and xenobiotic/drug metabolism are regulated primarily by DAF-16, while N-glycan, inositol phosphate, alpha-linolic acid, an amino sugar, purine, propanoate, RNA/DNA processing, etc., are primarily regulated by HSF-1. Moreover, similar pathways are also found to be regulated by opposingly different TFs. For example, glycolysis, glycerophospholipid, sphingolipid, biosynthesis of unsaturated fatty acids, lysine degradation, Wnt, and TGF-beta signaling pathways are regulated both by DAF-16 and HSF-1, but inversely. It could be due to their nonoverlapping set of genes involved in similar processes but regulated differently by distinct TFs. Thus, it shows the existence of a significant degree of overlap among regulatory functions despite their independent nature of gene regulation. Further, close observations in the networks indicate that the same genes differently controlled by these TFs are involved in regulating a particular biological process. For example, common genes *asm-3* and *sip-1* were found to be activated by DAF-16 and repressed by HSF-1 to regulate sphingolipid and longevity pathways, respectively. Conversely, some genes such as *rpc-2* and *sur-5* found to be repressed by DAF-16 and activated by HSF-1 were involved in the regulation of nucleotide and amino-acid (valine, leucine, and isoleucine) metabolism, respectively. In a nutshell, our study reveals several unidentified, as well as earlier reported, biological processes governed by the mechanisms regulating the complex biology of aging.

3. Discussion

There are several phenotypes associated with long-lived mutants, in addition to longevity, such as larval arrest, oxidative and heat stress resistance, pathogen resistance, reproduction, adult behavior, and metabolism [52,53]. In fact, the genes linked with these associated phenotypes were characterized first and subsequently found to be contributing to longevity modulation. The IIS pathway contains many evolutionarily conserved components, including downstream transcription factors that regulate most of these associated phenotypes in addition to prolonged longevity, but in a condition-specific manner [3,4,7]. Despite our extensive knowledge of the IIS pathway that leads to the activation of DAF-16, SKN-1, and HSF-1, the way TFs relay their transcriptional output in a comparable genetic condition to benefit the organism has long remained elusive. This study provides the first systematic rIIS-dependent TF target identification and regulation in a comparable experimental condition with the same genetic background.

Our data indicate that DAF-16 regulates a relatively small fraction of *C. elegans* genes, but under the rIIS condition, it regulates the majority. On the contrary, SKN-1 controls a large proportion of genes under normal conditions but a relatively smaller proportion under the rIIS condition. From the perspective of the total transcriptional response perspective, HSF-1 regulated genes were comparable to those of SKN-1, but under the rIIS condition, it regulates more than double the genes regulated by SKN-1. This implies that SKN-1 may have more important roles under normal conditions than in the rIIS condition, while the opposite is true for DAF-16. HSF-1, on the other hand, seems to play an important role both under normal and rIIS conditions. This seems plausible, as removing DAF-16 slightly affects many phenotypes, including lifespan in wild-type worms [54]. However, SKN-1 and HSF-1 removal affect many phenotypes, including development, normal lifespan, oxidative stress, pathogen resistance, and heat stress to a greater extent [55–57]. We presume this could be due to the different levels of TF molecules present in the nucleus under varied conditions. However, under basal conditions, the nucleus to cytoplasmic ratios of all three transcription factors was reported to be significantly lower as compared to the rIIS condition, where it increases mani-fold in the nucleus [2,3,7,58]. This hints that it is not only the dosage of the TFs translocated into the nucleus but may possibly be the active TF molecules that regulate the target gene expression in a context-specific manner. Therefore, it is possible that under the rIIS condition, a relatively smaller number of SKN-1 molecules translocated and/or are activated into the nucleus compared to DAF-16 and/or HSF-1, which corresponds to the lower number of genes regulated by them, as observed in this study. Moreover, the fraction of rIIS genes

controlled by these TFs are suggestive of the dominant DAF-16 activity due to its specificity to the rIIS condition, but the primary role of SKN-1 seems to be the basal condition, while HSF-1 seems to be necessary for both scenarios.

Analysis of all possible dimensions of the DAF-16 regulated rIIS-dependent common genes suggests that the direction of such genes is entirely coupled with DAF-16. It reflected the invincible and dominant role of DAF-16 over other TFs under rIIS. Surprisingly, the DAF-16 was independent, but SKN-1- and HSF-1-regulated common genes, where both TFs individually regulate them in a similar manner (Figure 4F), were found to behave differently under rIIS conditions. It hints at the involvement of some unidentified factor other than DAF-16, which acts antagonistically to the SKN-1 and HSF-1 under the rIIS condition.

The understanding of the specificity and complexity of the target genes provides insight into how they act and are targeted by the transcription factors during lowered insulin signaling. This systematic resolution of the TF-dependent transcriptional network identifies common and specific molecular signatures, which may contribute to different phenotypes of the rIIS condition. Our study identified overlapping but distinct molecular niches by comprehensive and well-interconnected TF-associated regulatory networks. We were able to resolve the rIIS-dependent TFs transcriptional complexity, which itself provides a significant resource for future studies. Finally, we would like to note that all these TFs are evolutionarily well conserved. Hence, their regulatory roles, including their complexity, specificity, overlapping, as well as distinct molecular niche described here, may be conserved in other organisms, and their further exploration may eventually benefit our understanding of human aging and age-linked diseases.

4. Materials and Methods

4.1. Strain Maintenance

Strains of *rrf-3(pk1426)*/[RRID:WB-STRAIN:WBStrain00028995], *rrf-3(pk1426);daf-2 (e1370)*/RRID:WB-STRAIN:WBStrain00004874, and *daf-2(e1368)*/RRID:WB-STRAIN:WBS train00006381 mutant worms were obtained from the Caenorhabditis Genetics Centre (Minneapolis, MN, USA). Double mutants *rrf-3(pk1426);daf-2(e1368)* were made by crossing *rrf-3(pk1426)* males and *daf-2(e1368)* hermaphrodites using standard genetic techniques. Throughout the manuscript, *rrf-3(pk1426)* and *rrf-3(pk1426);daf-2(e1368)* on empty vector [*E. Coli* HT115 (DE3) carrying L4440 vector]/RRID:WB-STRAIN:WBStrain00041074 are referred to as "control" and "reduced insulin signaling (rIIS) condition", respectively. Worms were grown at 20 °C unless otherwise mentioned. Animals were passaged frequently to avoid starvation and overcrowding during routine maintenance.

4.2. RNAi Plates Preparation

First, nematode growth medium (NGM) was prepared by mixing 3 g of NaCl (Merck Life Sciences Pvt. Ltd., Mumbai, India, Catalog #1.93606.0521), 2.5 g peptone (Himedia Laboratories, Mumbai, India, Catalog #RM001), and 17 g agar (Sisco Research Laboratories Pvt. Ltd., Mumbai, India, Catalog #24970) in 1 L double distilled water. After autoclaving and cooling down at 55–60 °C, 0.5 mL of cholesterol (Himedia Laboratories, Mumbai, India, Catalog #TC1101) [10 mg/mL in ethanol (Merck Life Sciences Pvt. Ltd., Mumbai, India, Catalog #1.00983.0511)], 1 mL of 1M $CaCl_2$ (Thermo Fisher Scientific, Waltham, Massachusetts, United States, Catalog #C614-500), 1 mL of 1M $MgSO_4$ (Himedia Laboratories, Mumbai, India, Catalog #GRM684), and 25 mL of 1M (pH 6.0) KPO_4. KPO4 (1 M) was made by mixing 10.83 g of KH_2PO_4 (Sisco Research Laboratories Pvt. Ltd., Mumbai, India, Catalog #54358) and 3.56 g of K_2HPO_4 (Himedia Laboratories, Mumbai, India, Catalog #GRM1045) in 100 mL of double-distilled water. Then, NGM was supplemented with 100 μg/mL ampicillin (Bio Basic Inc., Markham, Ontario, Canada, Catalog #AB0028) and 2 mM IPTG (BR Biochem Life sciences Pvt. Ltd., New Delhi, India, Catalog #BC0168). After pouring, plates were dried at room temperature for 2–3 days. *E. coli* bacterial strain HT115 containing the gene of interest for RNAi in the L4440 vector construct was cultured in

Luria Bertani (LB) media (Himedia Laboratories, Mumbai, India, Catalog #M1245) at 37 °C overnight in a shaker incubator. It was supplemented with 12.5 μg/mL tetracycline (Bio Basic Inc., Markham, Ontario, Canada, Catalog #TB0504) and 100 μg/mL ampicillin. The next day, overnight grown primary culture was inoculated in fresh LB media containing 100 μg/mL ampicillin in the ratio of 1:100 for secondary culture at 37 °C shaken until OD_{600} in the spectrophotometer (Shimadzu Corporation, Kyoto, Japan, Model #UV-1900) reached between 0.6–0.8. The secondary cultured bacterial cells were pelleted down by centrifuging at 5000× *g* for 10 min at 4 °C and resuspended in 1/10th volume of M9 buffer containing 1mM IPTG and100 μg/mL ampicillin. IPTG in the plates and M9 suspended culture was used to induce the T7 polymerase expression in the HT115 bacteria that transcribes the dsRNA in the plasmid. M9 culture suspension of 120 μL was seeded onto 60 mm RNAi plates and dried to develop a bacterial lawn at room temperature for nearly 2 days.

4.3. Synchronization of Worms by Hypochlorite Treatment

C. elegans worms were grown on *E. coli* OP50 bacteria (Caenorhabditis Genetics Centre, Minneapolis, MN, USA) until the egg-containing gravid adult stage. Worms from the plates were collected using M9 buffer in a 15 mL centrifuge tube. M9 buffer was made by mixing 6 g of Na_2HPO_4 (Himedia Laboratories, Mumbai, India, Catalog # TC051), 3 g of KH_2PO_4, 5 g of NaCl, and 0.25 g of $MgSO_4$ in 1 L double distilled water. Worms were centrifuged in a swing bucket rotor (Eppendorf India Pvt. Ltd., Chennai, India, Model #5810R) at 1200× *g* for 60 s followed by resuspension of the worm pellet in M9 buffer. This washing procedure was repeated three times. Then, worm pellet was dissolved in a bleach solution [double distilled H_2O, sodium hypochlorite (Merck Life Sciences Pvt. Ltd., Mumbai, India, Catalog #1.00983.0511), 5 N NaOH (Merck Life Sciences Pvt. Ltd., Mumbai, India, Catalog #1.06462.1000) in the ratio of 7:2:1]. To obtain hypochlorite-resistant eggs by dissolving gravid worm bodies, the above suspension was vortexed for 6–8 min in a vortex shaker (Tarsons, Kolkata, India, Model #Spinix). The eggs were washed 5–6 times by centrifuging at 2000 × g, then decanting the 1 × M9 with a suction pump (Rocker Scientific Co., Kaohsiung, Taiwan, Model #Rocker410) followed by resuspension in 1 × M9 buffer to remove traces of bleach and alkali. After the final wash, eggs were resuspended in 10 mL of M9 buffer and kept on a rocking shaker (Tarsons, Kolkata, India, Model #Rockymax) for 18–20 h at 21–22 °C for L1 offspring hatching and arrest. Hatching percentage was scored to confirm L1 synchronized animals' viability. L1 arrested worms were seeded on RNAi plates to grow until the L4 stage. Unhealthy and un-synchronized animals, if any were discarded at L4 stage. Remaining healthy and synchronized animals were grown further until young adult/early gravid stage for RNA isolation.

4.4. Lifespan Assays of TFs Gene Inactivation by RNAi

Gravid adult worms grown on *E. coli* OP50 were bleached as described above. The eggs were kept on different RNAi plates to hatch. On reaching adulthood, 80–90 young adult worms were transferred in triplicates to the corresponding RNAi plates containing Fluorodeoxyuridine (FudR) (Sisco Research Laboratories Pvt. Ltd., Mumbai, India, Catalog #81015) to a final concentration of 0.1 mg/mL of agar. On the 7th day of adulthood, sick, undeveloped, sluggish, and slow-dwelling worms were removed from the life span population, and the remaining were considered for scoring. The age-synchronized population of worms was scored every alternate day until they died. They were considered dead when they failed to respond to external stimuli. Percentage survival was plotted against the number of days.

4.5. Worm Sample Prep for RNA Seq

L1 synchronized worms were grown in three biological replicates on empty vector and test RNAi plates. Worms were collected at YA/gravid stage for RNA isolation in a 15 mL centrifuge tube using 1 × M9 buffer and washed at least four times to remove bacterial contamination. Before final wash, the suspension was transferred to the 2 mL cen-

trifuge tube, and 300 µL of Trizol (Invitrogen) reagent (ThermoFisher Scientific, Waltham, Massachusetts, United States, Catalog #15596026) was added to nearly 50–60 µL of the worm pellet. Samples were stored at −80 °C (Eppendorf North America, Connecticut, United States, Model #CryoCubeF740) until further processing. A few unhealthy, immotile animals in *rrf-3* strain were observed following heat shock, but we quickly removed most of them manually. After the RNA quality check, two biological replicates with the highest RIN value using automated electrophoresis (Agilent Technologies, Santa Clara, CA, United States, Model #Bioanalyzer2100) were selected for further downstream processing.

4.6. RNA Isolation

Frozen worms at −80 °C were lysed with three freeze-thaw cycles and intermittent vortexing in liquid nitrogen. To isolate RNA, 150 µL of chloroform (Merck Life Sciences Pvt. Ltd., Mumbai, India, Catalog #1.07024.0521) was added to the worm pellets, and tubes were gently inverted several times. After incubation for 3 min at room temperature, samples were centrifuged at 12,000× *g* for 15 min at 4 °C. The upper aqueous phase was gently removed into a fresh tube. An equal volume of isopropanol (Fisher Scientific, Ottawa, ON, Canada, Catalog #BP2618-500) was added, and the reaction was allowed to sit at room temperature for 10 min. After centrifugation at 12,000× *g* for 10 min at 4 °C, supernatants were carefully discarded, and the remaining pellets were washed using 1 mL 70% ethanol. After centrifugation at 12,000× *g* for 5 min at 4 °C, RNA pellets were dried at room temperature and then dissolved in nuclease-free water. It was kept at 65 °C for 10 min with intermittent tapping. RNA concentration was determined by fluorimeter (Invitrogen, California, United States, Model #Qubit3.0), and quality was checked using Bioanalyzer with RNA kit (Agilent Technologies, United States, Catalog #RNA6000Nano).

4.7. Real-Time Quantitative Reverse Transcription PCR (qRT-PCR)

RNAi knockdown efficiency of TF genes and validation of NGS data by selecting well-known genes was completed by quantifying their expression levels with Real-Time quantitative Reverse Transcription PCR (qRT-PCR). Complementary DNA (cDNA) was prepared using SuperScript III First-Strand Synthesis System Kit (ThermoFisher Scientific, Waltham, MA, United States, Catalog #18080051). Briefly, 1 µg of total RNA was used for cDNA preparation. Oligo dT primers and dNTPs (supplied with cDNA preparation kit) were mixed with it. The mixed solution was heated at 65 °C for 5 min followed by cooling at 4 °C for 1 min. To this mixture, dithiothreitol RNase OUT, 5 × reverse transcriptase buffer, and 1 µL/reaction of Superscript Reverse transcriptase III enzymes (supplied with cDNA preparation kit) were added in the required concentrations. The reaction was incubated at 42 °C for 50 min and later terminated by incubation at 70 °C for 15 min. Quantification of genes was done by qRT-PCR using Brilliant III Ultra-Fast SYBR QPCR Master Mix (Agilent Technologies, California, United States, Catalog #600882) and Real-Time PCR system (Bio-Rad, California, United States, Model #CFX96 Touch Real-Time PCR Detection System) as per the manufacturer's guidelines. The relative expression of genes was calculated according to the ΔΔCt method [59], where ΔCts of genes were obtained after normalization with Ct of actin. Primers used for quantitative RT-PCR are listed in Table S3.

4.8. RNA Sequencing and Analysis

Two biological replicates with RIN (RNA integrity number) values above 9 were selected for the study. The cDNA libraries were constructed with TruSeq RNA Library Prep Kit v2 (Illumina Inc., California, United States). Sequencing (72 or 50 bp single end) was performed using NGS platforms (Illumina Inc. California, United States, Models #Genome Analyzer IIx or HiSeq 2500 systems). Imaging, base calling, and quality scoring were done as per standard manufacturer's guidelines (Illumina Inc.). The demultiplexing and conversion of BCL file format reads to FASTQ file format was done with the Illumina-supported CASAVA v1.8.2 software package. Read counts were then aligned to the reference genome (WBcel 235), and their normalized abundances were calculated as Reads Per Kilobase Million (RPKM) using graphic user interface

NGS data analysis package (Qiagen, Germantown, Maryland, United States, Tool version # CLC Genomics Workbench v12.0.3). Gene fold changes were calculated among samples based on negative binomial Generalized Linear Models (GLM), which corrects for differences in library size between samples and the effects of confounding factors. Genes with an absolute fold change of at least 1.5 and standard *p*-values below 0.05 were considered as differentially expressed. To evaluate variance among biological replicates and conditions, normalized log counts per million (CPM) values and z-score normalization across samples for each gene were applied followed by PCA analysis and hierarchical clustering of the Euclidean distances [60].

4.9. Transcriptional Regulatory Network Analysis

Distinct TF-specific transcriptional regulatory networks were built by considering differentially expressed genes using Cytoscape v3.8.2 [61]. To visualize the non-redundant biological terms and for biological interpretation of a large set of genes in a functionally grouped network, Cytoscape plug-in ClueGO v2.5.7 was used [62]. Genes for TF-specific networks were made by selecting parameters of style as clusters, ontologies pathways-KEGG, a *p*-value of pathways $\leq$0.05, and by keeping other parameters at default values. Activated and repressed genes were represented with green and red color nodes and edges, respectively. Identification of individual clusters and annotation with an enclosing shape and labels were completed with the semi-automated Cytoscape plug-in AutoAnnotate v1.3.4 [63]. Individual clusters were further separated and aligned manually for clear representation.

4.10. Statistical Analysis

Basic survival analysis with the statistical test was conducted using the Mantel-Cox test using Oasis software available at (http://sbi.postech.ac.kr/oasis; Accessed on 9 May 2018). The difference in survival with a *p*-value $\leq$ 0.05 was considered significant. Differential expressed genes by RNA-Seq data were determined with standard *p*-values calculated by Baggerley et al.'s test [64]. Genes with a *p*-value $\leq$ 0.05 were considered with significant expression change. In all the Venn diagrams, hypergeometric *p*-values were calculated by online software (http://www.geneprof.org/GeneProf/tools/hypergeometric.jsp; accessed on 17 April 2020), and their exact *p*-values are indicated in the text as well as in figures. Statistical analysis of quantitative real-time PCR was performed using online statistical software (Systat Software Inc., Chicago, IL, United States, Tool version #SigmaPlot10.0; Accessed on 06-08-2021) with an unpaired two-tailed Student's *t*-test. These values were represented with * $\leq$0.05, ** $\leq$0.01 and *** $\leq$0.001.

Supplementary Materials: The following are available online at https://www.mdpi.com/article/10.3390/ijms222212462/s1.

Author Contributions: Conceptualization, A.M. and N.K. (Neeraj Kumar); data curation, N.K. (Neha Kaushik), S.R., and N.K. (Neeraj Kumar); formal analysis, N.K. (Neha Kaushik), S.V., and N.K. (Neeraj Kumar); funding acquisition, A.M. and N.K. (Neeraj Kumar); investigation, N.K. (Neha Kaushik), S.R., and N.K. (Neeraj Kumar); methodology, N.K. (Neha Kaushik), S.R., A.M., and N.K. (Neeraj Kumar); project administration, N.K. (Neeraj Kumar); resources, A.H., A.M., and N.K. (Neeraj Kumar); supervision, N.K. (Neeraj Kumar); validation, N.K. (Neha Kaushik), S.R., and S.V.; visualization, S.V. and N.K. (Neeraj Kumar); writing—original draft, N.K. (Neeraj Kumar); writing—review and editing, S.V., D.P., A.H., A.M., and N.K. (Neeraj Kumar). All authors have read and agreed to the published version of the manuscript.

Funding: This work was supported by a grant (BT/PR21105/BRB/10/1571/2016) from the Department of Biotechnology (DBT), (5/10/FR/57/2020-RBMCH) from the Indian Council of Medical Research and (ECR/2016/000017) from the Science and Engineering Research Board (SERB), Department of Science and Technology (DST), Government of India to N.K. A.M was supported by a National Bioscience Award for Career Development (BT/HRD/NBA/38/04/2016), DBT grant (BT/PR13720/BAB/10/1779/2010), and SERB-STAR award (STR/2019/000064).

Institutional Review Board Statement: The study waived ethical review and approval by the Institutional Ethics Committee of All India Institute of Medical Sciences, New Delhi (Ref. No. #IEC-2018/04.05.2018), which states, "as no human samples or subjects are involved, this project does not merit ethics approval". The approvals from the Institutional Biosafety Committee of the National Institute of Immunology are numbered IBSC#148/09 and IBSC #227/14.

Informed Consent Statement: Not applicable.

Data Availability Statement: Raw RNA-Seq data have been deposited in the Gene Expression Omnibus (GEO)-NCBI-NIH database under the Super Series accession number GSE184415. The list of genes generated for detailed analysis shown in the manuscript is being provided as processed data files.

Acknowledgments: We are grateful to the All India Institute of Medical Sciences (AIIMS), India, for providing resources for the *C. elegans* work. We are also thankful to the National Institute of Immunology (NII) and Centre for Cellular and Molecular Platforms (C-CAMP), India, for generously sharing its Next Generation Sequencing Facilities for sample sequencing.

Conflicts of Interest: The authors declare no competing or financial interests.

Appendix A

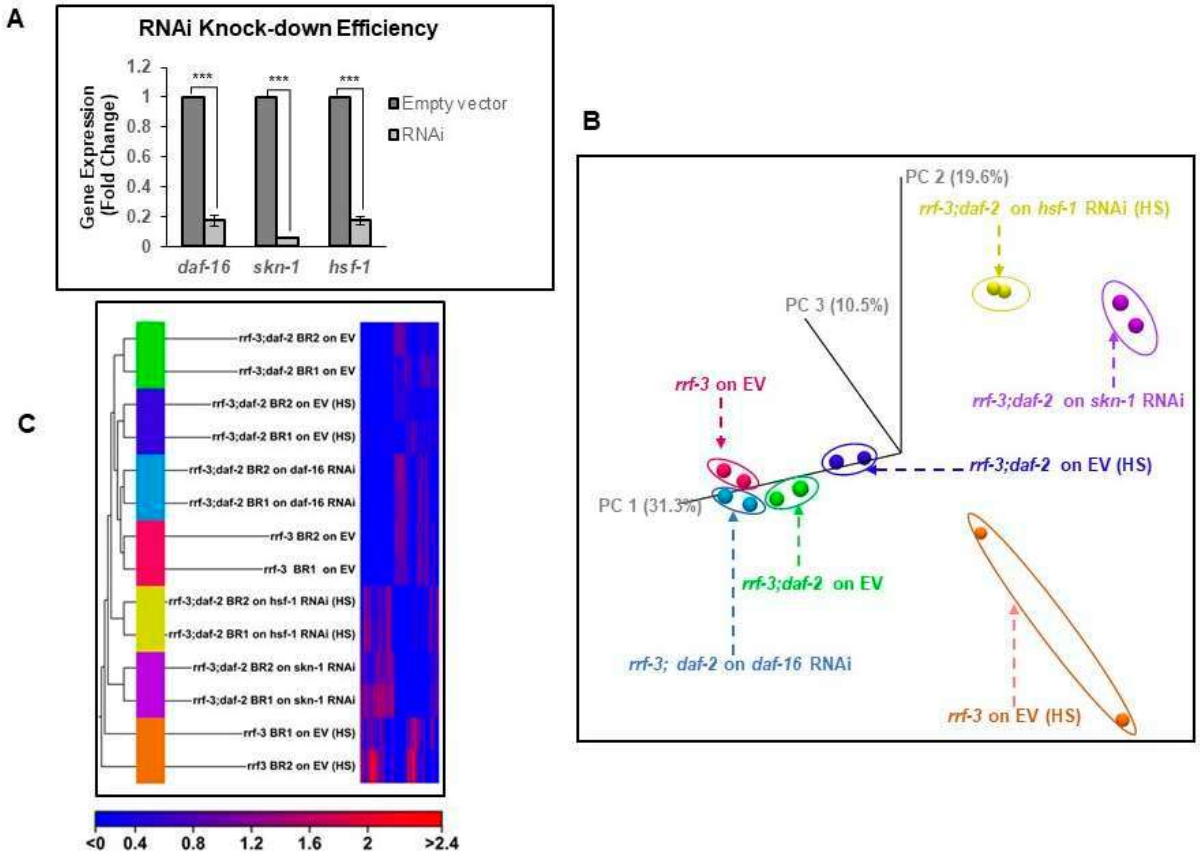

Figure A1. RNAi knockdown efficiency and data quality parameters. (**A**) RNA expression of the *hsf-1* genes was reduced by 80%, while for *skn-1* genes, it was reduced by more than 90%. (**B**) Principal component analysis (PCA) provides insights into the association between biological replicates. (**C**) Unsupervised hierarchical condition tree analysis clustered all the biological replicates under the same branch indicates a high degree of reproducibility with similar gene expression between biological replicates. *** $p \leq 0.001$.

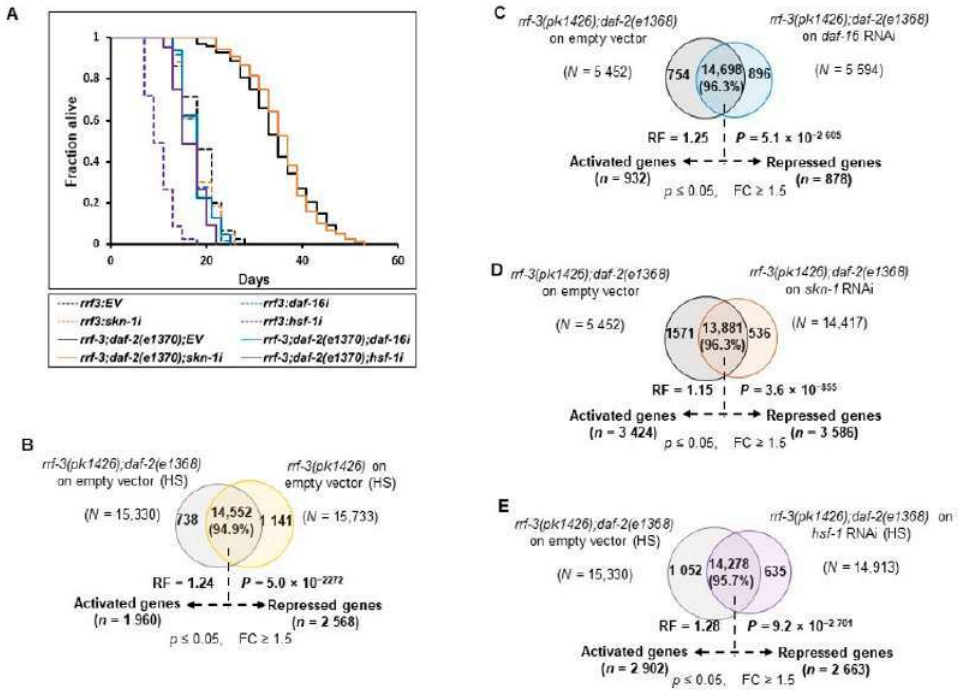

Figure A2. Lifespans of *daf-2* class 2 allele and genome-wide transcriptional output of transcription factors. (**A**) Lifespan of *daf-2* stronger class 2 allele does not depend on all three transcription factors. Life-spans of mutants *rrf-3(pk1426)* and *rrf-3(pk1426);daf-2(e1370)* on empty vector, *daf-16*, *skn-1*, and *hsf-1* RNAi. Knock-down of *daf-16* and *hsf-1* genes reverts the life-spans of rIIS mutant [*rrf-3(-);daf-2(-)*] near to control levels but *skn-1* knockdown does not suppress the life-span of *rrf-3(pk1426);daf-2 (e1370)* mutants. (**B**–**E**) Venn diagram shows the overlap among genes that are differentially expressed during low IIS (+HS), *daf-16*, *skn-1*, and *hsf-1* knockdown conditions respectively.

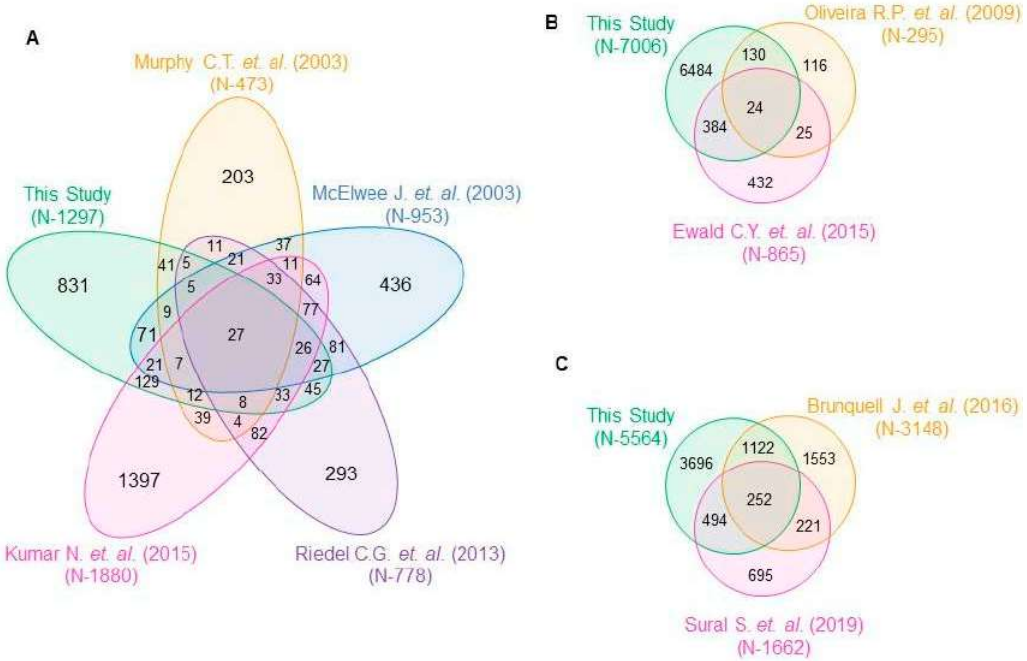

Figure A3. Reduced IIS condition-dependent gene comparison with earlier datasets. Venn diagrams represent the overlap with earlier published datasets. Differentially expressed genes were considered together to compare with earlier published (**A**) DAF-16, (**B**) SKN-1, and (**C**) HSF-1 datasets.

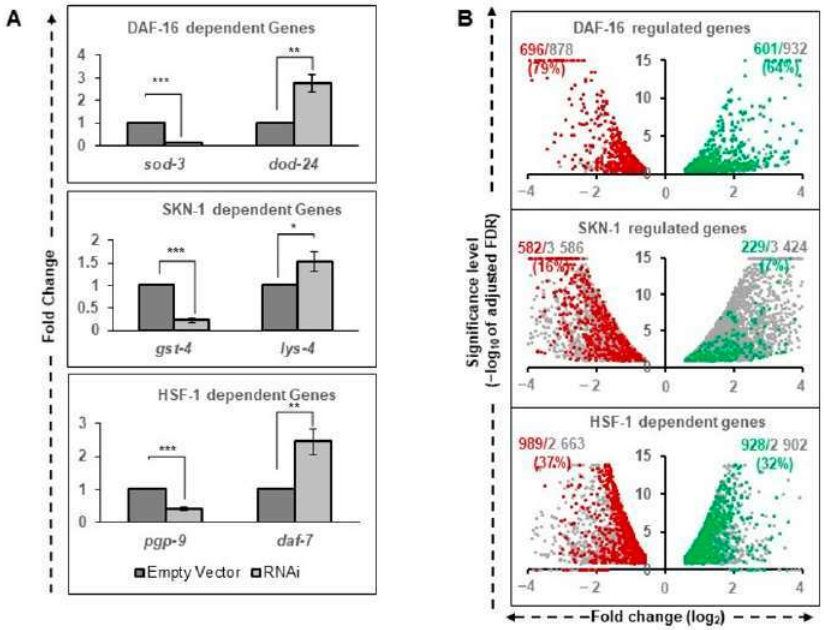

Figure A4. Quantification of rIIS-dependent targets and relative fraction of TF-dependent genes. (**A**) Quantitative real-time PCR of DAF-16 (upper panel), SKN-1 (middle panel), and HSF-1 (lower panel) well-known targets. One target each from the genes activated and repressed by the respective TF has been quantified in the *rrf-3(pk1426);daf-2 (e1368)* double mutants. (**B**) Volcano plots between $\log_{10}$ of adjusted FDR significance level and $\log_2$ fold change of TF-dependent genes (gray color dots). The fraction of these genes specific to the rIIS condition is represented by green and red coloring. Genes regulated by TFs and specific to rIIS condition are shown in percentage. The *p*-values were represented with * $\leq$0.05, ** $\leq$0.01 and *** $\leq$0.001.

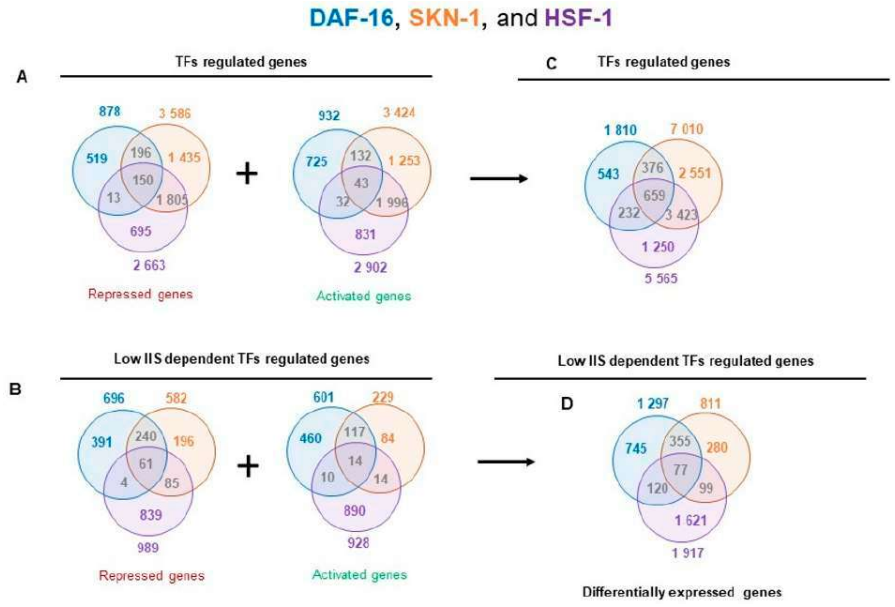

Figure A5. Gene expression profiles of rIIS associated TFs. (**A**) Venn diagram of TF-dependent repressed and activated genes. (**B**) Venn diagram of TF-dependent repressed and activated genes under reduced IIS condition. (**C**) A total of 9034 differentially expressed non-redundant genes regulated by all three TFs. (**D**) A total of 3297 non-redundant differentially expressed genes regulated by all three TFs under rIIS conditions.

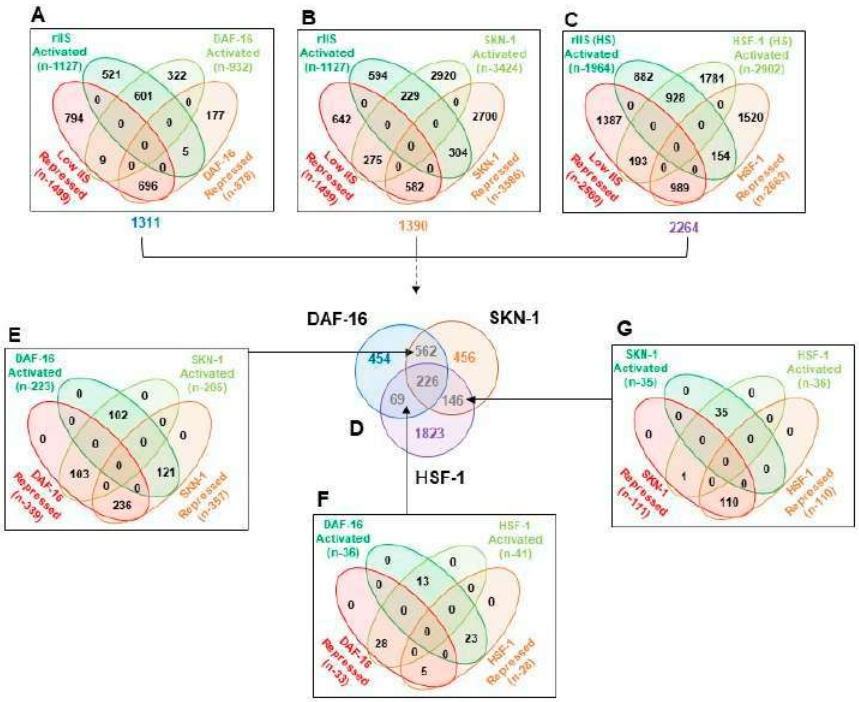

Figure A6. Identification of common genes. (**A**–**C**) Common genes between TFs and rIIS signaling were identified in all possible combinations. DAF-16 regulates a total of 1311, SKN-1-1390, and HSF-1 1831 under reduced IIS conditions. (**D**) Triple Venn diagram shows overlap among TF-regulated genes under rIIS condition. (**E**–**G**) Common activated and repressed genes by any two TFs under rIIS conditions were identified.

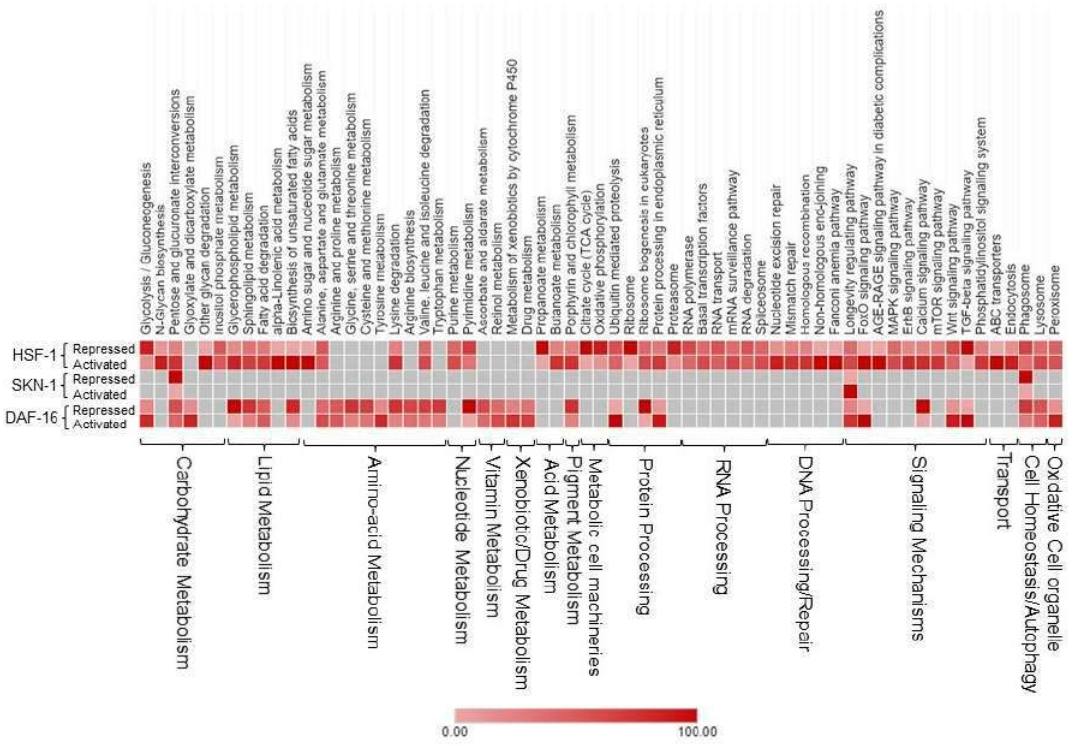

Figure A7. The relative percentage of differentially expressed genes regulated by the individual transcription factors are shown for each of the biological processes which were identified by gene network analysis.

References

1. Kenyon, C.J. The Genetics of Ageing. *Nature* **2010**, *464*, 504–512. [CrossRef] [PubMed]
2. Lin, K.; Hsin, H.; Libina, N.; Kenyon, C. Regulation of the Caenorhabditis Elegans Longevity Protein DAF-16 by Insulin/IGF-1 and Germline Signaling. *Nat. Genet.* **2001**, *28*, 139–145. [CrossRef]
3. Tullet, J.M.; Hertweck, M.; An, J.H.; Baker, J.; Hwang, J.Y.; Liu, S.; Oliveira, R.P.; Baumeister, R.; Blackwell, T.K. Direct Inhibition of the Longevity-Promoting Factor SKN-1 by Insulin-like Signaling in C. Elegans. *Cell* **2008**, *132*, 1025–1038. [CrossRef] [PubMed]
4. Hsu, A.-L.; Murphy, C.T.; Kenyon, C. Regulation of Aging and Age-Related Disease by DAF-16 and Heat-Shock Factor. *Science* **2003**, *300*, 1142–1145. [CrossRef] [PubMed]
5. Sarge, K.D.; Murphy, S.P.; Morimoto, R.I. Activation of Heat Shock Gene Transcription by Heat Shock Factor 1 Involves Oligomerization, Acquisition of DNA-Binding Activity, and Nuclear Localization and Can Occur in the Absence of Stress. *Mol. Cell. Biol.* **1993**, *13*, 1392–1407. [PubMed]
6. Sorger, P.K.; Lewis, M.J.; Pelham, H.R. Heat Shock Factor Is Regulated Differently in Yeast and HeLa Cells. *Nature* **1987**, *329*, 81–84. [CrossRef] [PubMed]
7. Chiang, W.-C.; Ching, T.-T.; Lee, H.C.; Mousigian, C.; Hsu, A.-L. HSF-1 Regulators DDL-1/2 Link Insulin-like Signaling to Heat-Shock Responses and Modulation of Longevity. *Cell* **2012**, *148*, 322–334. [CrossRef]
8. Accili, D.; Arden, K.C. FoxOs at the Crossroads of Cellular Metabolism, Differentiation, and Transformation. *Cell* **2004**, *117*, 421–426. [CrossRef]
9. Wolff, S.; Dillin, A. The Trifecta of Aging in Caenorhabditis Elegans. *Exp. Gerontol.* **2006**, *41*, 894–903. [CrossRef]
10. Mukhopadhyay, A.; Oh, S.W.; Tissenbaum, H.A. Worming Pathways to and from DAF-16/FOXO. *Exp. Gerontol.* **2006**, *41*, 928–934. [CrossRef]
11. Antebi, A. Genetics of Aging in Caenorhabditis Elegans. *PLoS Genet.* **2007**, *3*, e129. [CrossRef]
12. Lee, S.S.; Kennedy, S.; Tolonen, A.C.; Ruvkun, G. DAF-16 Target Genes That Control C. Elegans Life-Span and Metabolism. *Science* **2003**, *300*, 644–647. [CrossRef] [PubMed]
13. McElwee, J.; Bubb, K.; Thomas, J.H. Transcriptional Outputs of the Caenorhabditis Elegans Forkhead Protein DAF-16. *Aging Cell* **2003**, *2*, 111–121. [CrossRef] [PubMed]
14. McElwee, J.J.; Schuster, E.; Blanc, E.; Thomas, J.H.; Gems, D. Shared Transcriptional Signature in Caenorhabditis Elegans Dauer Larvae and Long-Lived Daf-2 Mutants Implicates Detoxification System in Longevity Assurance. *J. Biol. Chem.* **2004**, *279*, 44533–44543. [CrossRef] [PubMed]
15. Murphy, C.T.; McCarroll, S.A.; Bargmann, C.I.; Fraser, A.; Kamath, R.S.; Ahringer, J.; Li, H.; Kenyon, C. Genes That Act Downstream of DAF-16 to Influence the Lifespan of Caenorhabditis Elegans. *Nature* **2003**, *424*, 277–283. [CrossRef] [PubMed]
16. Shaw, W.M.; Luo, S.; Landis, J.; Ashraf, J.; Murphy, C.T. The C. Elegans TGF-β Dauer Pathway Regulates Longevity via Insulin Signaling. *Curr. Biol.* **2007**, *17*, 1635–1645. [CrossRef]
17. Halaschek-Wiener, J.; Khattra, J.S.; McKay, S.; Pouzyrev, A.; Stott, J.M.; Yang, G.S.; Holt, R.A.; Jones, S.J.; Marra, M.A.; Brooks-Wilson, A.R. Analysis of Long-Lived C. Elegans Daf-2 Mutants Using Serial Analysis of Gene Expression. *Genome Res.* **2005**, *15*, 603–615. [CrossRef] [PubMed]
18. Dong, M.-Q.; Venable, J.D.; Au, N.; Xu, T.; Park, S.K.; Cociorva, D.; Johnson, J.R.; Dillin, A.; Yates, J.R. Quantitative Mass Spectrometry Identifies Insulin Signaling Targets in C. Elegans. *Science* **2007**, *317*, 660–663. [CrossRef]
19. Schuster, E.; McElwee, J.J.; Tullet, J.M.; Doonan, R.; Matthijssens, F.; Reece-Hoyes, J.S.; Hope, I.A.; Vanfleteren, J.R.; Thornton, J.M.; Gems, D. DamID in C. Elegans Reveals Longevity-associated Targets of DAF-16/FoxO. *Mol. Syst. Biol.* **2010**, *6*, 399. [CrossRef] [PubMed]
20. Riedel, C.G.; Dowen, R.H.; Lourenco, G.F.; Kirienko, N.V.; Heimbucher, T.; West, J.A.; Bowman, S.K.; Kingston, R.E.; Dillin, A.; Asara, J.M. DAF-16 Employs the Chromatin Remodeller SWI/SNF to Promote Stress Resistance and Longevity. *Nat. Cell Biol.* **2013**, *15*, 491–501. [CrossRef]
21. Kumar, N.; Jain, V.; Singh, A.; Jagtap, U.; Verma, S.; Mukhopadhyay, A. Genome-Wide Endogenous DAF-16/FOXO Recruitment Dynamics during Lowered Insulin Signalling in C. Elegans. *Oncotarget* **2015**, *6*, 41418. [CrossRef] [PubMed]
22. An, J.H.; Vranas, K.; Lucke, M.; Inoue, H.; Hisamoto, N.; Matsumoto, K.; Blackwell, T.K. Regulation of the Caenorhabditis Elegans Oxidative Stress Defense Protein SKN-1 by Glycogen Synthase Kinase-3. *Proc. Natl. Acad. Sci. USA* **2005**, *102*, 16275–16280. [CrossRef] [PubMed]
23. Bowerman, B.; Eaton, B.A.; Priess, J.R. Skn-1, a Maternally Expressed Gene Required to Specify the Fate of Ventral Blastomeres in the Early C. Elegans Embryo. *Cell* **1992**, *68*, 1061–1075. [CrossRef]
24. An, J.H.; Blackwell, T.K. SKN-1 Links C. Elegans Mesendodermal Specification to a Conserved Oxidative Stress Response. *Genes Dev.* **2003**, *17*, 1882–1893. [CrossRef] [PubMed]
25. Li, X.; Matilainen, O.; Jin, C.; Glover-Cutter, K.M.; Holmberg, C.I.; Blackwell, T.K. Specific SKN-1/Nrf Stress Responses to Perturbations in Translation Elongation and Proteasome Activity. *PLoS Genet.* **2011**, *7*, e1002119. [CrossRef] [PubMed]
26. Wang, J.; Robida-Stubbs, S.; Tullet, J.M.; Rual, J.-F.; Vidal, M.; Blackwell, T.K. RNAi Screening Implicates a SKN-1–Dependent Transcriptional Response in Stress Resistance and Longevity Deriving from Translation Inhibition. *PLoS Genet.* **2010**, *6*, e1001048. [CrossRef]

27. Kahn, N.W.; Rea, S.L.; Moyle, S.; Kell, A.; Johnson, T.E. Proteasomal Dysfunction Activates the Transcription Factor SKN-1 and Produces a Selective Oxidative-Stress Response in Caenorhabditis Elegans. *Biochem. J.* **2008**, *409*, 205–213. [CrossRef] [PubMed]
28. Ewald, C.Y.; Landis, J.N.; Abate, J.P.; Murphy, C.T.; Blackwell, T.K. Dauer-Independent Insulin/IGF-1-Signalling Implicates Collagen Remodelling in Longevity. *Nature* **2015**, *519*, 97–101. [CrossRef] [PubMed]
29. Niu, W.; Lu, Z.J.; Zhong, M.; Sarov, M.; Murray, J.I.; Brdlik, C.M.; Janette, J.; Chen, C.; Alves, P.; Preston, E. Diverse Transcription Factor Binding Features Revealed by Genome-Wide ChIP-Seq in C. Elegans. *Genome Res.* **2011**, *21*, 245–254. [CrossRef]
30. Oliveira, R.P.; Abate, J.P.; Dilks, K.; Landis, J.; Ashraf, J.; Murphy, C.T.; Blackwell, T.K. Condition-adapted Stress and Longevity Gene Regulation by Caenorhabditis Elegans SKN-1/Nrf. *Aging Cell* **2009**, *8*, 524–541. [CrossRef]
31. Morley, J.F.; Morimoto, R.I. Regulation of Longevity in Caenorhabditis Elegans by Heat Shock Factor and Molecular Chaperones. *Mol. Biol. Cell* **2004**, *15*, 657–664. [CrossRef] [PubMed]
32. Seo, K.; Choi, E.; Lee, D.; Jeong, D.; Jang, S.K.; Lee, S. Heat Shock Factor 1 Mediates the Longevity Conferred by Inhibition of TOR and Insulin/IGF-1 Signaling Pathways in C. Elegans. *Aging Cell* **2013**, *12*, 1073–1081. [CrossRef]
33. Hajdu-Cronin, Y.M.; Chen, W.J.; Sternberg, P.W. The L-Type Cyclin CYL-1 and the Heat-Shock-Factor HSF-1 Are Required for Heat-Shock-Induced Protein Expression in Caenorhabditis Elegans. *Genetics* **2004**, *168*, 1937–1949. [CrossRef]
34. Walker, G.A.; Thompson, F.J.; Brawley, A.; Scanlon, T.; Devaney, E. Heat Shock Factor Functions at the Convergence of the Stress Response and Developmental Pathways in Caenorhabditis Elegans. *FASEB J.* **2003**, *17*, 1–19. [CrossRef] [PubMed]
35. Minsky, N.; Roeder, R.G. Direct Link between Metabolic Regulation and the Heat-Shock Response through the Transcriptional Regulator PGC-1α. *Proc. Natl. Acad. Sci. USA* **2015**, *112*, E5669–E5678. [CrossRef] [PubMed]
36. Douglas, P.M.; Baird, N.A.; Simic, M.S.; Uhlein, S.; McCormick, M.A.; Wolff, S.C.; Kennedy, B.K.; Dillin, A. Heterotypic Signals from Neural HSF-1 Separate Thermotolerance from Longevity. *Cell Rep.* **2015**, *12*, 1196–1204. [CrossRef] [PubMed]
37. Garigan, D.; Hsu, A.-L.; Fraser, A.G.; Kamath, R.S.; Ahringer, J.; Kenyon, C. Genetic Analysis of Tissue Aging in Caenorhabditis Elegans: A Role for Heat-Shock Factor and Bacterial Proliferation. *Genetics* **2002**, *161*, 1101–1112. [CrossRef]
38. Li, J.; Chauve, L.; Phelps, G.; Brielmann, R.M.; Morimoto, R.I. E2F Coregulates an Essential HSF Developmental Program That Is Distinct from the Heat-Shock Response. *Genes Dev.* **2016**, *30*, 2062–2075. [CrossRef] [PubMed]
39. Brunquell, J.; Morris, S.; Lu, Y.; Cheng, F.; Westerheide, S.D. The Genome-Wide Role of HSF-1 in the Regulation of Gene Expression in Caenorhabditis Elegans. *BMC Genom.* **2016**, *17*, 559. [CrossRef] [PubMed]
40. Sural, S.; Lu, T.-C.; Jung, S.A.; Hsu, A.-L. HSB-1 Inhibition and HSF-1 Overexpression Trigger Overlapping Transcriptional Changes to Promote Longevity in Caenorhabditis Elegans. *G3 Genes Genomes Genet.* **2019**, *9*, 1679–1692. [CrossRef] [PubMed]
41. Gems, D.; Sutton, A.J.; Sundermeyer, M.L.; Albert, P.S.; King, K.V.; Edgley, M.L.; Larsen, P.L.; Riddle, D.L. Two Pleiotropic Classes of Daf-2 Mutation Affect Larval Arrest, Adult Behavior, Reproduction and Longevity in Caenorhabditis Elegans. *Genetics* **1998**, *150*, 129–155. [CrossRef] [PubMed]
42. Sijen, T.; Fleenor, J.; Simmer, F.; Thijssen, K.L.; Parrish, S.; Timmons, L.; Plasterk, R.H.; Fire, A. On the Role of RNA Amplification in DsRNA-Triggered Gene Silencing. *Cell* **2001**, *107*, 465–476. [CrossRef]
43. Rabindran, S.K.; Haroun, R.I.; Clos, J.; Wisniewski, J.; Wu, C. Regulation of Heat Shock Factor Trimer Formation: Role of a Conserved Leucine Zipper. *Science* **1993**, *259*, 230–234. [CrossRef] [PubMed]
44. Clos, J.; Westwood, J.T.; Becker, P.B.; Wilson, S.; Lambert, K.; Wu, C. Molecular Cloning and Expression of a Hexameric Drosophila Heat Shock Factor Subject to Negative Regulation. *Cell* **1990**, *63*, 1085–1097. [CrossRef]
45. Beck, C.; Rankin, C.H. Heat Shock Disrupts Long-Term Memory Consolidation in Caenorhabditis Elegans. *Learn. Mem.* **1995**, *2*, 161–177. [CrossRef] [PubMed]
46. Lithgow, G.J.; White, T.M.; Melov, S.; Johnson, T.E. Thermotolerance and Extended Life-Span Conferred by Single-Gene Mutations and Induced by Thermal Stress. *Proc. Natl. Acad. Sci. USA* **1995**, *92*, 7540–7544. [CrossRef] [PubMed]
47. Steinkraus, K.A.; Smith, E.D.; Davis, C.; Carr, D.; Pendergrass, W.R.; Sutphin, G.L.; Kennedy, B.K.; Kaeberlein, M. Dietary Restriction Suppresses Proteotoxicity and Enhances Longevity by an Hsf-1-dependent Mechanism in Caenorhabditis Elegans. *Aging Cell* **2008**, *7*, 394–404. [CrossRef]
48. Oh, S.W.; Mukhopadhyay, A.; Dixit, B.L.; Raha, T.; Green, M.R.; Tissenbaum, H.A. Identification of Direct DAF-16 Targets Controlling Longevity, Metabolism and Diapause by Chromatin Immunoprecipitation. *Nat. Genet.* **2006**, *38*, 251–257. [PubMed]
49. Barna, J.; Princz, A.; Kosztelnik, M.; Hargitai, B.; Takács-Vellai, K.; Vellai, T. Heat Shock Factor-1 Intertwines Insulin/IGF-1, TGF-β and CGMP Signaling to Control Development and Aging. *BMC Dev. Biol.* **2012**, *12*, 32. [CrossRef] [PubMed]
50. Mansfeld, J.; Urban, N.; Priebe, S.; Groth, M.; Frahm, C.; Hartmann, N.; Gebauer, J.; Ravichandran, M.; Dommaschk, A.; Schmeisser, S. Branched-Chain Amino Acid Catabolism Is a Conserved Regulator of Physiological Ageing. *Nat. Commun.* **2015**, *6*, 10043. [CrossRef]
51. Dhondt, I.; Petyuk, V.A.; Cai, H.; Vandemeulebroucke, L.; Vierstraete, A.; Smith, R.D.; Depuydt, G.; Braeckman, B.P. FOXO/DAF-16 Activation Slows down Turnover of the Majority of Proteins in C. Elegans. *Cell Rep.* **2016**, *16*, 3028–3040. [CrossRef] [PubMed]
52. Kenyon, C. The Plasticity of Aging: Insights from Long-Lived Mutants. *Cell* **2005**, *120*, 449–460. [CrossRef]
53. Proshkina, E.N.; Solovev, I.A.; Shaposhnikov, M.V.; Moskalev, A.A. Key Molecular Mechanisms of Aging, Biomarkers, and Potential Interventions. *Mol. Biol.* **2020**, *54*, 777–811. [CrossRef]
54. Kenyon, C.; Chang, J.; Gensch, E.; Rudner, A.; Tabtiang, R. A C. Elegans Mutant That Lives Twice as Long as Wild Type. *Nature* **1993**, *366*, 461–464. [CrossRef]

55. Tullet, J.M.; Green, J.W.; Au, C.; Benedetto, A.; Thompson, M.A.; Clark, E.; Gilliat, A.F.; Young, A.; Schmeisser, K.; Gems, D. The SKN-1/Nrf2 Transcription Factor Can Protect against Oxidative Stress and Increase Lifespan in C. Elegans by Distinct Mechanisms. *Aging Cell* **2017**, *16*, 1191–1194. [CrossRef] [PubMed]
56. Singh, V.; Aballay, A. Heat-Shock Transcription Factor (HSF)-1 Pathway Required for Caenorhabditis Elegans Immunity. *Proc. Natl. Acad. Sci. USA* **2006**, *103*, 13092–13097. [CrossRef] [PubMed]
57. Morton, E.A.; Lamitina, T. Caenorhabditis Elegans HSF-1 Is an Essential Nuclear Protein That Forms Stress Granule-like Structures Following Heat Shock. *Aging Cell* **2013**, *12*, 112–120. [CrossRef] [PubMed]
58. Papp, D.; Csermely, P.; Sőti, C. A Role for SKN-1/Nrf in Pathogen Resistance and Immunosenescence in Caenorhabditis Elegans. *PLoS Pathog.* **2012**, *8*, e1002673. [CrossRef] [PubMed]
59. Schmittgen, T.D.; Livak, K.J. Analyzing Real-Time PCR Data by the Comparative C T Method. *Nat. Protoc.* **2008**, *3*, 1101. [CrossRef]
60. Love, M.I.; Huber, W.; Anders, S. Moderated Estimation of Fold Change and Dispersion for RNA-Seq Data with DESeq2. *Genome Biol.* **2014**, *15*, 550. [CrossRef] [PubMed]
61. Shannon, P.; Markiel, A.; Ozier, O.; Baliga, N.S.; Wang, J.T.; Ramage, D.; Amin, N.; Schwikowski, B.; Ideker, T. Cytoscape: A Software Environment for Integrated Models of Biomolecular Interaction Networks. *Genome Res.* **2003**, *13*, 2498–2504. [CrossRef] [PubMed]
62. Bindea, G.; Mlecnik, B.; Hackl, H.; Charoentong, P.; Tosolini, M.; Kirilovsky, A.; Fridman, W.-H.; Pagès, F.; Trajanoski, Z.; Galon, J. ClueGO: A Cytoscape Plug-in to Decipher Functionally Grouped Gene Ontology and Pathway Annotation Networks. *Bioinformatics* **2009**, *25*, 1091–1093. [CrossRef] [PubMed]
63. Kucera, M.; Isserlin, R.; Arkhangorodsky, A.; Bader, G.D. AutoAnnotate: A Cytoscape App for Summarizing Networks with Semantic Annotations. *F1000Research* **2016**, *5*, 1717. [CrossRef] [PubMed]
64. Baggerly, K.A.; Deng, L.; Morris, J.S.; Aldaz, C.M. Differential Expression in SAGE: Accounting for Normal between-Library Variation. *Bioinformatics* **2003**, *19*, 1477–1483. [CrossRef] [PubMed]

PLOS GENETICS

RESEARCH ARTICLE

A novel gene-diet pair modulates *C. elegans* aging

Sonia Verma, Urmila Jagtap¤, Anita Goyala, Arnab Mukhopadhyay*

Molecular Aging Laboratory, National Institute of Immunology, Aruna Asaf Ali Marg, New Delhi, India

¤ Current address: CSIR-Institute of Genomics & Integrative Biology, South Campus, New Delhi, India
* arnab@nii.ac.in, mukhopadhyayarn@gmail.com

OPEN ACCESS

Citation: Verma S, Jagtap U, Goyala A, Mukhopadhyay A (2018) A novel gene-diet pair modulates *C. elegans* aging. PLoS Genet 14(8): e1007608. https://doi.org/10.1371/journal.pgen.1007608

Editor: Siu Sylvia Lee, Cornell University, UNITED STATES

Received: October 10, 2017

Accepted: August 2, 2018

Published: August 20, 2018

Data Availability Statement: The RNA sequencing data is available at NCBI SRA (https://www.ncbi.nlm.nih.gov/sra) with a BioProject ID: PRJNA362992.

Funding: The study was funded by Department of Biotechnology (DBT)-Ramalingaswami fellowship (BT/HRD/35/02/12/2008; http://www.dbtindia.nic.in/), Department of Science and Technology-Science and Engineering Research Board (SERB) (EMR/2014/000377; http://serbonline.in/SERB/) and by Core funding from the National Institute of Immunology (www.nii.res.in). SV is supported by

Abstract

Diet profoundly affects metabolism and incidences of age-related diseases. Animals adapt their physiology to different food-types, modulating complex life-history traits like aging. The molecular mechanisms linking adaptive capacity to diet with aging are less known. We identify FLR-4 kinase as a novel modulator of aging in *C. elegans*, depending on bacterial diet. FLR-4 functions to prevent differential activation of the p38MAPK pathway in response to diverse food-types, thereby maintaining normal life span. In a kinase-dead *flr-4* mutant, *E. coli* HT115 (K12 strain), but not the standard diet OP50 (B strain), is able to activate p38MAPK, elevate expression of cytoprotective genes through the nuclear hormone receptor NHR-8 and enhance life span. Interestingly, *flr-4* and dietary restriction utilize similar pathways for longevity assurance, suggesting cross-talks between cellular modules that respond to diet quality and quantity. Together, our study discovers a new *C. elegans* gene-diet pair that controls the plasticity of aging.

Author summary

For animals living in the wild, being able to utilize a wide range of diet is evolutionarily advantageous as they can survive even when their optimal diet is depleted. Since diet is known to influence the rate of aging, animals seem to have evolved intricate mechanisms to maintain homeostasis and normal life span, but the molecular mechanisms are less understood. Using a small nematode, *C. elegans* as a model, we show that the adaptive capacity to different diet is maintained by a kinase gene. When this gene is mutated, worms start living longer on one strain of bacterial diet but not on the other. We identify the molecular cascade required for this food-type-dependent longevity. We show that this cascade of events significantly overlaps with the pathway that determine food quantity-dependent life span enhancement. Our study thus elucidates a part of the molecular monitoring system that regulates longevity dependent on the available quality and quantity of diet.

Introduction

Animals dwell in a complex ecosystem where they interact with a host of other organisms; some of them may alter their life history traits. For example, the nematode *Caenorhabditis*

UGC-JRF fellowship. The funders had no role in study design, data collection and analysis, decision to publish, or preparation of the manuscript.

Competing interests: The authors have declared that no competing interests exist.

elegans is found in decaying moist vegetation that is co-inhabited by different types of bacteria that they feed on. So, the worms are often exposed to various pathogenic bacteria that they either avoid or use a conserved innate immunity pathway to counter. The worms are also presented with a range of bacteria of different nutritional values that they choose between [1–3]. They encounter *E. coli*¸ *Bacillus* and *Comamonas* etc. that are known to modulate development, reproduction, fat storage and life span [2, 4–7]. In the laboratory, worms are mostly maintained on *E. coli* OP50 but are often exposed to the RNAseIII-deficient HT115 during RNAi experiments. The two strains differ considerably, particularly in terms of carbohydrate content, with the OP50 strain considered as a low quality diet that induces less satiety and promotes higher fat storage [3, 6–9]. Since the rate of aging is greatly influenced by dietary composition, worms seem to have evolved intricate adaptive strategies to maintain normal aging [10, 11]. As a result, although the two diets differentially affect metabolism, the worms are able to ensure relatively normal life span when fed either bacteria [7]. How *C. elegans* sense different diet to alter metabolism and life history traits, including complex traits like aging, is an emerging area of research. These studies are being facilitated by the discovery of gene-diet pairs where the function of a gene becomes discernible only on a particular diet [12].

Previous work has shown that sensory neurons may process signals that differentiate between different food-types and regulate life span in flies and worms [10, 13, 14]. In *C. elegans*, the neuromedin U receptor-like gene, *nmur-1* mutant as well as *osm-3* (kinesin motor protein required for cilia formation) mutant has extended life span on OP50 but not on HT115 [10, 14]. These life spans were found to be dependent on the FOXO transcription factor, DAF-16 [14]. On the other hand, the proline metabolism gene *alh-6* works in the muscle to preserve mitochondrial structure and functional homeostasis in response to OP50 [11]. This requires a functional NMUR-1 receptor signalling [11]. Interestingly and intuitively, it would appear that the intestine may also contribute to this phenomenon as it gets to sample different food that the worms ingest. However, the role of intestine in food-type-dependent life span regulation is not as well-characterized.

Here we show that a serine-threonine kinase gene, *flr-4* regulates food-type-dependent life span by functioning both in the neurons and the intestine. We find that when *flr-4* is knocked down by RNAi or its function disrupted by a P223S missense mutation in its kinase domain, life span is dramatically increased. The life span of the kinase-dead mutant *flr-4(n2259)* is increased only when the mutant is fed HT115 and not OP50. We show that knocking down *flr-4* leads to increased cytoprotective xenobiotic detoxification pathway (XDP) gene expression, through the nuclear hormone receptor NHR-8, that plays a causal role in its increased life span. Interestingly, this elevated gene expression as well as the increased life span is dependent on the conserved p38 MAPK signalling. In *flr-4(n2259)*, OP50 is unable to strongly activate the p38 MAPK while HT115 leads to increased phosphorylation of the MAPK. Consequently, in the mutant, HT115 is able to increase the levels of the XDP genes while OP50 does not. Finally, we demonstrate that FLR-4 uses a pathway similar to DR to ensure longevity, dependent on FOXA/PHA-4 but independent of FOXO/DAF-16. Together, our study establishes *flr-4* as a new longevity gene that controls adaptive capacity of *C. elegans* towards bacterial diet by preventing differential activation of XDP genes through p38MAPK pathway, dependent on food-type.

Results

Knocking down *flr-4* increases life span in a food-type dependent manner

Flr-4 was originally identified in a screen for genes that regulate fluoride resistance and the mutants exhibit temperature-sensitive defecation defects [15]. However, at 20 ^{o}C they do not

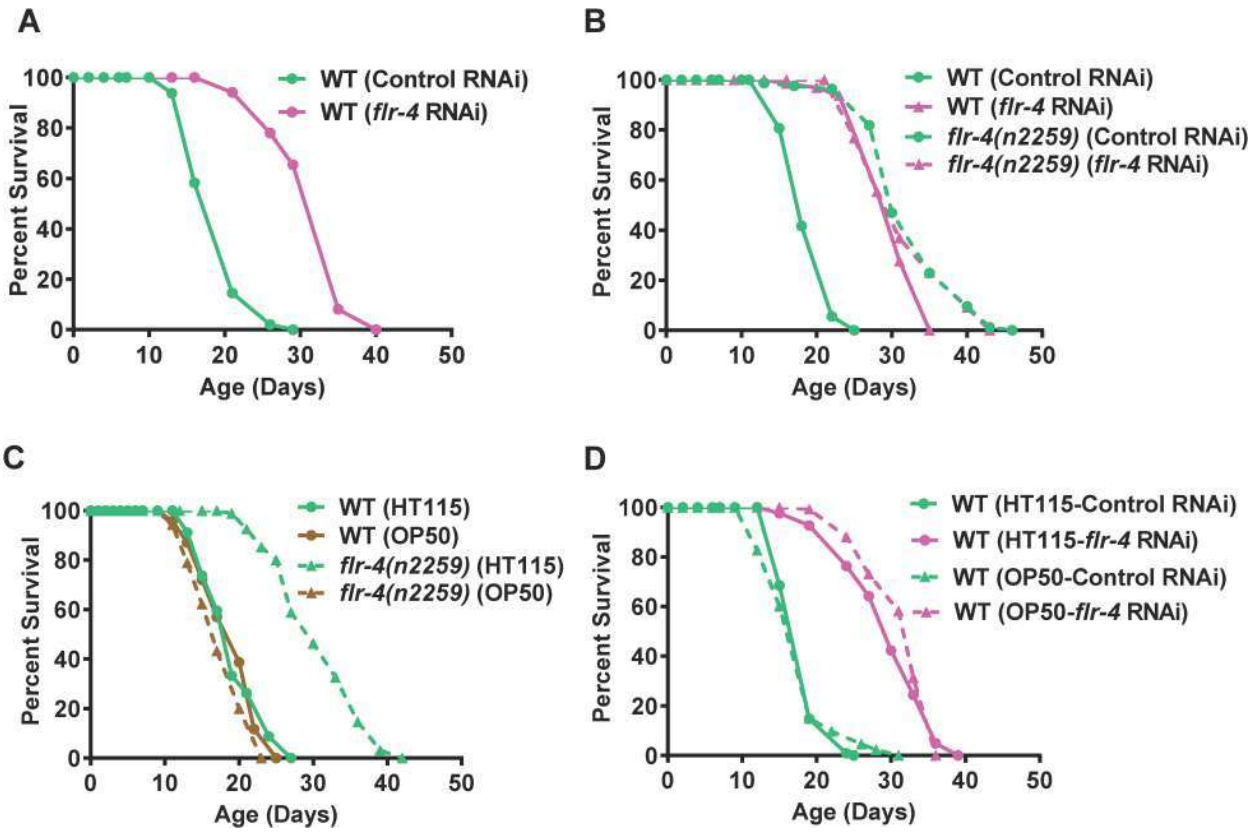

Fig 1. Knocking down *flr-4* increases life span in a food-type-dependent manner. (A) Knocking down *flr-4* by RNAi increases life span. (B) The *flr-4(n2259)* allele has increased life span that is not further extended when *flr-4* is knocked down using RNAi. (C) The *flr-4(n2259)* allele has increased life span only when the mutant worms are maintained on *E. coli* HT115 but not on *E. coli* OP50. (D) Knocking down *flr-4* using an OP50-based RNAi system increased life span comparable to HT115-based RNAi. Life spans were performed at 20˚C.

https://doi.org/10.1371/journal.pgen.1007608.g001

have defects in defecation [15]. We initially became interested in the *flr-4* gene as it has 26% homology and 40% identity to *drl-1* [16], a gene we have recently characterized to be involved in Dietary Restriction (DR). Knocking down *flr-4* using a cDNA RNAi construct increased life span dramatically (average life span increase 40–60%, Fig 1A, S1 and S2 Tables). Similar life span extension was observed in absence of FUDR, a DNA synthesis inhibitor used to arrest confounding effects of progeny population during life span analysis (S1A Fig). The increased life span was also associated with better health as evident from lower lipofuscin pigment accumulation (S2A Fig), lesser muscular atrophy with age (S2B Fig) and consequently, better motility (S2C Fig). These worms were smaller in size (S2D Fig) but did not have any major defects in developmental rates (S3 Fig). However, the increase in life span was not associated with enhanced tolerance towards heat stress (S4B Fig); UV stress tolerance was only increased 13–15% compared to 40–60% increase in life span (S4A Fig). The increased life span of *flr-4* knock down was also not dependent on the heat shock transcription factor *hsf-1* (S4C and S4D Fig). Thus, *flr-4* seems to decouple longevity from stress resistance and is a novel longevity modulator.

Next, we asked whether an *flr-4* mutant has attributes similar to the *flr-4* RNAi. We used the *flr-4(n2259)* allele that has a P223S missense mutation in the activation loop of the protein kinase domain and shows increased fluoride resistance [15]. This allele has similar

developmental rates as wild-type (S5 Fig) and shows no dauer arrest [15]. We found that *flr-4 (n2259)* increased life span that was not further increased when grown on *flr-4* RNAi (Fig 1B, S1 and S2 Tables). The life span of the mutant was also not affected by the presence of FUDR (S1B Fig). This suggests that *flr-4(n2259)* behaves as a null allele to regulate life span.

C. elegans is known to respond differentially to bacterial diet to modulate life history traits, including life span [5–7, 14, 17]. Interestingly, we found that the life span extension in *flr-4 (n2259)* is dependent on the food-type. When the mutant was grown on the *E. coli* HT115 (a K12 strain), life span was dramatically extended (Fig 1C, S1 and S2 Tables). In contrast, when grown on *E. coli* OP50 (a B strain), no extension of life span was observed (Fig 1C). We checked for differences in pumping under these conditions and found no change (S2E Fig). Also, ingestion of RFP-labelled beads was similar in WT and *flr-4(n2259)* (S2F Fig), suggesting that the differences in life span are not due to altered feeding behaviour. Furthermore, the developmental rate was similar in both the strains when grown on the two *E. coli* strains (S5 Fig). Remarkably, knocking down *flr-4* using an OP50-based RNAi system [18] increased life span similar to that of the HT115-based system (Fig 1D), suggesting that the food-type-dependent life span extension may be attributed to the kinase function of FLR-4. This conclusion is further supported by the observation that rescuing *flr-4(n2259)* with a kinase-proficient wild-type transgene suppresses the increased life span on HT115 (S16 Fig). Together, FLR-4 kinase suppresses pro-longevity cues in a food-type dependent manner.

Flr-4 functions in the intestine and neurons, during larval development to regulate adult life span

Next, we asked where FLR-4 functions to regulate longevity. We constructed a *flr-4p*::*gfp* transgenic line and found that the *flr-4* promoter drove expression of *gfp* in the intestine and a few neurons (Fig 2A). We used a tissue-specific RNAi system to determine the tissue where *flr-4* functions. We found that *flr-4* knockdown specifically in the intestine or the neurons was sufficient for life span extension; no extension in life span was observed when the gene is solely knocked down in muscle or hypodermis (Fig 2B–2E, S1 and S2 Tables). Together, *flr-4* functions in the intestine and neurons to negatively regulate life span of the worms.

In *C. elegans*, longevity genes need to be knocked down at temporally distinct points in development to increase life span. For example, the mitochondrial electron transport gene *cco-1* or the MEKK-3-like kinase *drl-1* needs to be knocked down early in development to increase life span while insulin-like signalling pathway functions in adulthood to exhibit the beneficial longevity effects [16, 19, 20]. We initiated *flr-4* RNAi at different stages of development of the worms and found that knocking down at L1 or L2 produced maximum life span extension; knocking down at L3 or later had diminished or no effect (S6A–S6E Fig). Together, *flr-4* functions in the intestine and neurons, during larval development to regulate adult life span.

Flr-4 requires p38 MAPK pathway for longevity

Since FLR-4 is required to suppress the effect of food-type on longevity, we asked what signalling cascade may be mediating this effect. The p38 MAPK pathway is a central signalling mediator required for mounting the innate immune response when worms are challenged with pathogens [21–25]. The worm p38 homolog PMK-1 is activated by its upstream MAPKKK NSY-1 and MAPKK SEK-1 [26, 27]. The TIR domain adaptor protein TIR-1, an ortholog of human SARM [28, 29] and UNC-43, a Ca^{2+}/calmodulin-dependent protein kinase II (CaMKII) [30] lie further upstream of these serine-threonine kinases. While TIR-1 works upstream of the p38 MAPK pathway to regulate innate immunity genes [28, 29], both TIR-1 and UNC-43 functions in the neurons to control neuronal cell fate and asymmetric patterns of odorant

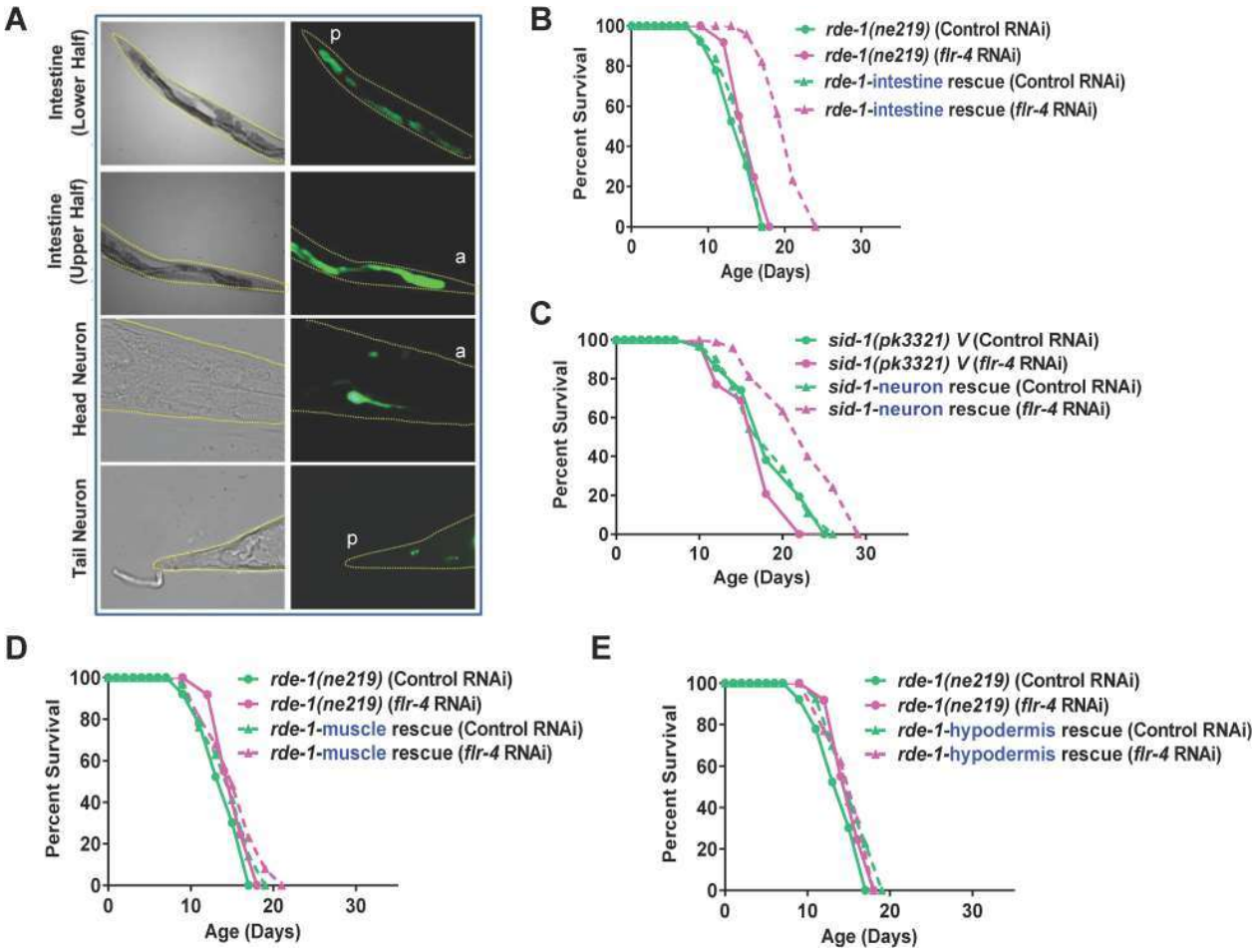

Fig 2. FLR-4 functions in the intestine and neurons to regulate life span. (A) The expression of *Pflr-4*::*gfp* is localized to the intestine and a few neurons. The anterior (a) or the posterior (p) ends of the worms are marked. Upper two panel 100X, lower two panels 630X magnification. L4 stage worms shown. (B-E) The *flr-4* RNAi had limited effect on the life span of RNAi-deficient *rde-1(ne219)*. Life span is extended only in *rde-1(ne213); kbIs7* where the *rde-1* gene is rescued in the intestine of *rde-1(ne219)* or in *sid-1(pk3321);uIs69* where *sid-1* is rescued in the neurons of *sid-1(pk3321)*. No extension was noticed in *rde-1(ne219);kzIs20* (muscle rescue) or *rde-1(ne219);kzIs9* (hypodermis rescue). Life spans were performed at 20 °C.

https://doi.org/10.1371/journal.pgen.1007608.g002

receptor expression [30, 31]. We grew wild-type, *pmk-1(km25)*, *sek-1(km4)*, *nsy-1(ag3)*, *nsy-1(ok593)*, *tir-1(tm3036)* and *unc-43(e403)* on control or *flr-4* RNAi and performed life span analysis. We found that increased life span on *flr-4* RNAi is suppressed when any of the kinases in the p38 MAPK pathway or *tir-1* or *unc-43* is mutated (Fig 3A, S1 and S2 Tables). Interestingly, *pmk-3* is not required for the life span extension, showing specificity of the process (S1 and S2 Tables). Similar suppression of life span was observed when *flr-4(n2259)* was grown on *sek-1* RNAi (S7A Fig). We also created a *flr-4(n2259)*:*sek-1(km4)* double mutant and found that the life span was suppressed (S7B Fig). Further, in order to determine biochemically whether knocking down *flr-4* activates the p38 MAPK, we performed western blot analysis using a phospo-PMK-1-specific antibody (Figs 3B and S14). We found that in WT worms when *flr-4* is knocked down, PMK-1 phosphorylation increases in a *sek-1*-dependent manner. Further, TIR-1 or UNC-43 seems to be working in the same linear pathway as *flr-4*; in the *tir-1(3036)* and *unc-43*(*e408*), *flr-4* knockdown failed to increase phosphorylation of PMK-1 (S7C Fig). Together, the FLR-4 longevity signals are mediated by the p38 MAPK pathway.

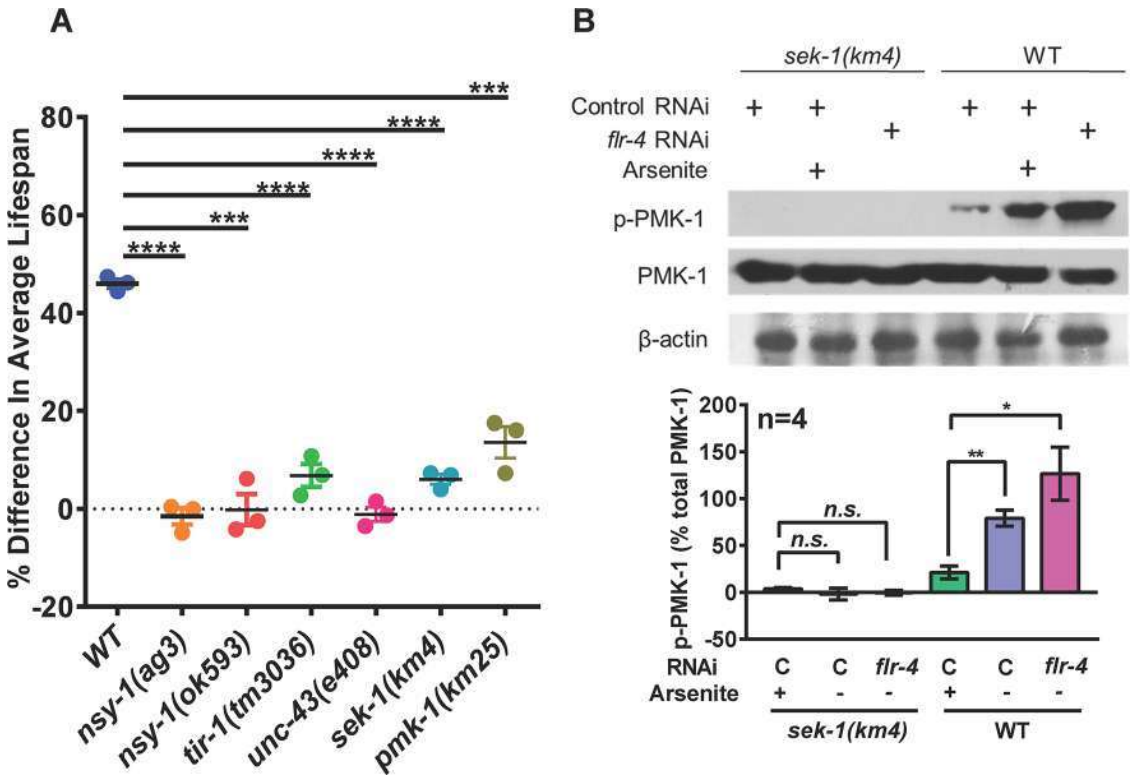

Fig 3. FLR-4 requires p38 MAPK pathway components to regulate life span. (A) The *flr-4* RNAi increased life span only in WT, but not to the same extent in *tir-1(tm3036)*, *unc-43(e408)*, *nsy-1(ag3)*, *nsy-1(ok593)*, *sek-1(km4)* or *pmk-1(km25)* mutants. The percent change in average life span on *flr-4* RNAi compared to control RNAi is plotted on the Y-axis. Error bar indicates SEM. $^{****}P \leq 0.0001$, $^{***}P \leq 0.001$, Student's *t* test. All life spans were performed at 20 °C. (B) Western blot analysis of young-adult WT or *sek-1(km4)* grown on control or *flr-4* RNAi using anti-phospho-PMK-1, anti-total PMK-1 or anti-β-actin antibodies. Quantification of the blot is shown below. The intensity of pPMK-1 and PMK-1 bands were normalized to beta-actin bands. Percent intensity of pPMK-1 with respect to total PMK is plotted. Average of 4 experiments shown. Error bar indicates SEM. $^{**}P \leq 0.01$, $^{*}P \leq 0.05$, n.s. not significant, Student's *t* test. The activation of p38 MAPK pathway with 20 mM Arsenite was used as a control. Blots from 4 biological replicates available in S14 Fig.

https://doi.org/10.1371/journal.pgen.1007608.g003

Flr-4 knockdown activates XDP genes in a p38 MAPK-dependent manner

In order to understand how *flr-4* knockdown increases life span, we performed transcriptomic analysis of wild-type worms grown on control or *flr-4* RNAi. We found that 1957 genes were upregulated (> 2 folds, $P \leq 0.05$) while 538 genes were down-regulated. We determined the biological functions of these genes using DAVID [32] and show that they are significantly enriched for genes involved in the Xenobiotic Detoxification Pathway (XDP) (Figs 4A and S8A). All these cytoprotective XDP genes are expressed in the intestine of the worms (www.wormbase.org). Using quantitative reverse transcriptase PCR (qRT-PCR), we verified 13 genes that were upregulated in our RNA-seq experiment (Figs 4B and S8B). We also used a transgenic worm expressing *gfp* driven by the *cyp-35B1* promoter and show that the expression of GFP is enhanced in the hind-gut region, when the worms were grown on *flr-4* RNAi (S8C Fig).

Next, in order to determine whether p38 MAPK pathway has any role in the regulation of these cytoprotective genes, we performed qRT-PCR analysis of these genes after knocking down *flr-4* in *sek-1(km4)*. Interestingly, majority of the XDP genes that were upregulated in the wild-type failed to do so in *sek-1(km4)* (Figs 4C and S8D). Since the levels of some of the genes do not fall back to basal level, it is possible that other signalling pathways or transcriptional

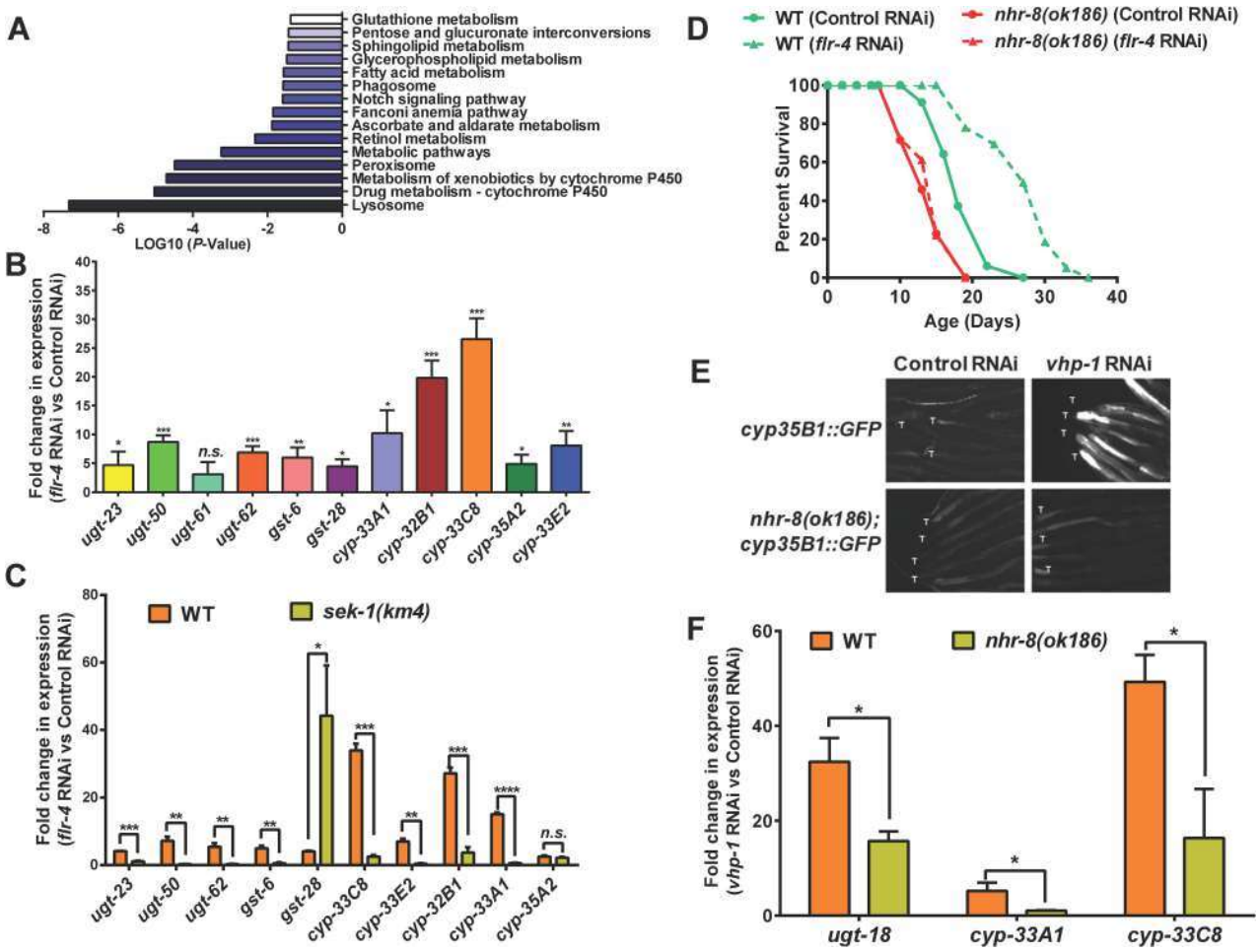

Fig 4. Knocking down *flr-4* transcriptionally activates the XDP genes in a p38 MAPK-dependent manner. (A) Enrichment of genes involved in xenobiotic metabolism among those that are upregulated when *flr-4* is knocked down using RNAi in WT, in comparison to control RNAi. Gene expression profiling was performed using RNA-seq and GO analysis performed using DAVID. Day 1 adult worms were used for RNA-seq. (B) Quantitative RT-PCR validation of expression of selected xenobiotic detoxification pathway (XDP) genes that were found to be upregulated using RNA-seq. (C) The expression of XDP genes is upregulated in WT in a *sek-1*-dependent manner when *flr-4* is knocked down. (D) In the *nhr-8(ok168)* mutant, life span is not extended when *flr-4* is knocked down. (E) Knocking down *vhp-1* using RNAi induced expression of GFP in *cyp-35B1p:gfp* but not in the *nhr-8(ok186);cyp-35B1p:gfp* transgenic worms. Images are of worms 48 hours post L4. Tails are marked by 'T'. Images captured at 100x magnification. (F) The expression of *ugt-18*, *cyp-33A1* and *cyp-33C8* are not upregulated in *nhr-8(ok186)* to the same extent as in WT, when *vhp-1* is knocked down using RNAi. Day 1 adult worms were used for RNA-seq and QRT-PCR. Error bar indicates SEM. $^{****}P \leq 0.0001$, $^{***}P \leq 0.001$, $^{**}P \leq 0.01$, $^{*}P \leq 0.05$, n.s. not significant, Student's *t* test.

https://doi.org/10.1371/journal.pgen.1007608.g004

regulators are also involved. These experiments suggested that p38 MAPK pathway regulates XDP genes downstream of *flr-4*.

Suppressing XDP genes prevent *flr-4*-mediated life span extension

In order to determine whether XDP genes are indeed required for life span extension brought about by *flr-4* knockdown, we used a mutant of *nhr-8*, a transcription factor required for XDP gene expression [16, 33]. First, we knocked down *flr-4* by RNAi in *nhr-8(ok186)* and found that it failed to increase life span to the same extent as in wild-type (Fig 4D). We also knocked down *nhr-8* using RNAi in *flr-4(n2259)*, and found that the life span of the mutant is significantly suppressed (S8E Fig). Finally, we show that in *nhr-8(ok186)*, the XDP genes fail to

upregulate to the same extent as in WT, when *flr-4* is knocked down (S8F Fig). Thus, increased expression of XDP genes is required for life span extension by *flr-4* knockdown.

Next, we asked whether NHR-8 functions downstream of p38 MAPK pathway to regulate XDP genes. For this, we decoupled p38 MAPK from *flr-4* and activated it by knocking down the phosphatase VHP-1 using RNAi [34, 35]. Knocking down *vhp-1* led to upregulation of *cyp-35B1*, as measured by increased GFP expression in the *cyp-35B1p*::*gfp* transgenic line. This enhancement was suppressed in the *cyp-35B1p*::*gfp;nhr-8(ok1853)* worms, showing that NHR-8 functions downstream of p38MAPK (Fig 4E). QRT-PCR analysis showed that three other XDP genes that are upregulated on *vhp-1* knockdown are dependent of NHR-8 (Fig 4F). Interestingly, knocking down *vhp-1* was not sufficient to increase life span of WT (S8G Fig), suggesting that additional downstream events may have to be coactivated in order to get life span benefits similar to *flr-4* knockdown.

Diet-specific activation of p38 MAPK and XDP genes in *flr-4(n2259)*

Since *flr-4(n2259)* shows differential response to OP50 and HT115 to extend life span, we suspected that this may be due to the ability of a diet to upregulate a specific set of genes. So, we performed transcriptomic analysis of wild-type and the mutant on the two bacterial diets. We found that the XDP genes are upregulated only when *flr-4(n2259)* was grown on HT115 but not when grown on OP50 (Fig 5A). We verified several of these genes using qRT-PCR and found them to be upregulated only on HT115 (Figs 5B and S9A). Additionally, we used the *flr-4(n2259);cyp-35B1p*::*gfp* strain to show that the expression of GFP is induced only when the worms are grown on HT115 (Fig 5C). Together, this shows that *flr-4* mutant worms mount a specific p38-dependent transcriptional response when fed HT115 that provide cytoprotective benefits leading to enhanced life span.

Next, we asked whether only HT115 can differentially activate the p38 MAPK pathway. For this, we performed western blot analysis with WT and *flr-4(n2259)* grown on HT115 or OP50. Interestingly, we found that *flr-4(n2259)* grown on HT115 showed enhanced phosphorylation of PMK-1 compared to wild-type (Figs 5D, S9B and S15). However, the levels of phosphorylation were unchanged in WT maintained on the two bacteria. Thus, FLR-4 prevents differential activation of p38 MAPK dependent on diet, maintaining adaptive capacity in *C. elegans*.

FLR-4 utilizes similar pathway as dietary restriction for longevity assurance

Since *flr-4* mutant worms responded differentially to diet, we evaluated the interaction of the gene with two nutrient sensing pathways. First, using RNAi we knocked down *flr-4* in the IIS pathway mutant *daf-2(e1370)* and found that the life span of the mutant is further extended, suggesting independent mechanisms (Fig 6A, S1 and S2 Tables). On the other hand, the life span of *eat-2(ad1116)* is not further extended; in fact, the life span was suppressed by 10–14% (Fig 6B). However, *flr-4* knockdown does not affect pharyngeal pumping of *eat-2(ad1116)*, similar to wild-type (S13 Fig), showing that the lack of additive effect on life span with *eat-2 (ad1116)* is not mechanical. In case of another genetic mimic of DR [16], the extended life span of *drl-1* RNAi worms was also not extended further by *flr-4* mutation (S10A Fig). This suggested that *flr-4* uses cellular signalling pathways utilized by DR, but not the IIS pathway to ensure longevity. This was further supported by the fact that life span of *flr-4* RNAi, as in *eat-2* mutants and on *drl-1* knockdown, was dependent only on the FOXA transcription factor PHA-4, and not the FOXO factor DAF-16 that is required by IIS pathway mutants (Figs 6C, 6D and S10B). In the *pha-4(zu225)*, life span extension by *flr-4* knockdown was completely abrogated. Interestingly, the life span of the *flr-4(n2259)* or *flr-4* RNAi worms was independent

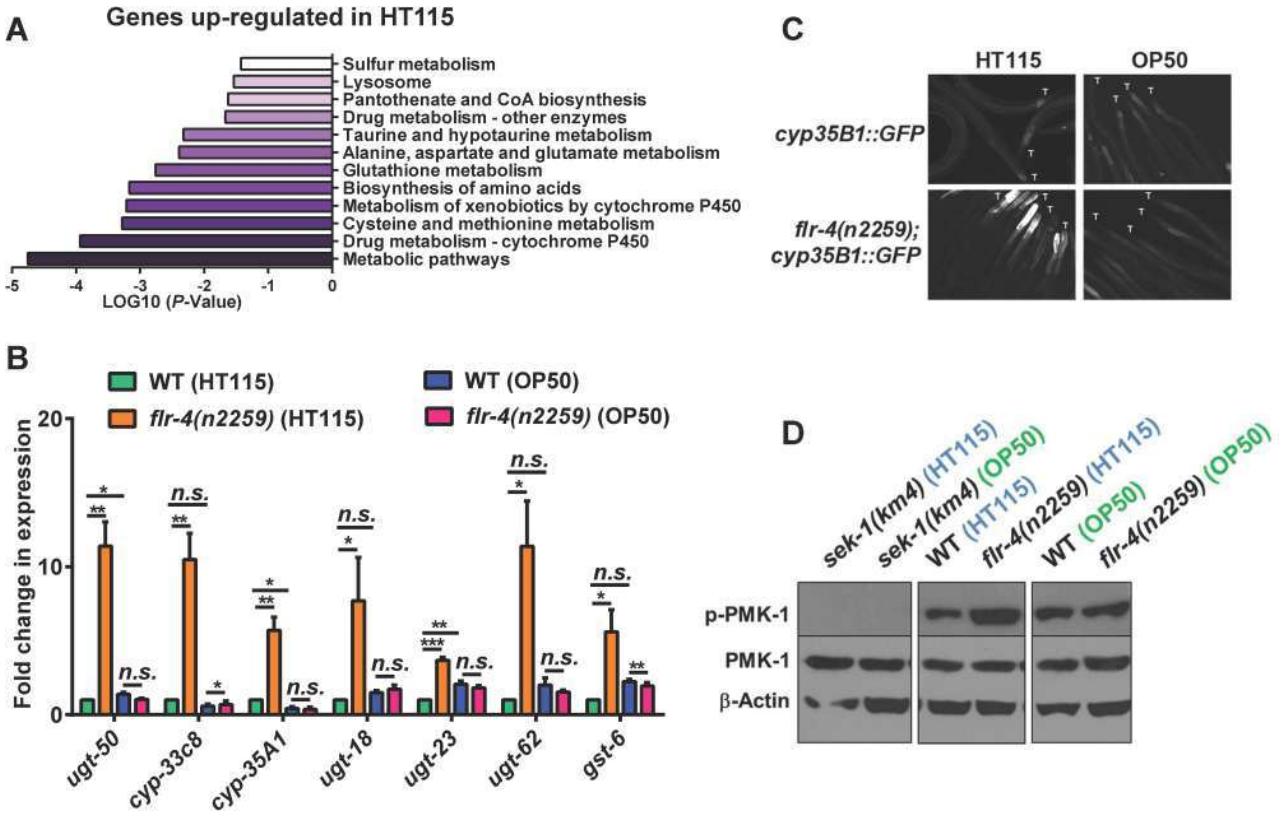

Fig 5. HT115 activates p38 MAPK pathway in *flr-4(n2259)*. (A) RNA-seq of *flr-4(n2259)* shows that genes involved in xenobiotic detoxification pathway (XDP) are upregulated only when worms were fed *E. coli* HT115. RNA from WT or *flr-4(n2259)* worms grown on HT115 or OP50 were used for sequencing. Genes upregulated on HT115 but not on OP50 were analyzed using DAVID. (B) Quantitative RT-PCR validation of RNA-seq data for selected XDP genes. These genes were upregulated only when *flr-4(n2259)* worms were fed HT115. Error bar indicates SEM. $^{****}P \leq 0.0001$, $^{***}P \leq 0.001$, $^{**}P \leq 0.01$, $^{*}P \leq 0.05$, n.s. not significant, Student's *t* test. (C) Expression of GFP in *cyp-35B1p::gfp* was upregulated only when the worms were fed HT115. Images are of worms 48 hours post L4. Tails are marked by 'T'. Images captured at 100x magnification. (D) Western blot analysis of WT or *flr-4(n2259)* grown on HT115 or OP50 using anti-phospho-PMK-1, anti-total PMK-1 or anti-β-actin antibodies. Quantification of the blot is shown in S9B Fig. Blots from 4 biological replicates available in S16 Fig. Day 1 adult worms were used for RNA-seq and QRT-PCR analysis.

https://doi.org/10.1371/journal.pgen.1007608.g005

of the NRF2 ortholog, SKN-1, a common output of insulin-like signalling and DR [36, 37] (S10C and S10D Fig); *skn-1* abrogation by mutation or RNAi affects the life span of WT and *flr-4* knockdown worms to similar extent. Further, similar to DR [16, 38], the *flr-4* RNAi did not further extend the already long life span of germline defective mutants (S11 Fig). Like many long lived mutants, *flr-4* mutants have delayed reproductive span and lower brood size compared to WT, mainly on HT115 (S12 Fig). This may be due to more resource allocation towards somatic maintenance during DR [39] and may be caused by lower germ cell proliferation as seen in case of insulin-IGF-1 signalling pathway mutants [40]. The fact that FLR-4 utilizes the DR machinery for longevity assurance is also consistent with its role in ensuring adaptive capacity to diet.

Discussion

A complex interaction between genes and diet determines the rate of aging and predisposes an individual to age-related diseases. The term gene-diet pair is used when the consequences of mutating a gene is visible only on a specific diet [12]. Surprisingly, only a few gene-diet pair have been identified that regulates aging, mainly through studies in *C. elegans* [12]. In this

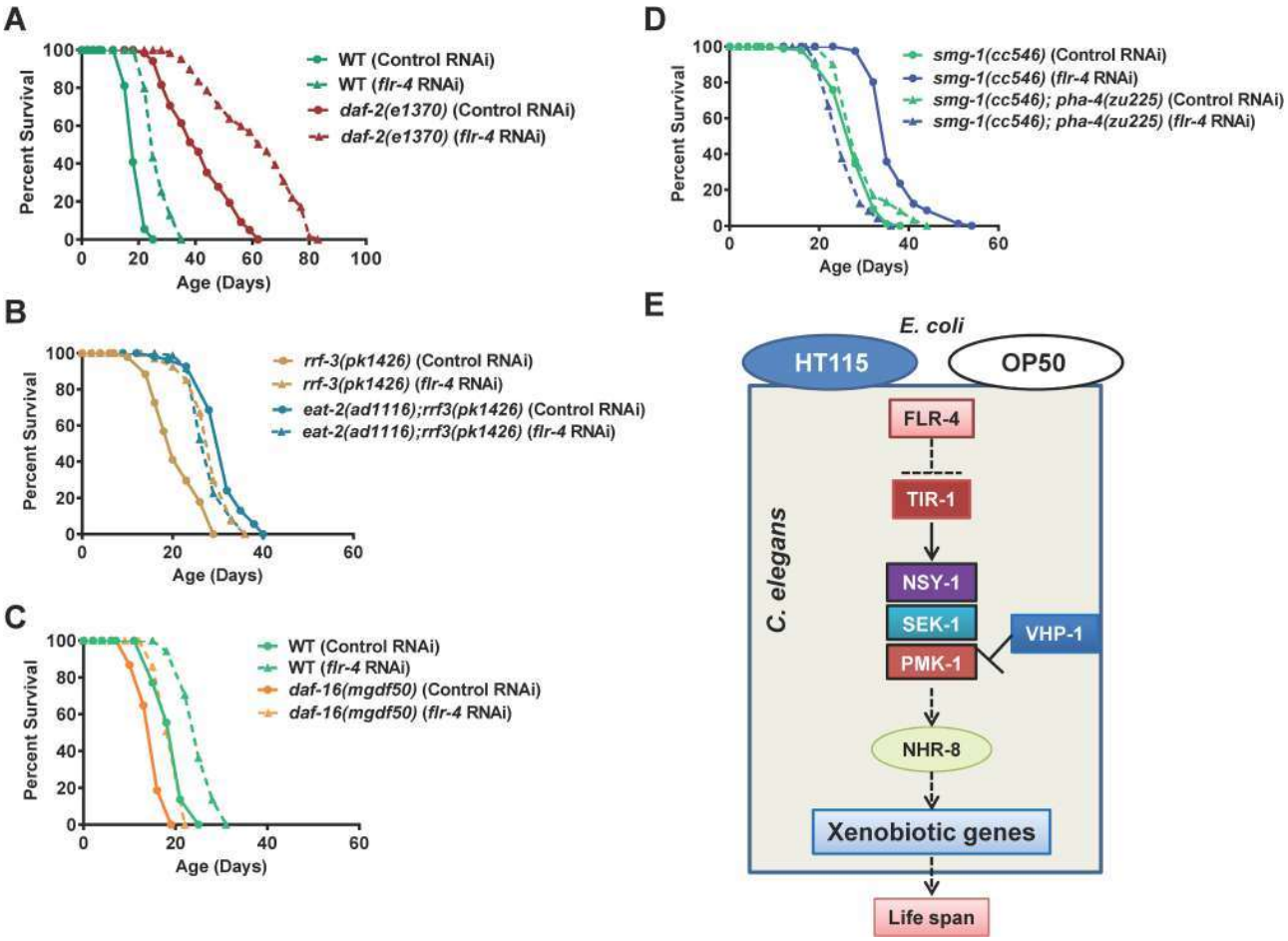

Fig 6. FLR-4 and dietary restriction use similar mechanisms for longevity assurance. (A) The life span of *daf-2(e1370)* was further increased when *flr-4* was knocked down using RNAi. (B) The life span of *eat-2(ad1116)* was not further extended when grown on *flr-4* RNAi. The RNAi hypersensitive strain *rrf-3(pk1426)* was used to ensure maximum RNAi efficiency in the feeding defective *eat-2* mutant. (C) The extended life span of *flr-4* RNAi worms is not dependent on *daf-16*. Life spans were performed at 20 °C. (D) The life span extension on *flr-4* knockdown is dependent on *pha-4*. The *smg-1 (cc546)* as well as *pha-4(zu225);smg-1(cc546)* were maintained at 25 °C and the life span was performed at 15 °C to inactivate PHA-4. (E) A model of FLR-4 function. FLR-4 negatively regulates the p38 MAPK pathway. RNAi knockdown or mutation in *flr-4* activates the pathway and leads to xenobiotic gene upregulation through NHR-8, providing life span benefits. In the kinase-dead *flr-4(n2259)* mutant, the pathway is only activated on HT115 and not OP50.

https://doi.org/10.1371/journal.pgen.1007608.g006

report, we identify a novel gene-diet pair and show that the adaptive capacity to different food-type is modulated by the protein kinase FLR-4. This protein prevents differential activation of the p38 MAPK pathway dependent on the food-type and consequently, the expression of cyto-protective genes by transcription factor NHR-8 (Fig 6E). Interestingly, this pathway overlaps with the DR pathway, suggesting a cross-talk between cellular signalling that senses food quality and quantity to regulate life history traits like aging.

FLR-4 is a serine-threonine protein kinase similar to mammalian Cyclin-dependent protein kinase 3 (31% identity, 50% similarity, E value 8e-22). It was initially identified in a screen for genes involved in fluoride tolerance [41], but was subsequently shown to have defects in ultradian rhythm in the intestine that controls defecation [15]. In this study, we elucidate a novel function for FLR-4 in the intestine and neurons that is independent of its role in defection. The temperature-sensitive kinase dead mutant *flr-4(n2259)* has normal defecation cycle at 20 °C [15], a temperature at which most of our assays were performed. In view of the central role

that this kinase plays in controlling multiple important phenotypes, future research needs to be directed towards finding its immediate cellular targets. This is particularly important as we found that the food-type-dependence is specific to the kinase dead mutant; RNAi knockdown using an OP50-based system also increased life span. This suggests that the kinase-dead mutant may not be able to phosphorylate a substrate(s) that is required to maintain life span homeostasis on the different bacterial diets.

Considering the importance of gene-diet pairs in aging and disease, our understanding of the mechanisms of adaptive capacity to food-type is still in its infancy. Previous studies have identified a few genes that play a role in this process. Notably among them are the RICTOR ortholog *rict-1* [6], neuromedin U receptor ortholog *nmur-1* [14] and mitochondrial 1-pyrroline-5-carboxylate dehydrogenase (P5CDH) *alh-6* [11]. The *rict-1* mutants have phenotypes similar to *flr-4* mutant worms such that they have shorter life span on OP50 while exhibiting life span extension on HT115 [6]. However, in contrast to the *flr-4*, *rict-1* regulates feeding behaviour when an animal encounters diets of different qualities. The *rict-1* mutants have different pumping rates and exhibit avoidance behaviour on food of diverse quality [6, 12]. The *alh-6* mutants, on the other hand, show accelerated aging when fed OP50 while retaining normal rates of aging on HT115 [11]. Interestingly, the *nmur-1* mutants have longer life span on OP50 but not on HT115 [14]. Thus, these gene-diet pairs seem to control diverse aspects of an animal's response to different food. In future, it will be interesting to study the interaction of these genes with *flr-4*, considering the fact that opposing phenotypes controlled by these genes may indicate homeostatic control of life span in response to different diet.

As the above mutants differ in their response to different diet, they may also activate diverse signalling cascades. This is apparent from the fact that *rict-1* and *nmur-1* interact differentially with the downstream components of the insulin signalling pathway [6, 14, 42]. While the life span extension of *rict-1* knockdown is dependent on NRF2 ortholog *skn-1*, *nmur-1* mutants require the FOXO transcription factor DAF-16. We found that the *flr-4* mutants require the FOXA transcription factor PHA-4 for life span extension and is independent of DAF-16; its transcriptional response may thus be different from other gene-diet pairs. Since both *alh-6* and *flr-4* may signal through a pathway used by the *eat-2* model of DR, it will be interesting to study the transcription factor requirements of the former. Comparative gene expression profiles of these mutants on different diet will help us understand the complex gene expression modalities controlled by these gene-diet pairs.

Gustatory and olfactory neurons that perceive chemical signals have previously been shown to affect life span [10, 14, 43]. Here we show that *flr-4* knockdown in the neurons can also increase life span. In fact, the life span extension by *flr-4* RNAi requires the CAMKII ortholog UNC-43 and SARM ortholog TIR-1 that is known to act in the neurons to determine cell fate. On the other hand, intestine-specific knockdown of *flr-4* also increases life span. Although it appears intuitive to suggest that the gut may play an important role in sensing different diet that is ingested, the role of the intestine in food-type-dependent life span extension is less known. Interestingly, TORC2 that also regulates food-type-dependent life span, requires SKN-1/NRF2 in the intestine to regulate life span [42]. However, FLR-4 life span is independent on *skn-1*, indicating to extensive insulation as well as cross-talks among these pathways. Future research needs to be directed to understand the partitioning of the p38 MAPK pathway in the neurons and intestine as well as their cross-talk to regulate *flr-4*-mediated life span.

Animals in the wild, unlike those in laboratories, are exposed to a wide variety of food that they have adapted to. Being able to utilize a wide range of diet is evolutionarily advantageous as the animals can survive when their optimal diet is depleted. Giant panda that depend mainly on bamboo for nutrition is facing extinction due to loss of habitat (wwf.panda.org)[44]. Since diet influences the rate of aging, the animals have evolved intricate mechanisms to maintain

homeostasis. In addition to the quality of diet, the quantity of food regulates the plasticity of aging. As a result, DR is able to delay aging and increase life span across the animal kingdom [45, 46]. In our study as well as in that of *alh-6* [11], we observe genetic overlap with DR, suggesting that organisms have evolved cellular modules that evaluate both quality and quantity of diet to regulate life span.

We show that FLR-4 signals through the p38 MAPK pathway to regulate the expression of cytoprotective genes dependent on diet. In *C. elegans*, this pathway has been extensively characterized for its role in mediating innate immune response towards pathogenic bacteria as well as in mounting an oxidative stress response [21, 23, 47–49]. On the other hand, the XDP genes have been shown to provide cytoprotective effects leading to enhanced life span in multiple models of longevity [16, 50–52]. The fact that FLR-4 would signal differences of diet through the p38 MAPK seems quite intuitive for an organism that feeds on bacteria and uses this same pathway to differentially activate immune genes on encountering pathogens. But in case of *flr-4* knock down, immune effector genes are not upregulated, showing specificity of this module. However, in mammals, the p38 MAPK has important role in regulating metabolism in liver and adipocytes during fasting, mediated by glucagon and insulin [53]. It will be interesting to study the role of p38 MAPK pathway in gene-diet interaction networks in mammals.

How *flr-4* mutants sense the differences in bacterial food remains to be answered. One possibility is that the mutants become sensitive to the presence or absence of a metabolite secreted by the bacteria and mount the specific response, whereas the WT worms are able to maintain homeostasis. Detailed metabolomics study will be able to reveal the exact nature of the molecule. One interesting observation is that genes that are upregulated in *flr-4(n2259)*, grown specifically on HT115, are enriched in amino acid metabolism. Previous studies have shown that methionine metabolism greatly influences life span, metabolism, and stress resistance [54–56]. Vitamin B12 acts an important cofactor in methionine as well as propionic acid metabolism, maintaining optimal level of Homocysteine and propionic acid, thereby preventing toxicity [54]. It is possible that the molecule may be vitamin B12, as seen in case of *Comamonas* [17, 57, 58]. In line with this idea, we found that the levels of the metabolic sensor *acdh-1* is much suppressed in HT115-fed *flr-4(n2259)* in our RNA-seq data, similar to the effect of vitamin B12 treatment. However, *flr-4* mutants do not have any significant defect in development or fat storage. In future, why *flr-4* mutants become sensitive to a metabolite or whether the two bacteria differ in production of soluble metabolites needs to be addressed. We also need to understand why the RNAi knockdown of the gene do not induce food-type-dependent life span response.

Together, our study discovers a new gene-diet pair that controls the plasticity of aging in *C. elegans* and reveals a complete signal transduction cascade involved in this process.

Materials and methods

C. elegans strains and maintenance

C. elegans strains used in this study were obtained from the Caenorhabditis Genetics Center and maintained on NGM agar plates at 20˚C, unless otherwise stated, on *Escherichia coli* OP50 lawns. All RNAi experiments were initiated with synchronized L1 worms. Strains used in the study are: N2 Bristol as wild-type, *flr-4(n2259)X*, *rde-1(ne219) V*, *rde-1(ne219) V;kzIs9*, *rde-1 (ne219) V;kzIs20*, *rde-1(ne213) V;kbIs7*, *sid-1(pk3321) V*, *sid-1(pk3321) V;uIs69 V*, *ccIs4251* [pSAK2 (*myo-3*::*NGFP-LacZ*)], *tir-1(tm3036)III*, *unc-43(e408)IV*, *nsy-1(ag3)II*, *nsy-1(ok593)II*, *sek-1(km4)X*, *pmk-1(km25)IV*, *pmk-3(ok169)IV*, *flr-4(n2259)X; sek-1(km4)X*, *nhr-8(ok186) IV*, *daf-2(e1370)III*, *bvIs5* [*cyp-35B1p*::*GFP* + *gcy-7p*::*GFP*] referred to as *cyp-35B1p*::*gfp* in this manuscript, *nhr-8(ok186) IV;bvIs5*, *flr-4(n2259)X;bvIs5*, *rrf-3(pk1426)II;eat-2(ad1116)II*, *rrf-3*

(pk1426)II, *daf-16(mgdf50)I*, *smg-1(cc546)*, *smg-1(cc546)I;pha-4(zu225)V*, *skn-1(zu169) IV/nT1 [unc-?(n754) let-?](IV;V)*, *glp-1(e2141)III*, *gld-1(op236)I*, *glp-4(bn2ts)I*, *hsf-1(sy441)*.

Lifespan analysis

Gravid adult worms, initially grown on *E. coli* OP50, were bleached and the eggs were L1 synchronized in M9 buffer for 16 hours before placing them on the respective RNAi plates (say 'X' gene RNAi). Once worms reached L4 stage, they were transferred to intermediate RNAi plates (seeded with the same 'X' gene RNAi) for 12 hours. After that, the worms were picked onto fresh 'X' gene RNAi plates overlaid with 5-fluorodeoxyuridine (FUDR, final concentration 0.1 mg/ml of media). For life span analysis on plates without FUDR, worms were transferred to fresh plates on alternate days till the end of the reproductive span. Life span scoring was initiated at day 7 of adulthood and continued every alternate day. For statistical analyses of survival, OASIS software (http://sbi.postech.ac.kr/oasis) was used and *P*-values were calculated by using a log rank (Mantel-Cox method) test.

For temporal requirement experiments, L1 synchronized worms were placed on control RNAi plates. Worms from the plates were transferred to *flr-4* RNAi plates at L2, L3, L4 or YA stages. FUDR was overlaid on the plates 12 hrs after the worms reached L4.

For life span on different bacterial feed, L1 synchronized worms were placed on HT115 and OP50-seeded plates and the lifespan was initiated as mentioned above.

All life span analysis referred in the main text is provided in the S1 Table. Two independent biological replicates are provided in S2 Table.

Body bend assay

A total of 20 worms each from control or *flr-4* RNAi plates were transferred to an unseeded plate on day 2, 5 and 10 of adulthood. Each worm was gently prodded on the tail with a platinum wire and total number of body bends per 30 seconds was counted. A body bend was scored every time the area behind the pharynx reached a maximum bend in the opposite direction from the last bend counted.

Muscle integrity measurements

The *ccIs4251* [pSAK2 (*myo-3*::*NGFP-LacZ*)] worms were grown on control or *flr-4* RNAi plates. On day 2, 5 and 10 of adulthood, the worms were paralyzed on 2% agarose pads in the presence of 20 mM sodium azide. Photographs of the worms were captured at 630X magnification using an AxioImager M2 microscope (Carl Zeiss, Germany) fitted with Axiocam MRm [Excitation 488nm and Absorbance at 520nm]. For each RNAi, at least 10 nuclei of 10 worms each were photographed. Morphology of each muscle nuclei was scored as 'intact', 'moderately damaged' or 'severely damaged'. A nucleus was scored as 'intact' if it had intact membrane with no degradation, 'moderately damaged' when the nuclear membrane appeared to disintegrate but the nucleoplasm displayed no or very little dark patches and 'severely damaged' when the nuclei had increased nucleolar size, dark patches in the nucleoplasm, distorted appearance and membrane disintegration.

Lipofuscin autofluorescence

To determine lipofuscin autofluorescence, 20 worms each grown on control or *flr-4* RNAi were anesthetized in 20mM Sodium Azide and mounted on 2% agarose pads on day 1, 5 and 10 of adulthood. The worms were visualized under microscope using FITC filter and images were captured using a constant exposure time (1.2 sec).

RFP beads ingestion assay

Twenty five L4 worms, grown on respective bacterial feed, were picked and placed onto NGM plates seeded with 250:1 (vol:vol) of bacteria and Fluoresbrites Multifluorescent microspheres/ RFP beads (0.2 μm diameter, Polyscience Inc., USA). After 10 minutes, worms were collected and washed twice with 1X M9 buffer to remove any bead attached to the body surface. Worms were finally re-suspended in 30 μl of 1X M9 buffer and transferred to a freshly prepared 2% agarose pad slides. The images of worms were taken using AxioImager M2 microscope (Carl Zeiss, Germany). Quantification was performed using NIH ImageJ software.

Pharyngeal pumping rate

An one minute video of Day 1 adult worms was taken using Axiocam MRm camera attached to M205FA microscope (Leica, Germany). The video was slowed down and pharyngeal pumping was counted for that 10 second period.

Body size

Worms were imaged one day after they reached L4 using Axiocam MRm camera attached to an AxioImager M2 microscope (Carl Zeiss, Germany). Area of the worms was quantified using NIH ImageJ software.

Cloning

flr-4 RNAi: The full length cDNA sequence of *flr-4* was amplified using primers listed in S3 Table and cloned into pL4440 RNAi vector.

Generation of *flr-4* transgenic worms

A transcriptional fusion of the *flr-4* promoter and a green fluorescent protein (GFP) gene was constructed in pPD95.75. The 3.5 kb promoter region upstream of start codon of *F09B12.6* was amplified using primers listed in S3 Table and HiFidelity PCR system (Kapa Biosystems, USA) and cloned into pPD95.75 using *Bam*HI and *Kpn*I restriction sites. The recombinant plasmid was injected at a concentration of 5ng/μl into the syncytial gonad of wild-type worms along with 100ng/μl pRF4 (*rol-6)* co-injection marker using a Microinjection setup consisting of Nikon TiS inverted microscope fitted with Eppendorf Femtojet Express and Transferman NK2. Transformants were selected based on the rolling phenotype as well as the presence of GFP expression. Fluorescence images of transgenic worms were captured under AxioImager M2 microscope (Carl Zeiss, Germany) fitted with Axiocam MRm at 40X magnification [Excitation 488nm and Absorbance at 520nm].

The full length cDNA sequence of *flr-4* was amplified using primers listed in S3 Table. The *gfp* sequence of *Pflr-4*::*gfp* plasmid was then excised using *Kpn*I and *Eco*RI and replaced with the amplified *flr-4* cDNA sequence, generating the *Pflr-4*::*flr-4 cDNA* construct. The *Pflr-4*::*flr-4* cDNA construct and pRF4 were co-injected in the germline of *flr-4(n2259)* (concentrations: 150 ng/μL pRF4 and 5 ng/μL *Pflr-4*::*flr-4 cDNA*). Wild-type and *flr-4(n2259)* roller lines were generated by injecting 150 ng/μL pRF4. Lines were maintained by picking rollers.

RNA isolation

Synchronized L1 worms grown on OP50 or RNAi plates were collected at Day 1 of adulthood in M9 buffer and washed thrice using M9 buffer. Then, Trizol was added to about 4 times the volume of the worm pellet and the worms lysed using two freeze thaw cycles, followed by vigorous vortexing. RNA was purified by phenol:chloroform:isoamylalcohol extraction and

isopropanol precipitation. For quantitative Reverse Transcriptase PCR (qRT-PCR) experiments, the concentrations of the RNA were determined using NanoDrop 2000 (Thermo Scientific, USA) and the quality of the ribosomal 28 S and 18 S on denaturing agarose gel was used for evaluation of RNA integrity. For transcriptomic analysis, the quality was evaluated using Bioanalyzer (Agilent, USA) and only RNA with RIN number above 9 was used for RNA-seq.

QRT-PCR analysis

About 2.5 μg of RNA was converted to cDNA using Superscript III Reverse Transcriptase enzyme and poly-T primers (Invitrogen, USA). QRT-PCR analysis was performed using the DyNAmo Flash SYBR Green mastermix (Thermo Scientific, USA) and Realplex PCR system (Eppendorf, USA) to determine the relative gene expression levels. Statistical analysis was performed using GraphPad 7.0. All the primers used are listed in S3 Table.

Transcriptomic analysis

RNA-Sequencing (RNA-seq) libraries of WT grown on Control RNAi or *flr-4* RNAi, and WT or *flr-4(n2259)* grown on HT115 or OP50 at Day 1 adulthood were prepared as recommended by the Illumina TruSeq RNA Sample Preparation kit using Low-Throughput (LT) Protocol (Illumina, Inc., USA). Sequencing of libraries was performed using Illumina GAII_X for 78 cycles including 6 additional cycles for index read. Sequence reads were aligned using CLC Genomics Workbench 6.5.1 with default setting against *C. elegans* genome assembly (WS231). Unpaired group comparisons, based on RPKM (Reads per Kilobase per Million mapped reads), were chosen as expression values for comparing the samples. A fold change ±2.0 and *P* value $\leq$0.05 (Kal's Z test) were used to filter the differentially expressed genes. GO-term enrichment analysis was performed using the DAVID Bioinformatics Database [32]. The sequencing data is available as BioProject ID: PRJNA362992.

Western blotting

Synchronized L1 worms, grown on OP50 or HT115-seeded plates, were collected at Day 1 of adulthood in 1xM9 buffer and washed thrice using the same buffer. The pellet was freeze-thawed 3 times in a protein extraction buffer (20 mM Hepes buffer pH 7.9, 25% glycerol, 0.42 mM NaCl, 1.5 mM $MgCl_2$ hexahydrate, 0.2 mM EDTA dihydrate, 0.5 mM DTT) in presence of a protease inhibitor cocktail (Sigma, USA), sonicated in a waterbath-based sonicator (Diagenode, USA) and centrifuged at 10,000 rpm for 10 mins. The protein concentration in the supernatant was estimated by using Bradford reagent (BioRad, USA).

About 30 μg of protein was separated on a 12% SDS-PAGE and transferred to Nitrocellulose membrane. The membranes were blocked for 1 hour in 5% non-fat milk and 5% BSA dissolved in 1X TBST (TBS with 0.1% Tween 20) and probed with anti-PMK-1 antibody (1:2,000 dilution in blocking buffer; Cell Signaling Technology, USA) or anti-phospho-PMK-1 antibody (1:2,000 dilution in blocking buffer; Cell Signaling Technology, USA), incubated overnight at 4˚C. Next day, the membranes were washed thrice with 1X TBST and further incubated with 1:10,000-diluted secondary antibody (anti-rabbit conjugated to HRP, Cell Signaling Technology, USA) for 1 hr at room temperature. The blots were then washed 4–5 times with 1X TBST, each wash lasting 10 min. The blots were developed using enhanced chemiluminiscent substrate (Millipore, USA).

For the quantification of PMK-1 activity, the band intensities of pPMK-1 and total PMK-1 were quantified using ImageJ software (National Institutes of Health, Bethesda, MD; http://rsb.info.nih.gov/ij/) and divided with the intensity of the beta-actin bands. The value thus

acquired for pPMK-1 was then divided by that of total PMK-1 and represented as percentage. The immunoblots of four independent experiments were quantified.

Arsenite treatment

Well-fed young adult worms from control RNAi-seeded plates were collected and washed thrice in M9 buffer. The worm pellet was then divided into two halves; to one half 120 μl of 1X M9 buffer was added while to the other half 120 μl of 1X M9 buffer containing 20mM sodium arsenite was added. After incubation at 20˚C for 20 minutes, the worms were washed thrice with M9 buffer. The worm pellet was then processed for protein isolation and western blotting using the above-mentioned method.

UV-resistance assay

Worms were grown on respective RNAi from L1 onwards. For each RNAi, four 60 mm unseeded NGM plates with approximately 25 L4 worms per plate were irradiated using a 254 nm UV bulb at $10Jm^{-2}min^{-1}$ in a CL-1000 UV Crosslinker (Ultra-Violet Products Limited), followed by transfer to the respective RNAi-seeded NGM. All UV-resistance assays were performed at 20 ^{o}C. Survival to stress was scored every 24 hrs post UV exposure.

Heat-resistance assay

The worms were grown on RNAi plate as above. For each RNAi, three 60 mm NGM plates with approximately 40 L4 worms per plate were incubated at 35 ^{o}C. Animal survival was scored every 60 min.

Reproductive span and brood size assay

Wild-type or *flr-4(n2259)* mutant worms were grown on two different *E. coli* feed, OP50 or HT115 till late L4 stage. Five worms were picked onto fresh plates (OP50 or HT115 seeded) and allowed to lay eggs for 24 hours. Three such plates were used for each assay so that 'n' was 15 per experiment. The worms were then transferred to fresh plates every day and the eggs/L1s on previous day's plate were counted. Worms that crawled off the plates or ruptured before the fertile period ended were discarded. Eggs that produced viable progeny were considered as total L1s and the un-hatched eggs were considered as dead eggs. Pool of total L1s and dead eggs are defined as brood size. Data is presented as brood size ± SEM. For calculating reproductive span, total number of L1s is expressed per worm per day. Data is shown as viable progenies plotted against number of days, with SEM at each time point.

Development rate

Gravid adult worms, initially grown on *E. coli* OP50, were bleached and the eggs were L1 synchronized in M9 buffer for 16 hours before placing them on seeded NGM plates. The worms were then scored every 12 hours till 60th hour for their development stage.

Ethics statement

The study was performed with approval from the Institutional Biosafety committee. Only invertebrate nematodes were used for the study.

Supporting information

S1 Fig. (A) Life span of WT worms is extended to same extent in absence or presence of FUDR, when *flr-4* is knocked down using RNAi. In absence of FUDR, worms were transferred to fresh plates every day during the reproductive phase. (B) The *flr-4(n2259)* worms have increased life span when grown on HT115 compared to OP50, both in absence as well as in presence of FUDR. Life spans performed at 20 ^{o}C.
(PDF)

S2 Fig. (A) The *flr-4* RNAi worms have lower lipofuscin accumulation with age as compared to age-matched WT worms. Images captured at 100x magnification. (B) Muscle nuclei degeneration was delayed in *myo-3*::*gfp* transgenic worms grown on *flr-4* RNAi. Nuclei were categorized as intact, moderately or severely degraded according to representative photographs in the left (refer to materials and methods). n > 20. Images captured at 630x magnification. (C) Analysis of age-dependent changes in number of body bends in worms grown on control or *flr-4* RNAi. Student's *t* test was used to determine statistical significance on each day between control and *flr-4* RNAi-treated worms, n>40. (D) The *flr-4* RNAi worms have smaller body size compared to control RNAi. (E) Pharyngeal pumping does not change significantly when day 1 adult WT or *flr-4(n2259)* was grown on either HT115 or OP50. Average of 6 biological replicates shown. In each replicate, >15 worms were monitored. (F) WT as well as *flr-4(n2259)* worms ingest similar amounts of RFP-tagged beads when maintained on HT115 or OP50. For analysis of body size and RFP beads ingestion, Day 1 adult worms were used.
Error bars indicate SEM. $^{****}P\leq0.0001$, $^{**}P\leq0.01$,$^{*}P\leq0.05$, n.s. is not significant. Student's t-test.
(PDF)

S3 Fig. Developmental rate of WT and *flr-4(n2259)* worms when maintained on control RNAi or flr-4 RNAi. Worms were synchronized at L1 and stages were determined at the indicated hours. *P*-value not significant in all except at 60th hour between WT and *flr-4(n2259)* on control RNAi (Two-way ANOVA).
(PDF)

S4 Fig. (A) UV stress tolerance assay was performed with WT worms grown on control or *flr-4* RNAi. The L4 stage worms were exposed to 10 J m^{-2} min^{-1} of UV and mortality was scored every day. (B) Heat stress assay was performed by exposing the L4 stage WT worms grown on control or *flr-4* RNAi to 35 ^{o}C and mortality scored every hour. (C) The life span of WT and *hsf-1(sy441)* are extended to the similar extent when *flr-4* is knocked down. (D) *Hsf-1* RNAi suppressed the life span of WT and *flr-4(n2259)* to similar extent. Life span performed at 15 ^{o}C.
(PDF)

S5 Fig. Developmental rate of WT and *flr-4(n2259)* worms when maintained on HT115 or OP50. Worms were synchronized at L1 and stages were determined at the indicated hours. *P*-value not significant (Two-way ANOVA).
(PDF)

S6 Fig. *Flr-4* knockdown is required early in life to increase life span. Maximum life span is observed when *flr-4* is knocked down starting at L1 or L2 (A-B). The effect decreases when knockdown is initiated at L3 or L4 (C-D). No life span increase was observed when knockdown was initiated on day 1 of adulthood (E). All life spans were performed at 20 ^{o}C.
(PDF)

S7 Fig. (A) The extended life span of *flr-4(n2259)* is suppressed by *sek-1* RNAi. (B) The life span of *flr-4(n2259)* is suppressed to the levels of *sek-1(km4)* in the double mutant *flr-4(n2259);*

sek-1(km4). Life spans performed at 20 °C. (C) Western blot analysis of day 1 adult WT, *unc-43(e408)* or *tir-1(tm3036)* grown on control or *flr-4* RNAi using anti-phospho-PMK-1, anti-total PMK-1 or anti-β-actin antibodies. Quantification of the blot is shown below. The intensity of pPMK-1 and PMK-1 bands were normalized to beta-actin bands. Percent intensity of pPMK-1 with respect to (w.r.t.) total PMK is plotted. Average of 3 experiments shown. Error bars are SEM. $^{**}P \leq 0.01$, n.s. not significant, Student's *t* test. The activation of p38 MAPK pathway with 20 mM Arsenite was used as a control.
(PDF)

S8 Fig. (A) Fold changes based on RPKM values between WT on control or *flr-4* RNAi as determined by RNA-seq. (B) The expression of *ugt-16* and *ugt-18* are upregulated when *flr-4* is knocked down using RNAi. (C) The expression of GFP in *cyp-35B1p::gfp* was induced in the lower gut region when *flr-4* is knocked down using RNAi. Head and tail are marked with H and T, respectively. Images are of worms 48 hours post L4. Images captured at 100x magnification. (D) The expression of *ugt-16* and *ugt-18* are not upregulated in *sek-1(km4)* to the same extent as in WT, when *flr-4* is knocked down using RNAi. (E) The life span of *flr-4(n2259)* is suppressed to a greater extent (35% against 21%) compared to WT when these worms were grown on *nhr-8* RNAi. (F) The expression of *ugt-18*, *cyp-32B1* and *gst-28* are not upregulated in *nhr-8(ok186)* to the same extent as in WT, when *flr-4* is knocked down using RNAi. Error bar indicates SEM. $^{****}P \leq 0.0001$, $^{***}P \leq 0.001$, $^{**}P \leq 0.01$, $^{*}P \leq 0.05$, n.s. not significant, Student's *t* test. Day 1 adult worms were used for RNA-seq and QRT-PCR. (G) The life span of WT worms does not change when *vhp-1* is knocked down using RNAi. Life spans were performed at 20 °C.
(PDF)

S9 Fig. (A) QRT-PCR validation of RNA-seq data for *ugt-16* which is upregulated only when *flr-4(n2259)* worms were fed HT115. (B) Quantitation of data of Fig 5D. The intensity of pPMK-1 and PMK-1 bands were normalized to beta-actin bands. Percent intensity of pPMK-1 with respect to (w.r.t.) total PMK is plotted. Average of four experiments shown. Error bars are SEM. $^{***}P \leq 0.001$, $^{**}P \leq 0.01$, $^{*}P \leq 0.05$, n.s. not significant, Student's *t* test. Day 1 adult worms were used for QRT-PCR and western blot analysis.
(PDF)

S10 Fig. (A) Knocking down *drl-1* by RNAi does not further prolong the extended life span of *flr-4(n2259)*. (B) The *daf-16* RNAi suppresses life span of WT and *flr-4(n2259)* to similar extent. (C) The *skn-1* RNAi suppresses life span of WT and *flr-4(n2259)* to similar extent. (D) The *flr-4* RNAi extends life span of WT and *skn-1(zu169)* to similar extent. Life spans were performed at 20 °C.
(PDF)

S11 Fig. (A-C) Life span analysis was performed on different germline-defective mutants that were grown on control or *flr-4* RNAi. The worms were maintained at 15 °C and life spans performed at 25 °C.
(PDF)

S12 Fig. (A) Reproductive span analysis of WT or *flr-4(n2259)* grown on HT115 or OP50. Number of eggs that hatched are plotted against the number of days. (B) Total number of eggs hatched over the entire reproductive span in shown. Comparisons are made between the WT and mutant on a particular diet. Error bars are SEM. $^{***}P \leq 0.001$, $^{**}P \leq 0.01$, $^{*}P \leq 0.05$, n.s. not significant, Student's t test.
(PDF)

S13 Fig. Pharyngeal pumping of wild-type or *eat-2(ad1116)* on control or *flr-4* RNAi. Error bars are SEM. $^{**}P \leq 0.01$, n.s. not significant, Student's t test.
(PDF)

S14 Fig. All four biological replicates that were used for quantification of data is shown. Refers to Fig 3B.
(PDF)

S15 Fig. All four biological replicates that were used for quantification of data is shown. Refers to Figs 5D and S9B.
(PDF)

S16 Fig. Rescuing *flr-4*(n2259) with a wild-type copy of *flr-4* cDNA suppresses life span to the level of WT. Transgenic worms were generated by injecting WT and *flr-4(n2259)* with pRF4 (*rol-6*) plasmid as well as *flr-4(n2259)* with *Pflr-4*::*flr-4* cDNA along with pRF4. Life spans performed at 20 °C.
(PDF)

S1 Table. Life span details reported in the main text.
(XLSX)

S2 Table. Two representative sets of biological replicates for the life spans reported in the main text.
(XLSX)

S3 Table. Details of primers used in this study.
(XLSX)

Acknowledgments

We thank all members of the Molecular Aging lab for their support, A. Siddiqui for helping in generating transgenic worms, Dr. A. Pandit and V. Jain for RNA-seq analysis as well as Drs. Satyajit Rath and Ranjan Sen for their critical inputs. We are grateful to the Department of Biotechnology (DBT), Government of India for supporting the establishment of the NII NGS core facility. Some strains were provided by the Caenorhabditis Genetics Center (CGC), which is funded by NIH Office of Research Infrastructure Programs (P40 OD010440).

Author Contributions

Conceptualization: Arnab Mukhopadhyay.

Data curation: Sonia Verma.

Formal analysis: Sonia Verma, Arnab Mukhopadhyay.

Funding acquisition: Arnab Mukhopadhyay.

Investigation: Sonia Verma, Urmila Jagtap, Anita Goyala.

Methodology: Sonia Verma, Urmila Jagtap.

Resources: Arnab Mukhopadhyay.

Supervision: Arnab Mukhopadhyay.

Validation: Sonia Verma, Urmila Jagtap.

Visualization: Sonia Verma.

Writing – original draft: Arnab Mukhopadhyay.

Writing – review & editing: Arnab Mukhopadhyay.

References

1. Avery L, You YJ. C. elegans feeding. WormBook. 2012:1–23. https://doi.org/10.1895/wormbook.1.150.1 PMID: 22628186; PubMed Central PMCID: PMCPMC3590810.
2. Coolon JD, Jones KL, Todd TC, Carr BC, Herman MA. Caenorhabditis elegans genomic response to soil bacteria predicts environment-specific genetic effects on life history traits. PLoS Genet. 2009; 5(6): e1000503. https://doi.org/10.1371/journal.pgen.1000503 PMID: 19503598; PubMed Central PMCID: PMCPMC2684633.
3. Shtonda BB, Avery L. Dietary choice behavior in Caenorhabditis elegans. J Exp Biol. 2006; 209(Pt 1):89–102. https://doi.org/10.1242/jeb.01955 PMID: 16354781; PubMed Central PMCID: PMCPMC1352325.
4. Macneil LT, Walhout AJ. Food, pathogen, signal: The multifaceted nature of a bacterial diet. Worm. 2013; 2(4):e26454. https://doi.org/10.4161/worm.26454 PMID: 24744980; PubMed Central PMCID: PMC3917966.
5. MacNeil LT, Watson E, Arda HE, Zhu LJ, Walhout AJ. Diet-induced developmental acceleration independent of TOR and insulin in C. elegans. Cell. 2013; 153(1):240–52. https://doi.org/10.1016/j.cell.2013.02.049 PMID: 23540701; PubMed Central PMCID: PMC3821073.
6. Soukas AA, Kane EA, Carr CE, Melo JA, Ruvkun G. Rictor/TORC2 regulates fat metabolism, feeding, growth, and life span in Caenorhabditis elegans. Genes Dev. 2009; 23(4):496–511. https://doi.org/10.1101/gad.1775409 PMID: 19240135; PubMed Central PMCID: PMCPMC2648650.
7. Brooks KK, Liang B, Watts JL. The influence of bacterial diet on fat storage in C. elegans. PLoS One. 2009; 4(10):e7545. https://doi.org/10.1371/journal.pone.0007545 PMID: 19844570.
8. You YJ, Kim J, Cobb M, Avery L. Starvation activates MAP kinase through the muscarinic acetylcholine pathway in Caenorhabditis elegans pharynx. Cell Metab. 2006; 3(4):237–45. https://doi.org/10.1016/j.cmet.2006.02.012 PMID: 16581001; PubMed Central PMCID: PMCPMC3433278.
9. Juozaityte V, Pladevall-Morera D, Podolska A, Norgaard S, Neumann B, Pocock R. The ETS-5 transcription factor regulates activity states in Caenorhabditis elegans by controlling satiety. Proc Natl Acad Sci U S A. 2017; 114(9):E1651–E8. https://doi.org/10.1073/pnas.1610673114 PMID: 28193866; PubMed Central PMCID: PMCPMC5338484.
10. Alcedo J, Kenyon C. Regulation of C. elegans Longevity by Specific Gustatory and Olfactory Neurons. Neuron. 2004; 41(1):45–55. PMID: 14715134.
11. Pang S, Curran SP. Adaptive capacity to bacterial diet modulates aging in C. elegans. Cell Metab. 2014; 19(2):221–31. https://doi.org/10.1016/j.cmet.2013.12.005 PMID: 24440036; PubMed Central PMCID: PMCPMC3979424.
12. Yen CA, Curran SP. Gene-diet interactions and aging in C. elegans. Exp Gerontol. 2016; 86:106–12. https://doi.org/10.1016/j.exger.2016.02.012 PMID: 26924670; PubMed Central PMCID: PMCPMC5001925.
13. Libert S, Zwiener J, Chu X, Vanvoorhies W, Roman G, Pletcher SD. Regulation of Drosophila life span by olfaction and food-derived odors. Science (New York, NY). 2007; 315(5815):1133–7. https://doi.org/10.1126/science.1136610 PMID: 17272684
14. Maier W, Adilov B, Regenass M, Alcedo J. A neuromedin U receptor acts with the sensory system to modulate food type-dependent effects on C. elegans lifespan. PLoS Biol. 2010; 8(5):e1000376. https://doi.org/10.1371/journal.pbio.1000376 PMID: 20520844; PubMed Central PMCID: PMCPMC2876044.
15. Take-uchi M, Kobayashi Y, Kimura KD, Ishihara T, Katsura I. FLR-4, a novel serine/threonine protein kinase, regulates defecation rhythm in Caenorhabditis elegans. Molecular biology of the cell. 2005; 16(3):1355–65. https://doi.org/10.1091/mbc.E04-04-0273 PMID: 15647385
16. Chamoli M, Singh A, Malik Y, Mukhopadhyay A. A novel kinase regulates dietary restriction-mediated longevity in Caenorhabditis elegans. Aging Cell. 2014; 13(4):641–55. https://doi.org/10.1111/acel.12218 PMID: 24655420; PubMed Central PMCID: PMCPMC4326946.
17. Watson E, MacNeil LT, Arda HE, Zhu LJ, Walhout AJ. Integration of metabolic and gene regulatory networks modulates the C. elegans dietary response. Cell. 2013; 153(1):253–66. https://doi.org/10.1016/j.cell.2013.02.050 PMID: 23540702; PubMed Central PMCID: PMC3817025.
18. Xiao R, Chun L, Ronan EA, Friedman DI, Liu J, Xu XZ. RNAi Interrogation of Dietary Modulation of Development, Metabolism, Behavior, and Aging in C. elegans. Cell Rep. 2015; 11(7):1123–33. https://doi.org/10.1016/j.celrep.2015.04.024 PMID: 25959815; PubMed Central PMCID: PMCPMC4439342.

19. Dillin A, Hsu AL, Arantes-Oliveira N, Lehrer-Graiwer J, Hsin H, Fraser AG, et al. Rates of behavior and aging specified by mitochondrial function during development. Science. 2002; 298(5602):2398–401. https://doi.org/10.1126/science.1077780 PMID: 12471266.

20. Dillin A, Crawford DK, Kenyon C. Timing requirements for insulin/IGF-1 signaling in C. elegans. Science. 2002; 298(5594):830–4. https://doi.org/10.1126/science.1074240 PMID: 12399591.

21. Kim DH, Feinbaum R, Alloing G, Emerson FE, Garsin DA, Inoue H, et al. A conserved p38 MAP kinase pathway in Caenorhabditis elegans innate immunity. Science. 2002; 297(5581):623–6. https://doi.org/10.1126/science.1073759 PMID: 12142542.

22. Aballay A, Drenkard E, Hilbun LR, Ausubel FM. Caenorhabditis elegans innate immune response triggered by Salmonella enterica requires intact LPS and is mediated by a MAPK signaling pathway. Curr Biol. 2003; 13(1):47–52. PMID: 12526744.

23. Troemel ER, Chu SW, Reinke V, Lee SS, Ausubel FM, Kim DH. p38 MAPK regulates expression of immune response genes and contributes to longevity in C. elegans. PLoS Genet. 2006; 2(11):e183. https://doi.org/10.1371/journal.pgen.0020183 PMID: 17096597.

24. Shivers RP, Youngman MJ, Kim DH. Transcriptional responses to pathogens in Caenorhabditis elegans. Curr Opin Microbiol. 2008; 11(3):251–6. https://doi.org/10.1016/j.mib.2008.05.014 PMID: 18567532.

25. Gravato-Nobre MJ, Hodgkin J. Caenorhabditis elegans as a model for innate immunity to pathogens. Cell Microbiol. 2005; 7(6):741–51. https://doi.org/10.1111/j.1462-5822.2005.00523.x PMID: 15888078.

26. Kurz CL, Tan MW. Regulation of aging and innate immunity in C. elegans. Aging Cell. 2004; 3(4):185–93. https://doi.org/10.1111/j.1474-9728.2004.00108.x PMID: 15268752.

27. Sakaguchi A, Matsumoto K, Hisamoto N. Roles of MAP Kinase Cascades in Caenorhabditis elegans. J Biochem (Tokyo). 2004; 136(1):7–11. https://doi.org/10.1093/jb/mvh097 PMID: 15269234.

28. Couillault C, Pujol N, Reboul J, Sabatier L, Guichou JF, Kohara Y, et al. TLR-independent control of innate immunity in Caenorhabditis elegans by the TIR domain adaptor protein TIR-1, an ortholog of human SARM. Nat Immunol. 2004; 5(5):488–94. https://doi.org/10.1038/ni1060 PMID: 15048112.

29. Liberati NT, Fitzgerald KA, Kim DH, Feinbaum R, Golenbock DT, Ausubel FM. Requirement for a conserved Toll/interleukin-1 resistance domain protein in the Caenorhabditis elegans immune response. Proc Natl Acad Sci U S A. 2004; 101(17):6593–8. https://doi.org/10.1073/pnas.0308625101 PMID: 15123841.

30. Sagasti A, Hisamoto N, Hyodo J, Tanaka-Hino M, Matsumoto K, Bargmann CI. The CaMKII UNC-43 activates the MAPKKK NSY-1 to execute a lateral signaling decision required for asymmetric olfactory neuron fates. Cell. 2001; 105(2):221–32. PMID: 11336672.

31. Chuang CF, Bargmann CI. A Toll-interleukin 1 repeat protein at the synapse specifies asymmetric odorant receptor expression via ASK1 MAPKKK signaling. Genes Dev. 2005; 19(2):270–81. https://doi.org/10.1101/gad.1276505 PMID: 15625192; PubMed Central PMCID: PMCPMC545892.

32. Dennis G Jr., Sherman BT, Hosack DA, Yang J, Gao W, Lane HC, et al. DAVID: Database for Annotation, Visualization, and Integrated Discovery. Genome Biol. 2003; 4(5):P3. PMID: 12734009.

33. Lindblom TH, Pierce GJ, Sluder AE. A C. elegans orphan nuclear receptor contributes to xenobiotic resistance. Curr Biol. 2001; 11(11):864–8. PMID: 11516648.

34. Mizuno T, Hisamoto N, Terada T, Kondo T, Adachi M, Nishida E, et al. The Caenorhabditis elegans MAPK phosphatase VHP-1 mediates a novel JNK-like signaling pathway in stress response. Embo J. 2004; 23(11):2226–34. https://doi.org/10.1038/sj.emboj.7600226 PMID: 15116070.

35. Kim DH, Liberati NT, Mizuno T, Inoue H, Hisamoto N, Matsumoto K, et al. From the Cover: Integration of Caenorhabditis elegans MAPK pathways mediating immunity and stress resistance by MEK-1 MAPK kinase and VHP-1 MAPK phosphatase. Proc Natl Acad Sci U S A. 2004; 101(30):10990–4. https://doi.org/10.1073/pnas.0403546101 PMID: 15256594.

36. Bishop NA, Guarente L. Two neurons mediate diet-restriction-induced longevity in C. elegans. Nature. 2007; 447(7144):545–9. https://doi.org/10.1038/nature05904 PMID: 17538612

37. Tullet JM, Hertweck M, An JH, Baker J, Hwang JY, Liu S, et al. Direct inhibition of the longevity-promoting factor SKN-1 by insulin-like signaling in C. elegans. Cell. 2008; 132(6):1025–38. https://doi.org/10.1016/j.cell.2008.01.030 PMID: 18358814.

38. Crawford D, Libina N, Kenyon C. Caenorhabditis elegans integrates food and reproductive signals in lifespan determination. Aging Cell. 2007; 6(5):715–21. https://doi.org/10.1111/j.1474-9726.2007.00327.x PMID: 17711560.

39. Mukhopadhyay A, Tissenbaum HA. Reproduction and longevity: secrets revealed by C. elegans. Trends Cell Biol. 2006. https://doi.org/10.1016/j.tcb.2006.12.004 PMID: 17187981.

40. Michaelson D, Korta DZ, Capua Y, Hubbard EJ. Insulin signaling promotes germline proliferation in C. elegans. Development. 2010; 137(4):671–80. https://doi.org/10.1242/dev.042523 PMID: 20110332; PubMed Central PMCID: PMCPMC2827619.

41. Katsura I, Kondo K, Amano T, Ishihara T, Kawakami M. Isolation, characterization and epistasis of fluoride-resistant mutants of Caenorhabditis elegans. Genetics. 1994; 136(1):145–54. PMID: 8138152

42. Mizunuma M, Neumann-Haefelin E, Moroz N, Li Y, Blackwell TK. mTORC2-SGK-1 acts in two environmentally responsive pathways with opposing effects on longevity. Aging Cell. 2014; 13(5):869–78. https://doi.org/10.1111/acel.12248 PMID: 25040785; PubMed Central PMCID: PMCPMC4172656.

43. Kenyon CJ. The genetics of ageing. Nature. 2010; 464(7288):504–12. https://doi.org/10.1038/nature08980 PMID: 20336132.

44. Wei F, Swaisgood R, Hu Y, Nie Y, Yan L, Zhang Z, et al. Progress in the ecology and conservation of giant pandas. Conserv Biol. 2015; 29(6):1497–507. https://doi.org/10.1111/cobi.12582 PMID: 26372302.

45. Speakman JR, Mitchell SE. Caloric restriction. Mol Aspects Med. 2011; 32(3):159–221. https://doi.org/10.1016/j.mam.2011.07.001 PMID: 21840335.

46. Mair W, Dillin A. Aging and survival: the genetics of life span extension by dietary restriction. Annu Rev Biochem. 2008; 77:727–54. https://doi.org/10.1146/annurev.biochem.77.061206.171059 PMID: 18373439.

47. Engelmann I, Pujol N. Innate immunity in C. elegans. Adv Exp Med Biol. 2010; 708:105–21. PMID: 21528695.

48. Inoue H, Hisamoto N, An JH, Oliveira RP, Nishida E, Blackwell TK, et al. The C. elegans p38 MAPK pathway regulates nuclear localization of the transcription factor SKN-1 in oxidative stress response. Genes Dev. 2005; 19(19):2278–83. https://doi.org/10.1101/gad.1324805 PMID: 16166371.

49. Shivers RP, Pagano DJ, Kooistra T, Richardson CE, Reddy KC, Whitney JK, et al. Phosphorylation of the conserved transcription factor ATF-7 by PMK-1 p38 MAPK regulates innate immunity in Caenorhabditis elegans. PLoS Genet. 2010; 6(4):e1000892. https://doi.org/10.1371/journal.pgen.1000892 PMID: 20369020.

50. Shore DE, Carr CE, Ruvkun G. Induction of cytoprotective pathways is central to the extension of lifespan conferred by multiple longevity pathways. PLoS Genet. 2012; 8(7):e1002792. https://doi.org/10.1371/journal.pgen.1002792 PMID: 22829775.

51. Shore DE, Ruvkun G. A cytoprotective perspective on longevity regulation. Trends Cell Biol. 2013. https://doi.org/10.1016/j.tcb.2013.04.007 PMID: 23726168.

52. Steinbaugh MJ, Sun LY, Bartke A, Miller RA. Activation of genes involved in xenobiotic metabolism is a shared signature of mouse models with extended lifespan. Am J Physiol Endocrinol Metab. 2012;in press. https://doi.org/10.1152/ajpendo.00110.2012 PMID: 22693205.

53. Gehart H, Kumpf S, Ittner A, Ricci R. MAPK signalling in cellular metabolism: stress or wellness? EMBO Rep. 2010; 11(11):834–40. https://doi.org/10.1038/embor.2010.160 PMID: 20930846; PubMed Central PMCID: PMCPMC2966959.

54. Yilmaz LS, Walhout AJ. Worms, bacteria, and micronutrients: an elegant model of our diet. Trends in genetics: TIG. 2014; 30(11):496–503. https://doi.org/10.1016/j.tig.2014.07.010 PMID: 25172020; PubMed Central PMCID: PMCPMC4399232.

55. Lin CJ, Wang MC. Microbial metabolites regulate host lipid metabolism through NR5A-Hedgehog signalling. Nat Cell Biol. 2017; 19(5):550–7. https://doi.org/10.1038/ncb3515 PMID: 28436966; PubMed Central PMCID: PMCPMC5635834.

56. Ding W, Smulan LJ, Hou NS, Taubert S, Watts JL, Walker AK. s-Adenosylmethionine Levels Govern Innate Immunity through Distinct Methylation-Dependent Pathways. Cell Metab. 2015; 22(4):633–45. https://doi.org/10.1016/j.cmet.2015.07.013 PMID: 26321661; PubMed Central PMCID: PMCPMC4598287.

57. Watson E, MacNeil LT, Ritter AD, Yilmaz LS, Rosebrock AP, Caudy AA, et al. Interspecies Systems Biology Uncovers Metabolites Affecting C. elegans Gene Expression and Life History Traits. Cell. 2014; 156(6):1336–7. https://doi.org/10.1016/j.cell.2014.02.036 PMID: 28898637.

58. Watson E, Olin-Sandoval V, Hoy MJ, Li CH, Louisse T, Yao V, et al. Metabolic network rewiring of propionate flux compensates vitamin B12 deficiency in C. elegans. Elife. 2016; 5. https://doi.org/10.7554/eLife.17670 PMID: 27383050; PubMed Central PMCID: PMCPMC4951191.

Genome-wide endogenous DAF-16/FOXO recruitment dynamics during lowered insulin signalling in *C. elegans*

Neeraj Kumar[1,2], Vaibhav Jain[1,*], Anupama Singh[1,*], Urmila Jagtap[1], Sonia Verma[1] and Arnab Mukhopadhyay[1]

[1] Molecular Aging Laboratory, National Institute of Immunology, Aruna Asaf Ali Marg, New Delhi, India

[2] Current address: Centre for Human Genetics and Molecular Medicine, School of Health Sciences , Central University of Punjab, Bathinda, India

[*] These authors have contributed equally to this work

Correspondence to: *Neeraj Kumar*, ***email***: *neeraj@cup.ac.in*

Arnab Mukhopadhyay, ***email***: *arnab@nii.ac.in*

Keywords: DAF-16, FOXO, ChIP-seq, C. elegans, transcription, Gerotarget

Received: *August 31, 2015* ***Accepted***: *October 20, 2015* ***Published***: *November 02, 2015*

ABSTRACT

Lowering insulin-IGF-1-like signalling (IIS) activates FOXO transcription factors (TF) to extend life span across species. To study the dynamics of FOXO chromatin occupancy under this condition in *C. elegans*, we report the first recruitment profile of endogenous DAF-16 and show that the response is conserved. DAF-16 predominantly acts as a transcriptional activator and binding within the 0.5 kb promoter-proximal region results in maximum induction of downstream targets that code for proteins involved in detoxification and longevity. Interestingly, genes that are activated under low IIS already have higher DAF-16 recruited to their promoters in WT. DAF-16 binds to variants of the FOXO consensus sequence in the promoter proximal regions of genes that are exclusively targeted during low IIS. We also define a set of 'core' direct targets, after comparing multiple studies, which tend to co-express and contribute robustly towards IIS-associated phenotypes. Additionally, we show that nuclear hormone receptor DAF-12 as well as zinc-finger TF EOR-1 may bind DNA in close proximity to DAF-16 and distinct TF classes that are direct targets of DAF-16 may be instrumental in regulating its indirect targets. Together, our study provides fundamental insights into the transcriptional biology of FOXO/DAF-16 and gene regulation downstream of the IIS pathway.

INTRODUCTION

The evolutionarily conserved IIS pathway controls metabolism, development, stress response and longevity across the animal kingdom [1]. The Forkhead TFs (FOXO) play a critical role in sculpting the transcriptional topology downstream of the IIS in worms, flies and mammals. Considering the conservation of IIS, simple model organisms like *Caenorhabditis elegans* are instrumental in finding how FOXO recruits to its direct transcriptional targets to regulate gene expression in a context-dependent manner.

In *C. elegans*, mutations in the IIS receptor *daf-2* lower IIS leading to a dramatic increase in life span, stress tolerance, higher fat stores and tendency to arrest at an alternate developmental stage called dauer [1-4]. All these phenotypes are dependent on the single FOXO homolog, DAF-16. Only two studies have previously reported the genome-scale recruitment profile of DAF-16/FOXO under conditions of low IIS using DamID or ChIP-sequencing (ChIP-Seq) [5, 6]. However, both these studies used transgenic worms overexpressing a single isoform of DAF-16 tagged to GFP that may not precisely reproduce the endogenous situation, making it difficult to evaluate the role of the TF. Although these studies have provided indications towards the complexity of gene regulation by DAF-16, more detailed analysis is required to elucidate how this transcription factor works in the endogenous settings. In our previous study, we used an anti-DAF-16 antibody to immunoprecipitate chromatin-bound DAF-

16/FOXO and identified 33 direct target genes [7]. But the study failed to saturate the genome due to its low throughput nature. In this context, a genome-wide recruitment study in a non-manipulated worm will help tremendously in understanding *in vivo* DAF-16/FOXO transcriptional biology.

Here we report the first global chromatin recruitment dynamics of endogenous DAF-16/FOXO under wild-type (WT) and low IIS conditions using ChIP-Seq. Our data shows significantly more enrichment of DAF-16 binding compared to previous ChIP-seq using an overexpression strain [6] and we report ~4000 new binding events. We also present a more detailed analysis of the recruitment profile compared to previous studies. Interestingly, we find that genes that are activated under low IIS condition already have higher DAF-16 recruitment on their promoters in WT. Surprisingly, these genes are transcribed at a higher level compared to genes to whose promoters DAF-16 recruit only during low IIS. Comparing our data to other studies, we define a 'core' set of DAF-16 direct targets that we validate phenotypically for their contributions towards IIS pathway-dependent phenotypes; these targets will serve as an important resource for future studies on DAF-16/FOXO. Importantly, we show that DAF-16, *Drosophila* dFOXO and human FOXO3 bind orthologous genes when activated. Using this data, we identify TFs that may bind in close proximity of DAF-16 during lowered IIS conditions. Finally, we identify specific classes of TFs directly regulated by DAF-16 that may modulate the expression of DAF-16 indirect targets. Together, our analysis provides a robust framework to study the endogenous transcriptional dynamics of DAF-16/FOXO and provides a glimpse into the complexity of gene regulation downstream of the IIS pathway.

RESULTS AND DISCUSSION

Endogenous DAF-16/FOXO recruitment dynamics during low IIS

To uncover the chromatin occupancy pattern of endogenous DAF-16/FOXO, we generated a ChIP-grade antibody against the soluble protein. ChIP-qPCR using primers designed to amplify the promoter proximal

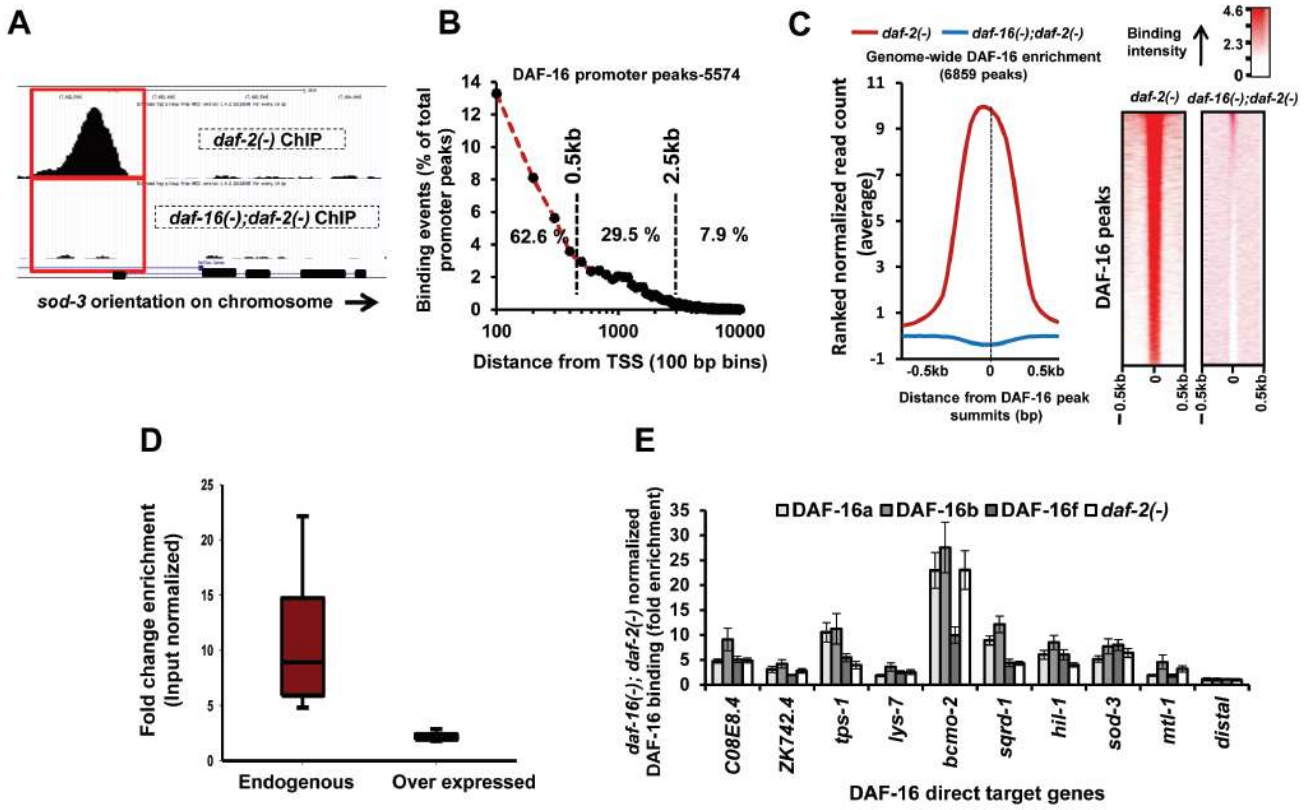

Figure 1: Genome-wide recruitment profile of DAF-16/FOXO. A. A DAF-16 peak on *sod-3* promoter in *daf-2(-)* is absent in *daf-16(-);daf-2(-).* **B.** Distribution of DAF-16 peaks with respect to TSS. **C.** Enrichment of ranked normalized reads at the DAF-16 peak summits (left panel) and its heat map representation (right panel) in *daf-2(-)* that is absent in *daf-16(-);daf-2(-)*. **D.** DAF-16 enrichment in *daf-2(-)* normalized to input samples. Enrichment was calculated using MACS in DAF-16 peaks that were common between this study (Endogenous DAF-16) and that of Riedel et al. (2013) (Overexpressed DAF-16). **E.** Recruitment profiles of DAF-16 isoforms in *daf-2(-)* compared to *daf-16(-);daf-2(-)* as determined by ChIP-Q PCR. DAF-16a, DAF-16b or DAF-16f represents transgenic lines where only one of the DAF-16 isoforms is expressed in a *daf-16(-);daf-2(-)* background [9].

region of *sod-3*, a bonafide DAF-16/FOXO direct target [7], showed that DAF-16-bound chromatin is enriched in the immune-complex immunoprecipitated from *daf-2(-)* as compared to the one from *daf-16(-);daf-2(-)* (Figure S1A). Such robust enrichment was not observed in a distal region of the gene. Validated ChIP-ed DNA were used as templates to prepare single-end ChIP-sequencing libraries (Illumina Inc., USA) that also retained the enrichment on *sod-3* promoter as above (Figure S1A). Following deep sequencing, we obtained 6860 input-normalized peaks ($P < 1x10^{-5}$, FDR < 5%) in case of *daf-2(-)* as against one significant peak in *daf-16(-);daf-2(-)*, showing the specificity of the ChIP experiments (Table S1; also Figure S2). As expected, we observed a single DAF-16 peak in the promoter of *sod-3* while no peak was detected in the 3' region or in *daf-16(-);daf-2(-)* (Figure 1A).

Majority of the DAF-16 peaks (5574) were positioned within the 0.5 kb region upstream of the transcription start site (TSS) (Figure 1B, S1B). About 68.4% or 4696 peaks in *daf-2(-)* were assigned to 3734 coding genes while the remaining were in the vicinity of non-coding genes, indicating extensive regulatory role of the TF (Table S2). This is also reflected in the distribution of DAF-16 peaks on the chromosomes that show enrichment on non-coding genes in Chr I, II, III, IV and X (Figure S1C). The mean read density (MRD) distribution analysis around the DAF-16 peak summits (±0.5 kb) shows clear enrichment within a narrow window of ~200 bp in *daf-2(-)* that is absent in *daf-16(-);daf-2(-)* (Figure 1C). Together, using a robust ChIP-seq procedure, we have generated the first endogenous genome-wide DAF-16/FOXO recruitment profile under low IIS conditions.

Previous studies to chart genome-wide DAF-16 binding used overexpression strains [5, 6]. We compared our data with these studies and report a large number of new genes with DAF-16 binding peaks in the promoter proximal region (4389 genes) (Figure S1D). This was surprising as we expected that DAF-16 overexpression would lead to more bound targets compared to endogenous DAF-16. This unexpected observation may be explained partly by the fact that we achieved more enrichment on the DAF-16 binding loci compared to the previous ChIP-seq study [6] (Figure 1D, S1E). The previous study used overexpression of only the DAF-16a isoform [8] for the ChIP-seq experiments. This may result in lower enrichment compared to our study since the antibody detects all the DAF-16 isoforms and reports the DAF-16 binding dynamics more accurately. Additionally, we used a mixed stage worm culture to capture maximum binding events while Riedel *et al.* used L4-staged worms. Together, endogenous ChIP-seq reported in this study may provide a more realistic estimate of DAF-16 recruitment profile under low IIS condition.

The *daf-16* gene codes for several isoforms; three of them are well-characterized and have overlapping as well as distinct functions [9]. To determine the relative recruitment dynamics of the DAF-16 isoforms, we used transgenic worms where only one isoform of DAF-16, i.e., DAF-16a, DAF-16b or DAF-16f has been rescued in *daf-16(-);daf-2(-)* [9]. ChIP-PCR analysis revealed that all DAF-16 isoforms bind DNA. However, the DAF-16b had comparatively higher binding to all the promoters, although it plays only a modest role in pharynx remodelling [10](Figure 1E). Thus, DAF-16b may have other undiscovered functions or alternatively, the dynamics of chromatin recruitment may change in scenarios where only one isoform is present.

TSS proximity of binding defines the strength of DAF-16/FOXO transcriptional response

To correlate DAF-16 chromatin recruitment to its transcriptional efficiency, we first compared expression profiles of WT, *daf-2(-)* and *daf-16(-);daf-2(-)* strains by RNA-seq (Table S3). This identified 667 genes that were up- (activated) and 1213 genes down-regulated (repressed) during low IIS compared to WT, in a *daf-16*- dependent manner (fold change ≥2; $P \leq 0.05$) (Figure 2A, upper circles). Among the activated genes, only 223 ($R = 2.2$, $P = 6.0x10^{-33}$) are direct targets of the TF (Figure 2A, lower circles). However, no significant overlap with binding data was observed in case of repressed genes, supporting previous suggestions that DAF-16 may act primarily as an activator [5, 6, 11]. The majority of the genes that are activated in *daf-2(-)* are indirect targets of DAF-16 as they lacked a DAF-16-binding peak in the promoter proximal region, suggesting a hierarchical control involving multiple downstream TFs. It appears that DAF-16 may be "parked" at multiple locations on the chromatin without apparent transcriptional activity, similar to dFOXO [12]. It is tempting to speculate that some of these binding may represent enhancer sites that regulate expression of distant genes. It is also possible that these genes may be transcribed at a low rate or in a tissue or context-specific manner.

We found that genes with binding peaks within 0.5 kb of TSS are more likely to be activated in *daf-2(-)* ($R = 1.5$; $P = 5.5x10^{-9}$) (Figure 2B) with the highest average mRNA fold change (Figure 2C). However, this was not the case with genes that are repressed (Figure 2C). Moreover, a single peak of DAF-16 in the promoter-proximal region resulted in higher transcriptional induction compared to two or more peaks (Figure S1F). Together, our data suggests that DAF-16/FOXO acts predominantly as an activator and TSS proximity correlates directly to transcriptional efficiency.

DAF-16 direct targets are enriched for genes involved in detoxification and longevity

We find that DAF-16 directly binds and transcriptionally regulates only a small subset of the genes that are upregulated during low IIS. These genes may comprise the immediate early response to lowering of IIS; the indirect targets possibly represent the outcome of a hierarchical response that may be relatively delayed in onset. So, to understand the biological role of the DAF-16/FOXO direct targets, we used DAVID [13] for Gene Ontology analysis. The direct and transcriptionally relevant activated targets (223) were found to be enriched in genes having oxidoreductase, antioxidant and monooxygenase activity with role in determination of adult life span (Figure 2D). On the other hand, DAF-16 indirect targets are also enriched in genes involved in metabolic processes (Figure S3). It is possible that worms respond to lowering of IIS by first upregulating the detoxification machinery through DAF-16 that is primarily responsible for life span extension. The secondary genes that are upregulated indirectly may be required to support the enhanced longevity.

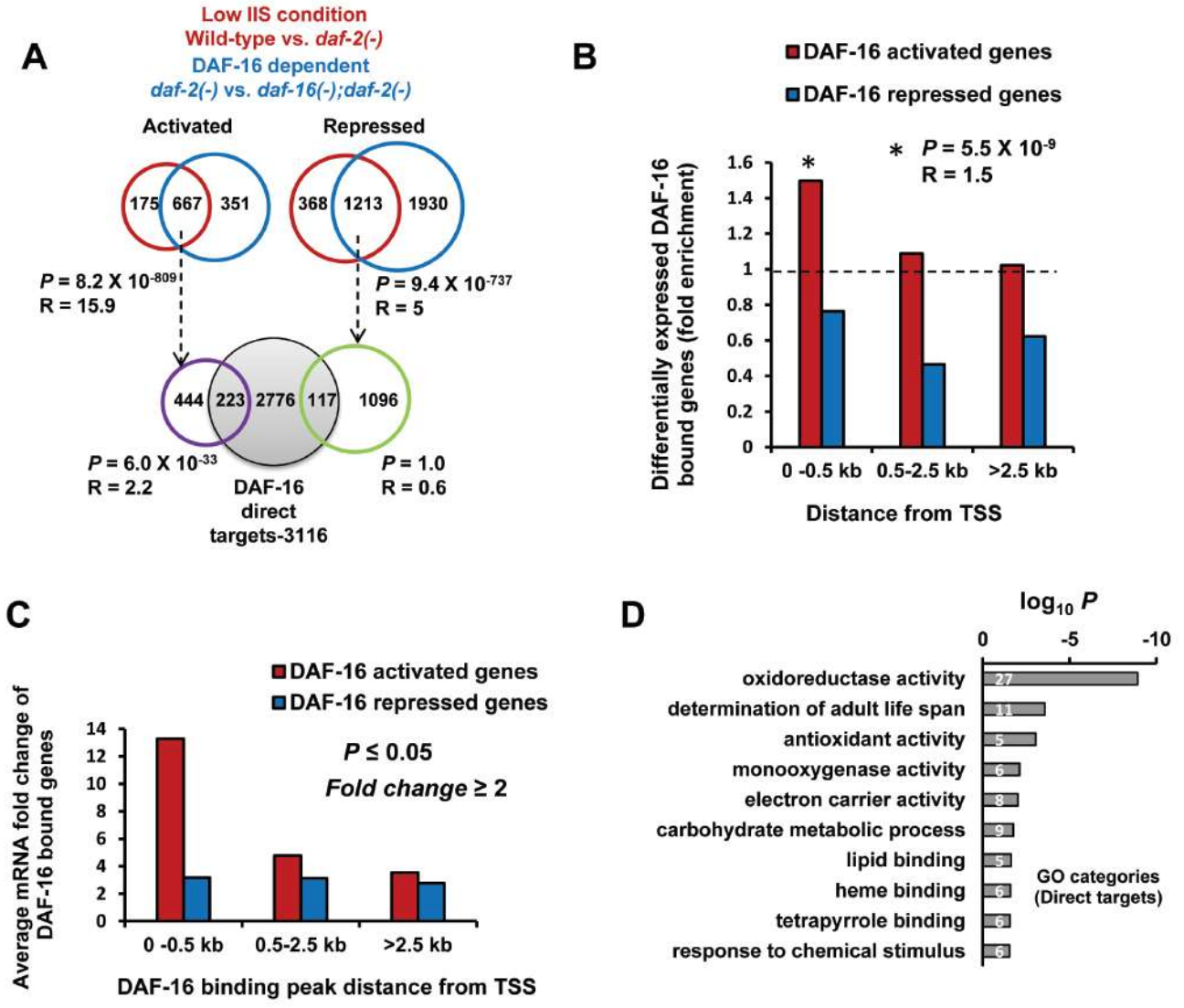

Figure 2: Promoter-proximal binding of DAF-16 ensures optimal transcriptional response. A. Genes activated (N=667) or repressed (N=1213) in *daf-2(-)* in a DAF-16-dependent manner were overlapped with genes in which DAF-16 binds within 2.5 kb promoter region upstream of TSS (Grey circle; lower panel) to obtain 223 significant (Hypergeometric test) DAF-16 direct targets that are transcriptionally relevant. **B.** DAF-16-dependent genes that have peaks located within 0.5 kb of TSS are more likely (Hypergeometric test) to be activated in *daf-2(-)*. **C.** Average mRNA fold change of genes activated or repressed in *daf-2(-)*. The genes were categorized based on distance of DAF-16 peaks from TSS. **D.** Gene annotation enrichment analysis highlights biological functions of genes directly activated by DAF-16.

DAF-12 and EOR-1 may bind chromatin at close proximity to DAF-16 during low IIS

As discussed above, lowering IIS leads to enhanced longevity, elevated stress tolerance and increased dauer formation. Although all these phenotypes are dependent on a functional DAF-16, other transcriptional regulators are also known to have important role to play in determining these phenotypes. For e.g., HSF-1 and SMK-1 are known to influence *daf-2(-)* longevity and/or stress tolerance [14, 15]. On the other hand, DAF-12 is required for enhanced dauer formation as well as longevity [16, 17]. In order to identify transcriptional regulators that may co-regulate DAF-16 direct targets, we searched for signatures of DNA-binding factors within the DAF-16 peaks. *De novo* motif search [18] revealed, as expected, the enrichment of 5'- sygGTAAACAasr -3' motif in 71.2% of the DAF-16 peaks (Figure 3A). This motif had strong Pearson correlation (0.998) with DAF-16 reference motif 5'-GTAAACA(A)-3' [11, 19, 20] (Figure 3A, lower panel). We used the position-specific scoring matrices (PSSMs) of this motif and scanned all DAF-16 peak regions (peak summits ± 250 bp) in our data to show that the matching frequency of DAF-16 motif is significantly higher as compared to the random sequences, specifically in the region of the higher PSSM hit score (Figure 3A, upper panel, S5A), indicating a robust enrichment of DAF-16 motifs. Importantly, the DAF-16 motifs were found to be distributed around the DAF-16-binding peaks (Figure S4A).

This analysis also revealed the presence of GATA-like motifs (present in 61.1 % of the DAF-16 peaks), a prospective DAF-12-binding motif (present in 40.4% of the peaks) as well as an EOR-1-binding motif (present in ~50% peaks), apart from unknown low-complexity motifs (Figure 3C, 3E, S5B, C, lower panels). However, the GATA motif and an unknown low complexity motif did not show much enrichment as compared to the random sequences (Figure S4B, C, upper panels). On the other hand, DAF-12 as well as the EOR-1 motif was overrepresented in the DAF-16 peaks across the range of PSSM hit score (Figure 3C, 3E, upper panel, S5B, C). Additionally, best PSSM hit scores for DAF-16, EOR-1 as well as DAF-12 motifs correlated better with DAF-16 peak height, compared to the GATA or the unknown motif (Figure 3B), suggesting that the occurrence of DAF-16, EOR-1 or DAF-12 motifs may ensure higher recruitment of DAF-16. Further, the DAF-12 as well as EOR-1 motifs within the DAF-16 peaks are tightly centred around the DAF-16 motifs (Figure 3D, 3F). Together, EOR-1 and DAF-12 can potentially bind chromatin at close proximity

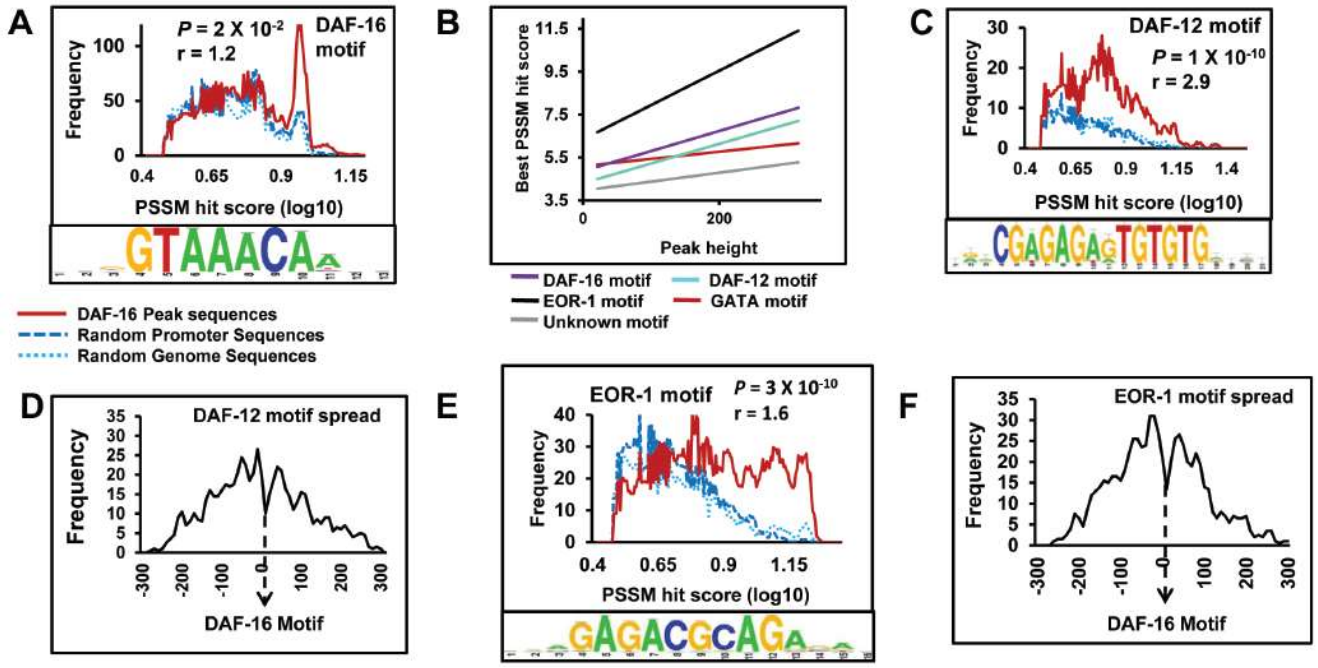

Figure 3: DAF-12 and EOR-1 may bind chromatin at close proximity to DAF-16 during low IIS. A. Upper panel shows the frequency of DAF-16 motif (red) within the DAF-16 peaks as compared to random sequences (blue). Lower panel contains the consensus DAF-16 motif identified by RSAT. **B.** Correlation of best PSSM hit scores of DAF-16, EOR-1, DAF-12, GATA or an unknown motif with DAF-16 peak heights. **C.** Upper panel shows the frequency of DAF-12 motif (red) within the DAF-16 peaks as compared to random sequences (blue). Lower panel contains the consensus DAF-12 motif identified by RSAT. **D.** Distribution of DAF-12 motifs with respect to DAF-16 motifs in *daf-2(-)*. **E.** Upper panel shows the frequency of EOR-1 motif (red) within the DAF-16 peaks as compared to random sequences (blue). Lower panel contains the consensus EOR-1 motif identified by RSAT. **F.** Distribution of EOR-1 motifs with respect to DAF-16 motifs in *daf-2(-)*. *P* values calculated using unpaired student's *t* test.

to DAF-16 under conditions of low IIS to regulate gene expression.

DAF-12 is a nuclear receptor that is homologous to the vertebrate farnesoid-X (FXR), liver-X and vitamin-D receptors. It binds to bile acid-like steroids known as the dafachronic acids (DAs), which regulate its transcriptional activity [21, 22]. DAF-12 acts as a molecular switch downstream of the IIS pathway (DAF-16/FOXO) and TGF-beta like pathway (DAF-3/SMAD and DAF-5/SKI) to determine the choice between dauer formation and reproductive growth [23]. DAF-12 affects multiple DAF-16-dependent phenotypes like dauer and longevity. Although these two factors are known to interact in worms and mammals, the molecular mechanism is less clear [24]. The *eor-1* encodes the ortholog of human PLZF, a BTB/zinc-finger transcription factor and functions downstream of the EGF pathway to regulate longevity [25]. The EGF and IIS pathways work in parallel, responding to different physiological or environmental cues to maintain protein homeostasis [26]. Our finding that DAF-12 and EOR-1 also may bind DAF-16 direct target genes suggests a novel mechanism by which hormone signalling and IIS pathway can impinge on the promoters of direct targets to co-ordinately regulate gene expression. This needs to be verified at the transcriptional and physiological level in future.

DAF-16 binds to variants of FOXO consensus sequence under low IIS

FOXO/DAF-16 is known to be majorly regulated at the level of nuclear translocation through phosphorylation by its upstream kinases [27]. To determine whether nuclear-cytoplasmic distribution of DAF-16 is reflected in

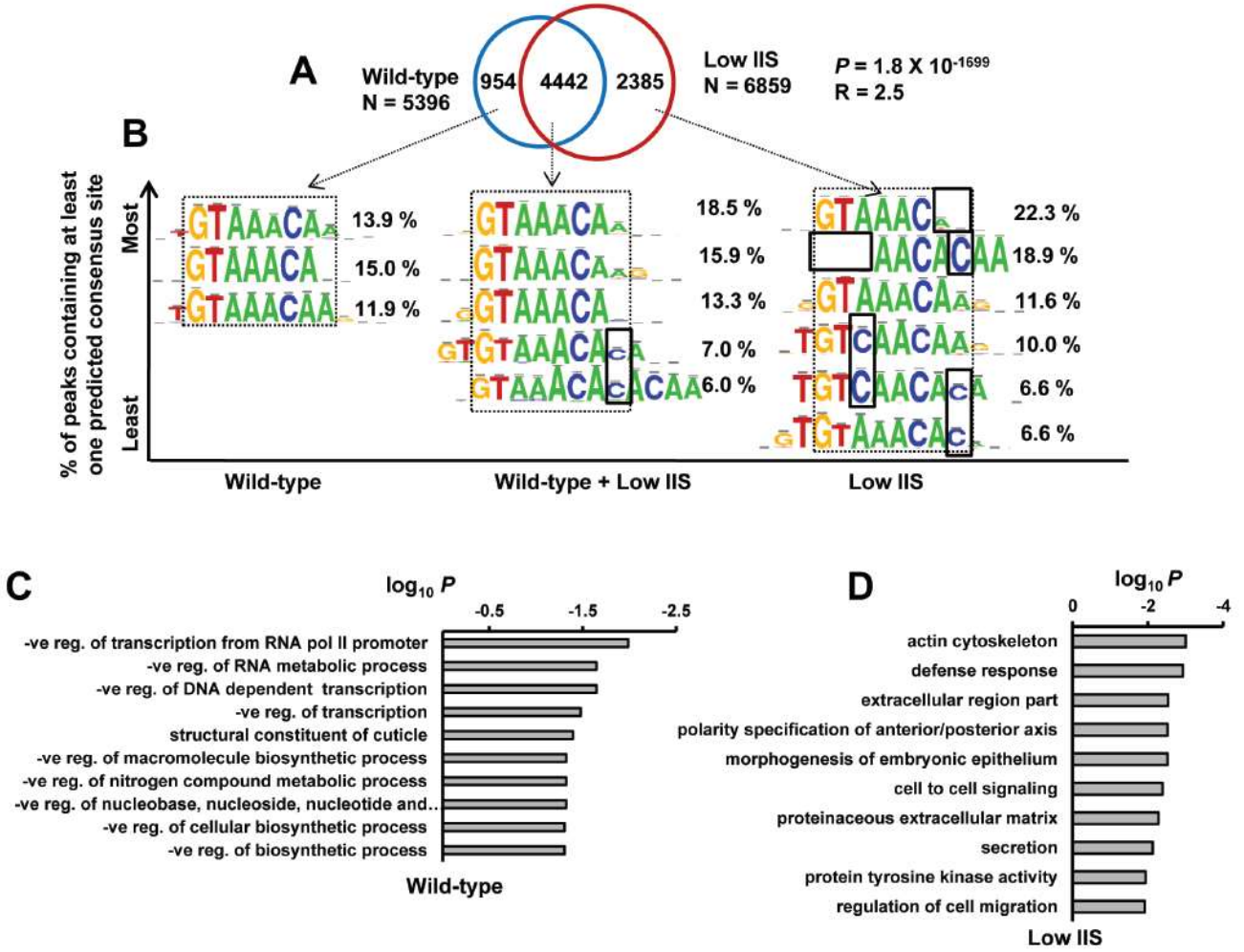

Figure 4: DAF-16 binds to variants of core FOXO consensus sequence on genes that it recruits to exclusively under low IIS. A. Overlap of DAF-16 binding peaks in WT and *daf-2(-)*. Many new peaks (2385) appear in *daf-2(-)*. *P* calculated using Hypergeometric test. **B.** FOXO consensus sequence was identified by RSAT *de novo* motif finding tool in DAF-16 binding peaks (within ± 250 bp of summit) for genes that the transcription factor recruits to in WT, *daf-2(-)* or both. Percentage occurrence of each consensus sequence is shown. **C.-D.** Gene annotation enrichment analysis highlights biological functions of genes that DAF-16 recruits to exclusively in WT **C.** or *daf-2(-)* **D.**

its recruitment pattern, we compared the binding dynamics of *daf-2(-)* with WT (Figure 4A). We find that DAF-16 binds to exclusive targets in WT (954) and *daf-2(-)* (2385) as well as a large number of common targets (4442). The relative positions of the common DAF-16 binding peaks in the two strains do not shift and exhibit normal distribution with respect to TSS (Figure S6A). This is in contrast to the observation in *Drosophila* [12], where only the extent of dFOXO binding changes at the target loci in WT vs a low IIS mutant. Together, the DAF-16 recruitment dynamics

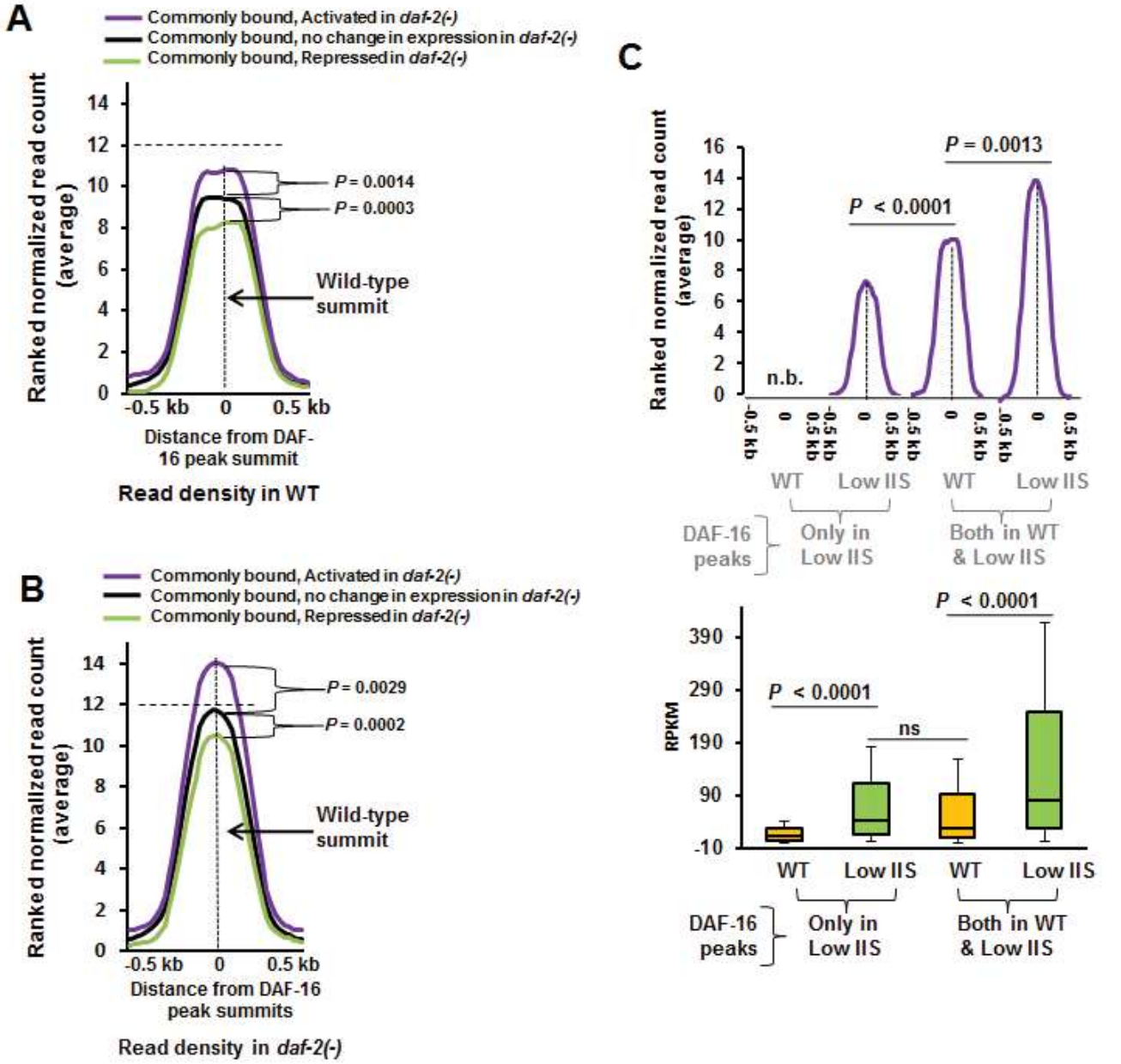

Figure 5: Genes that are activated under low IIS have higher DAF-16 recruitment in WT. A. Genes that are activated in *daf-2(-)* have higher DAF-16 recruitment on their promoters in WT compared to genes whose expression remain unchanged or are repressed. Ranked normalized read counts in WT were plotted against the distance from the peak summits (± 0.5 kb). Coding genes that are DAF-16-bound both in WT and *daf-2(-)* (2506) were considered. They were categorised as activated, repressed or no change based on their expression in *daf-2(-)* compared to WT. *P* calculated using Mann Whitney test. **B.** Ranked normalized read counts in *daf-2(-)* were plotted against the distance from the peak summits (± 0.5 kb) similar to **A.** *P* calculated using Mann Whitney test. **C.** RPKM of genes that are activated under low IIS condition as in *daf-2(-)* compared to WT (lower panel). Genes are categorized based on the fact that DAF-16 binds to the promoters exclusively in *daf-2(-)* or commonly in both WT as well as in *daf-2(-)*. *P* between WT and low IIS calculated by Wilcoxon signed rank test. *P* between low IIS (DAF-16 peaks only in Low IIS) and WT (DAF-16 peaks both WT and Low IIS) in calculated by Mann Whitney test. The corresponding ranked normalized read counts are provided in the upper panel. *P* calculated using Mann Whitney test. n.b. indicates no binding peaks observed.

partially reflect the nuclear-cytoplasmic distribution as not all DAF-16 may be excluded from the nucleus under WT condition. Since DAF-16 has multiple isoforms, it is also possible that one of the isoforms may be mostly chromatin bound while others shuttle between nucleus and cytoplasm in a context-dependent manner. Since our antibody recognizes all the isoforms, we were not in a position to resolve this mode of regulation. In line with this idea, the DAF-16f isoform is evenly distributed in the cytosol and nucleus even under the low IIS condition [9].

Next, we focused on the FOXO consensus sequences in the DAF-16 peaks found exclusively in WT or *daf-2(-)* as well as from those commonly observed in the two strains. DAF-16 peaks, present exclusively in WT, were near match to the core FOXO consensus sequence [11, 28] (Figure 4B, left). These genes were found to function mainly in negative regulation of transcription and metabolic processes, as determined by Gene Ontology analysis using DAVID [13] (Figure 4C). Interestingly, in DAF-16 peaks exclusive to *daf-2(-)*, several variants of the FOXO consensus sequences were found apart from the core consensus motif (Figure 4B, right). These categories of genes functions mostly in defence response, cell to cell signalling etc (Figure 4D).This suggests that activated DAF-16, as in *daf-2(-)*, may have higher binding affinity and bind imperfect FOXO consensus sequences. Alternatively, they may require other factors to assist in binding.

Genes activated in *daf-2(-)* already have higher DAF-16 recruitment in WT

To further study the dynamics of DAF-16 recruitment in normal and low IIS conditions, we correlated the extent of binding of the transcription factor to chromatin in WT and *daf-2(-)* with gene activation levels. We observed that genes that are activated in *daf-2(-)* already have higher DAF-16 recruitment in WT worms compared to genes whose expression remain unchanged, while those that are repressed have lower (Figure 5A). In *daf-2(-)*, the average peak heights of all the three categories increase, but only a subset is transcriptionally upregulated with respect to WT (Figure 5B). Thus, it appears that the genes that are destined to be activated under low IIS are already marked by presence of more DAF-16 on their promoter proximal regions (Figure 5B). More interestingly, no such difference in binding was noticed for genes that are bound by the transcription factor exclusively in *daf-2(-)* (Figure S6B). These genes may require additional factors to modulate gene expression.

Above, we observed two different dynamics of DAF-16-dependent gene activation under low IIS; one where DAF-16 binds to promoters in both WT as well as in *daf-2(-)*, the other where DAF-16 binds promoters exclusively in *daf-2(-)*. We asked whether these two scenarios lead to different levels of gene expression. We compared the RPKM of the genes under these two categories as determined by transcriptomics and only observed clear positive correlation between binding and activation of gene expression; no correlation was found in case of genes that are repressed or unchanged (Figure S6C). We find that in case of genes where DAF-16 binds in both WT and *daf-2(-)*, there is more robust gene transcription as compared to ones where DAF-16 binds exclusively under low IIS condition, as in *daf-2(-)* (Figure 5C, lower panel). This may not be directly attributed to the levels of recruitment as increased DAF-16 binding does not necessarily translate into more transcription [compare Figure 5C, blue with orange]. Importantly, this does not significantly affect the fold change in gene expression (data not shown). Put together, genes that are commonly bound by DAF-16 in WT and *daf-2(-)* are transcribed at a higher level in *daf-2(-)* compared to the ones to which the transcription factor recruits to under low IIS.

'Core' DAF-16 direct targets are often co-regulated and contribute robustly towards IIS pathway-dependent phenotypes

DAF-16 is a central regulator of gene expression and is involved in multiple biological processes [4]. Studies involving this TF often require experiments that follow its direct target genes transcriptionally as well as phenotypically. So using our dataset, we defined a 'core' set of DAF-16/FOXO direct and transcriptionally relevant targets by comparing our study to several previous studies that employed transcriptomics or microarray [6, 19, 29] (Figure 6A, 6B). We found 37 activated genes that overlap with all these previous studies and represent the "core" direct targets that are highly relevant (Figure 6A). No such significant overlap was observed among DAF-16 repressed genes (Figure 6B).

The *daf-2(-)* worms have increased stress tolerance, enhanced longevity, higher fat storage and propensity to arrest as dauers [30]. All these phenotypes are completely dependent on DAF-16. To evaluate the contributions of DAF-16 direct targets on these phenotypes, we systemically knocked down each one of them by RNAi in *daf-2(-)*. We found that most of the genes affect multiple phenotypes in *daf-2(-)* (Figure 6C), indicating that DAF-16 direct targets play important roles during low IIS. Importantly, these genes will now serve as essential reagents for pursuing *bonafide* DAF-16 direct targets for analysis.

Genes that function together often co-express [31]. We analyzed the co-expression profile of the 'core' DAF-16 direct targets using STRING database Version 10 (www.string-db.org/) (Figure 6D). We found that several of these genes are co-expressed under multiple conditions and may suggest linked functions. The *nnt-*

1 (putative proton-pumping nicotinamide nucleotide transhydrogenase), *far-7* (fatty acid/retinol binding protein) and *hil-1* (histone H1-like protein) are some of the annotated genes that show co-expression with other genes. This type of association may not occur by chance as in 5 sets of randomly generated list of 37 genes, co-expression was not observed (Figure 6D, S7). Thus, DAF-16 preferentially targets genes that are co-expressed to modulate phenotypes downstream of the IIS pathway.

Conservation of FOXO direct targets in worms, flies and human

The FOXO TF works in the adipocytes/fat bodies/ intestinal cells to modulate life span in mice, flies and worms [32-34]. To determine whether the direct targets of DAF-16 are conserved, we compared our data with that of human FOXO3 and fly dFOXO binding data-sets [35] [12] (Figure 7A). Among the orthologous genes between *C. elegans, Drosophila* and humans, 124 were found to be common and represent genes that are bound by FOXO in these species under low IIS conditions. Interestingly, these genes are enriched for GO terms involving vesicle-mediated endocytosis/membrane organization (Enrichment Score or ES 3.18), regulation of Rab protein signalling (ES 2.91), reproduction (ES 2.18), cell motility (ES 2.14), motor proteins (ES2.03), neurogenesis (ES 1.77), regulation of organismal growth (ES 1.41) etc. (Dataset 1). These genes may play important role in mediating the prolongevity effects associated with lowered IIS. Together,

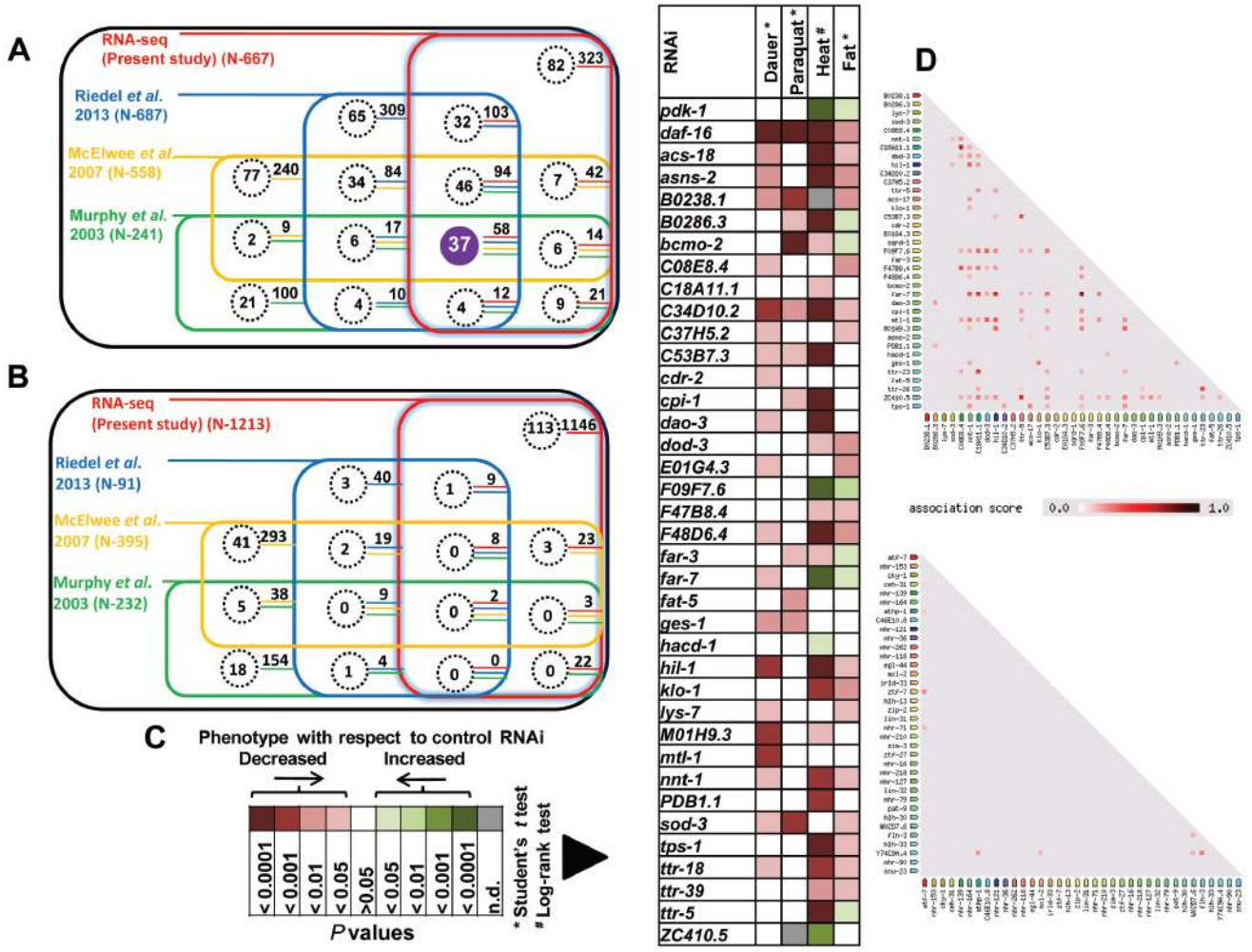

Figure 6: DAF-16 "core" direct targets contribute robustly towards IIS-regulated phenotypes. A. Comparison of DAF-16 ChIP-seq with transcriptomics data from multiple studies [6, 19, 29] reveals 37 "core" direct DAF-16 targets that are activated in *daf-2(-)*. Each coloured square represents a RNA-seq or microarray data taken from the indicated studies. Genes that were found to be common with our ChIP-seq data are highlighted by dotted circles (direct DAF-16 targets). The numbers adjoining the dotted circles represent genes that overlap with our transcriptomics data. **B.** No significant overlap was observed in case of repressed genes. **C.** IIS pathway-dependent phenotypes are differentially affected when the "core" DAF-16 targets are knocked down by RNAi. The *P* values (obtained either by Student's *t* test or log rank test) of significantly affected genes are plotted. Details of the phenotypic analysis experiments provided in Table S7. **D.** DAF-16 core direct target genes are co-expressed with each other as determined by STRING database analysis (upper panel). No such co-expression was observed in case of a randomly chosen set of 37 genes.

FOXO TFs bind an overlapping set of genes in worms, flies and human.

Transcription factors downstream of DAF-16 that it directly regulates

Comparing DAF-16 binding data to transcriptomics analysis indicates that DAF-16 directly regulates only a small fraction of the *daf-2(-)* transcriptome. Therefore, TFs within the directly targeted genes may act as second tier regulators that control the indirect targets of DAF-16. We found 21 TFs among upregulated and 53 TFs among down-regulated direct target genes (Figure 7B, Tables S4, S5). Interestingly, certain categories of transcription factors are enriched in each case. For example, among the activated genes, the winged helix forkhead TFs, the b-ZIP TFs and the zinc-finger nuclear hormone receptors are enriched. On the other hand, zinc finger containing GATA factors, C2H2 zinc-finger TFs, homeodomain CUT-like TFs and AT Hook TFs are enriched in the downregulated direct targets. Thus, DAF-16 may employ distinct categories of downstream TFs to coordinately control the indirect targets.

CONCLUSION

Based on this study, it appears that DAF-16 in general or some of its isoforms may remain parked in the immediate promoter proximal regions of genes that it regulates; the ones that it will eventually activate are marked with more bound transcription factor. During low IIS, due to influx of more DAF-16 molecules into the nucleus, binding at these sites increase while new regions are also recruited to. Interestingly, there is a differential requirement for FOXO consensus sequence for binding of DAF-16, with the regions that are exclusively recruited to in *daf-2(-)* having considerable variation. It is possible that different isoforms of DAF-16 have dissimilar binding consensus and may be assisted by other factors to promote/oppose binding. Our study thus highlights the complexity of gene regulation downstream of the IIS that is controlled by DAF-16/FOXO. With multiple isoforms that localize distinctly and modulate gene expression differentially, DAF-16 recruitment studied using a single isoform will not be sufficient to reveal the detailed mechanism of gene regulation by the transcription factor. On the other hand, our study using an anti-DAF-16 antibody that recognizes all the isoform will not have the adequate resolution to dissect isoform-specific regulation. In future, we envisage

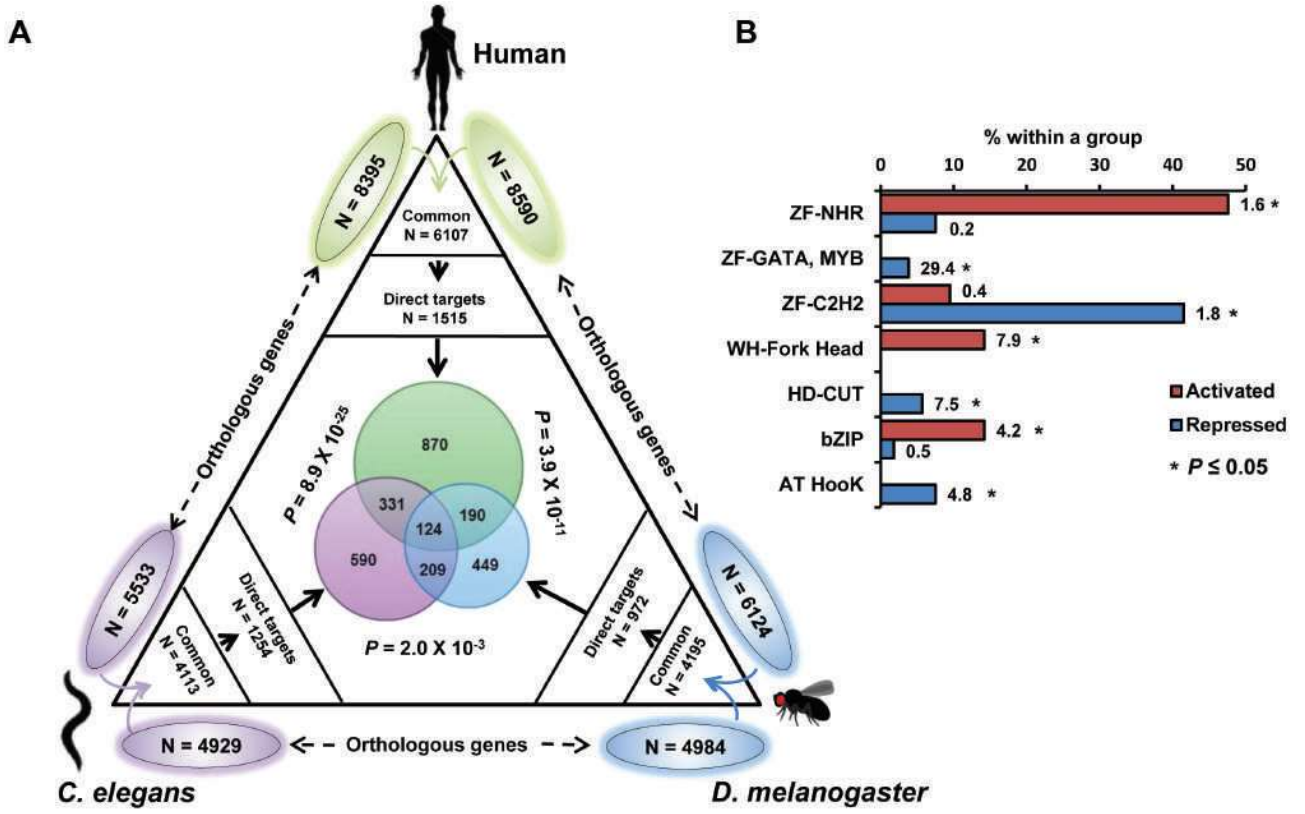

Figure 7: FOXO recruitment to its target genes is conserved. Orthologous genes between a pair of species is shown outside the triangle. Common orthologous genes were overlapped with the binding data (direct targets) from either human FOXO, dFOXO or DAF-16 (this study) as indicated. Species-specific direct targets were overlapped and are shown in the centre of the triangle along with *P* values calculated using Hypergeometric test. **B.** Relative enrichment of different types of transcription factors that are directly activated or repressed by DAF-16. Numbers indicate R = representation score. *$P \leq 0.05$ by Hypergeometric test.

that studies employing isoform-specific antibodies or tagging isoforms endogenously using genome editing will be required to understand the intricate transcriptional biology of DAF-16 downstream of the IIS.

MATERIALS AND METHODS

Strain maintenance

Wild-type (N2 Bristol), *daf-2(e1370)* and *daf-16(mgDf50);daf-2(e1370)* mutant worm strains were obtained from Caenorhabditis Genetics Centre (Minneapolis, MN, USA). Throughout the manuscript, the *daf-16(mgDf50)* and *daf-2(e1370)* alleles are referred to as *daf-16(-)* and *daf-2(-)*, respectively. Worms were grown at 20 °C unless otherwise mentioned.

Generation of anti-DAF-16 antibody

The DAF-16 cDNA was amplified using primers CCCAAGCTTGGCCTATACGGGAGCAATGAGC and CCGCTCGAGCGGACGGAAAGATGATGGAACG and cloned in PET24b (EMD Millipore Biosciences, USA). The protein was expressed in BL21(DE3) strain of *E. coli* and purified using Ni-NTA column under denaturing conditions (8M urea) as per protocol provided by the manufacturer (Qiagen, USA). Step-wise dialysis was performed with the purified protein. After the final dialysis step in 1X PBS pH 7.5, much of the protein precipitated. The remaining protein that was left in the soluble form was used to immunize rabbits (250 µg per immunization, 6 boosters) to generate polyclonal antibodies.

Chromatin immunoprecipitation (ChIP)

Mixed stage cultures of worms were grown on 15-20 *E. coli* OP50-seeded 150 X 15 mm NGM (Nematode Growth Media) agar petri-plates maintained at 20 °C. A previously published ChIP protocol was used [7], with few modifications. Briefly, the worms were harvested from plates with 1 X PBS buffer and washed four times in the same buffer. The compact worm slurry (250 µl) was resuspended in 4 ml cross-linking buffer (1% formaldehyde in 1 X PBS) followed by homogenization with 7 ml glass Dounce homogenizer. Cross-linking was allowed to proceed for 15 min at room temperature. The homogenized worm lysate was quenched with 200 µl of 2.5 M glycine (125 mM final concentration) for 10 minutes. The worm pellet was washed four times with 1 X PBS, frozen in liquid nitrogen and stored at -80 °C. The frozen pellet was resuspended and washed once in 2 ml of SDS lysis buffer (1% SDS, 10 mM EDTA and 50 mM Tris-Cl, pH 8.1) in presence of a protease inhibitor cocktail (Sigma, USA). The pellet was again resuspended in 2 ml of SDS lysis buffer and sonicated using Bioruptor Plus sonication device (Diagenode, Denville, NJ, USA) with output settings of 45 seconds on, 1 minute off at high intensity for 25 cycles in 10 ml tubes. The sonicated lysate was centrifuged at high speed for 20 minutes to collect the supernatant. Each lysate aliquot having 10 mg of protein was diluted 10 times with ChIP dilution buffer (1.1 % Triton X-100, 1.2 mM EDTA, 167 mM NaCl and 16.7 mM Tris-Cl, pH 8.0). One percent of the aliquot was saved as 'Input sample' and processed later along with ChIP samples. About 50 µl of salmon sperm DNA-coated protein A agarose beads (Millipore, USA) and 50 ul of pre-immune serum was added to the cell lysate and incubated for 1 hour at 4 °C for preclearing. After centrifugation at 400 x g, 35 µl of anti-DAF-16 antibody was added to the precleared supernatant and incubated overnight at 4 °C. Next day, the supernatant was incubated with 50 µl of salmon sperm DNA-coated protein A agarose beads for 2 hours at 4°C. The beads were transferred to a 1.5 ml micro-centrifuge tube , centrifuged at 400 x g and washed once with 1 ml of the low-salt-wash buffer (0.1% SDS, 1% Triton X-100, 2 mM EDTA, 150 mM NaCl and 20 mM Tris-HCl, pH 8.0), once with high salt wash buffer (same composition as of low salt wash buffer except 500 mM NaCl), once with LiCl was buffer (250 mM LiCl, 1% sodium deoxycholate, 1mM EDTA, 10 mM Tris-Hcl, pH 8.0) and three times with 1 X TE. ChIP-ed DNA was eluted with 500 µl elution buffer (1% SDS, 0.1 mM $NaHCO_3$) by heating at 45 °C for 10 minutes. Simultaneously, 400 µl of elution buffer was added to the input samples. 50 µl of 5M NaCl was added to each sample and kept for reverse cross-linking overnight at 65 °C. Next day, 25 µl (1 mg ml^{-1}) of DNase-free RNase (Roche Pharmaceuticals, Switzerland) was added and incubated at 37 °C for 2 h. Then, 10 µl of 500 mM EDTA, 20 µl of 1 M Tris-HCl (pH-6.5) and 10 µl of proteinase K (20 mg ml^{-1}) was added and incubated at 45 °C for 2 h. The DNA was purified using phenol-chloroform and dissolved in 10 µl (for ChIP sample) or 30 µl (for input sample) of 10 mM Tris-Cl pH 8.0. The expected range of sonicated DNA was confirmed by running 3 µl of the input sample in a 2% agarose gel. The samples were stored at -80 °C either for ChIP-PCRs or Next Generation Sequencing library preparations. All ChIP experiments were done with at least three biological replicates (each biological replicate with two technical replicates) and multiple samples were pooled for sequencing library preparation.

Quantitative real-time PCR

The enrichment of DAF-16 on the promoter regions of known or newly identified genes was determined by quantitative real time PCR (qRT-PCR) using the Mesagreen MasterMix (Eurogentec, Belgium) and Realplex PCR system (Eppendorf, USA) according to

manufacturer's specifications. The list of primers are provided in Table S6. The relative enrichment in *daf-2(-)* was determined after normalization with input and then compared with input-normalized *daf-16(-);daf-2(-)*. Fold change was calculated using ΔΔCT method [36] and statistical analysis was performed using SigmaPlot 10.0 (Systat software, USA).

Construction of next generation sequencing libraries

ChIP-ed DNA (1 µl) was quantified with Quant-iT™ dsDNA HS Assay Kit in a Qubit® fluorementer (Invitrogen, USA). A total of ~10 ng of DNA was used as a starting material for library preparation according to the manufacturer's instructions (Illumina, San Diego, CA, USA). Briefly, the DNA was end-repaired, 'A' tailed and adapters were ligated to both ends. The DNA was purified using MinElute PCR Purification Kit (Qiagen, USA) and size-selected in the range of 200 ± 50 bp after running in a 2% UltraPure™ Low Melting Point Agarose (Invitrogen, USA). The DNA was extracted from the gel using a Gel Extraction Kit (Qiagen, USA), then PCR amplified for 18 cycles using Illumina-supplied PCR primers 1.1 and 2.1 and purified with Qiagen MinElute PCR Purification Kit. The library was validated using a High Sensitivity DNA Kit and High Sensitivity DNA Reagents on a 2100 Bioanalyzer (Agilent Technologies, USA).

Next generation sequencing and analysis of ChIP-seq data

The ChIP or Input DNA was sequenced on a single lane of an Illumina Genome Analyzer IIx (GA IIx) for 36 cycles. Imaging, base calling and quality scoring were performed as per standard manufacturer's guidelines (Illumina, USA).

The de-multiplexing and conversion of BCL file format reads to FASTQ file format was done with Illumina-supported CASAVA v1.8.2 software package. Adapter and quality trimming was done with Cutadapt v1.2 using the parameters -m 15 -q 10 —quality-base 30. Quality-filtered reads were aligned to the *C. elegans* annotated reference genome (WS230) using Bowtie v.0.12.7 with parameters: -q -m 1 —best —strata. Peak calling was performed with uniquely-aligned reads, containing no more than one mismatch, using peak calling algorithm MACS v1.4.2 with parameters: —mfold = 5,30 —bw = 175 -w [37]. Statistically significant enriched peaks were selected with 5% FDR cut-off.

Assignment of DAF-16 peaks to the target genes was performed using PeakAnnotator, a PeakAnalyzer utility tool v1.4 [38]. The ChIP-seq peak summit (defined using MACS) was associated with a nearby gene transcription start site (TSS) and includes both coding as well as non-coding genes. In case of the presence of multiple genes in the vicinity of a summit, assignment was made to the closest TSS. For further analysis, peaks positioned within a window of 2.5 kb upstream or 300 bp downstream of a TSS were selected.

Metadata analysis

Following peak calling using MACS, the location of the reads were shifted towards 3' direction based on the mean fragment size [171 base pairs for WT, 158 base pairs for *daf-2(-)*, 200 base pairs for *daf-16(-);daf-2(-)*]. The genome was divided into 25-bp non-overlapping bins and the number of uniquely mapped reads in each bin was determined. The read counts per bin were normalized to the total number of uniquely mapped reads, both in the ChIP and input samples. The normalized input read counts were subtracted from the respective ChIP sample read counts, within each bin. To evaluate the average DAF-16 binding among different samples, the normalized genome-wide read counts were further quantile normalized, for statistical comparison, using preprocess Core R package. The bin containing each DAF-16 peak summit (determined by MACS) was identified and the mean normalized read count was determined for that bin. This procedure was repeated for 20 bins that were situated both upstream as well as downstream of the peak summit (25 bp x 20 = ± 500 bp). To show the spread of DAF-16 binding with respect to each peak, the above normalized read counts were plotted as heat map using MeV v.4.9. To visualize the aligned data as wig files (as in Figure 1A, S2), UCSC genome browser was used.

de novo motif discovery

DAF-16 peaks assigned to promoters were used for *de novo* motif discovery. The sequences of the complete peak region were retrieved by Galaxy [39]. *De novo* motifs were identified using the peak motifs module of RSAT (Regulatory Sequence Analysis Tools)[18, 40] by using the following parameters: cut peak sequences ± 1000 bp, discover motifs with oligo and position analysis with oligomer length above 6-8 bp, Markov order (m = 2), five motifs per algorithm searched on both stands. We also analyzed the data using MEME (Multiple Em for Motif Elicitation)[41] and obtained similar results; only RSAT analysis is shown in the manuscript. Similar motifs were clustered with Cytoscape [42] by using the input files from RSAT. The motif with the highest number of edges and strongest correlation index was selected for further analysis. The selected motifs were then compared with the JASPAR [43] or TRANSFAC database Professional version 9.3 (http://www.biobase.de) to determine their identity.

In silico validation of the discovered motifs

The discovered motifs were used to scan all the DAF-16 peak sequences (DAF-16 peak summits ± 250 bp) using the pattern matching module of RSAT, assuming that there is no more than one true binding site in the target sequence. Similar parameters were also considered for random promoters and genomic regions that were used as controls. Selections of the matched sequences were performed with a *P*-value ≤ 10^{-5} (based on the Markov model) with *C. elegans* reference genome WBcel230 as a background. The best match for the motifs (PSSMs match or weight score) was selected for downstream analysis including inter-motif distances *etc*. The statistical significance of the difference between the frequency of occurrence of the motifs within DAF-16 peaks lying in the promoter regions and the same number of randomly chosen promoter sequences was calculated using unpaired student *t*-test. We also calculated the 'r' or ratio of frequency of a motif's occurrence within the peak sequences to the random promoter sequences to evaluate the relative enrichment.

Inter-motif distances

For this, the central co-ordinates of the sequences that matched the motifs were first determined. The relative position (distance) of the central co-ordinates of one motif was determined with respect to the other, with due consideration to the strandedness of the promoter. These distances were used to plot the histogram (Figure 6D, 6F) where DAF-16 motif positions were used as the reference point. Similar process was also followed to plot the relative positions of DAF-16 motifs with respect to peak summits (Figure S5A) and while comparing the relative positions of DAF-16 summits in *daf-2(-)* vs WT (Figure 3A).

RNA-seq analysis and correlation with ChIP-seq data

For RNA isolation, mixed culture of worms was grown on *E. coli* OP_{50}-seeded 90 mm NGM agar plates. The pellet was collected, after washing four times in M9 buffer, in 250 µl TRIzol reagent (Invitrogen, USA) and stored at -80 °C. Total RNA was isolated as per manufacturer's recommendation.

Multiplexing was used while sequencing RNA with the help of indexed adapters as provided by manufacturer (Illumina, USA). Before library preparation, the quality of the RNA was checked on a 2100 Bioanalyzer by using the RNA 6000 Nano Kit (Agilent Technologies, USA). RNA with RNA integrity number (RIN) > 9 was selected for library preparation. The RNA library was prepared using the TrueSeq RNA SamplePrep V2 kit (Illumina, USA) according to manufacturer-provided specifications.

RNA-sequencing of WT, *daf-2(-)* and *daf-16(-);daf-2(-)*strains were performed using Illumina GAIIx. After de-multiplexing and adaptors trimming, reads were aligned to the annotated reference genome (WS230) using CLC Genomics Workbench v.6.5.1 and levels of the mapped genes (RPKM, Reads Per Kilobase of exon model per Million mapped reads) [44] were calculated using default parameters. Significant fold changes ($P \leq 0.05$, fold change ≥ 2) were selected by applying beta-binomial Baggerley's test [45]. Significance of overlap between different gene lists was calculated by hypergeometric distribution using GeneProf [46]. The fold enrichment of DAF-16-bound differentially expressed genes (DDEG) ($P \leq 0.05$, fold change ≥ 2) was calculated as follows: (number of DDEGs/number of DEG)/(number of DAF-16-bound expressed genes/number of expressed genes) (Figure 2B). Genes with RPKM >0 in the *daf-2(-)* and *daf-16(-);daf-2(-)* samples were considered as expressed genes. Further, the average mRNA fold change was calculated only for the genes having either single or double DAF-16 peaks within 0.5 kb promoter (Figure S1D).

Data availability

The sequencing data is available to the readers at the following links:

ChIP-seq-GSE63865

http://www.ncbi.nlm.nih.gov/geo/query/acc.cgi?token=ktsdemoqjjuxpqb&acc=GSE63865

RNA-seq-GSE67975-

http://www.ncbi.nlm.nih.gov/geo/query/acc.cgi?token=ypwjukqithsljaz&acc=GSE67975

List of genes generated for detailed analysis shown in the manuscript is being provided as Data Set 1.

Phenotypic analysis

Oxidative stress

Following hypochlorite treatment, eggs of *daf-2(e1370);rrf-3(pk1426)* were grown on RNAi-seeded NGM agar plates till they reached gravid adult stage. These worms were then transferred to respective RNAi plates that were overlaid with FUDR (final concentration of 50 µg/ml) and maintained at 20°C till Day 5 of adulthood. Approximately 10-12 adult worms were dispensed into each well of a 24-well tissue culture plate containing 400 µl of 100 mM paraquat (Sigma, USA) in 1X M9 buffer containing cholesterol. Worms were scored for survival at the 50th hour following the commencement of the experiment and those that failed to respond to gentle prodding were scored as dead. Data is presented as survival on 50th hour ± SD for each RNAi. Statistical

analysis performed using Student's *t* test and is plotted in Figure 6C.

Heat stress

After hypochlorite treatment, eggs of *daf-2(e1370);rrf-3(pk1426)* were grown on the different RNAi as above. Approximately 100 animals per RNAi were upshifted to 30 °C and scored for survival by gentle touching with a platinum wire every 6th hour. Statistical analyses for survival were conducted using Mantel-Cox log rank test through OASIS software available at http://sbi.postech.ac.kr/oasis [47] and plotted in Figure 6C.

Dauer

Dauer assay was performed at 22 °C in the liquid culture containing RNAi feed. An RNAi mini-library was prepared for direct targets of DAF-16. A day before setting up the assay, the bacterial glycerol stocks from the library were inoculated in 500 µl LB containing 100 µg/ml ampicillin in a 96-deep-well plate and incubated for 16 hours at 37°C with shaking at 240 rpm. After incubation, the culture was induced for an hour with IPTG at a final concentration of 4mM. The culture was then pelleted and resuspended in 250 µl NGM containing 100 µg/ml ampicillin and 4 mM IPTG. About 60 µl NGM RNAi per well was dispensed into a flat-bottomed 96-well plate in triplicate. Approximately 10-15 L1 starved *daf-2(e1370);rrf-3(pk1426)* animals were added to each well in a maximum volume of 10 µl. The worms were then maintained at 22°C with constant shaking at 200 rpm. On 5th day of the experiment, the worms were scored for dauer formation. The percentage dauer formation (6 wells for each RNAi) was calculated and compared to control RNAi-treated worms. Statistical analysis was performed using Student's *t* test and is plotted in Figure 6C.

Fat storage

Fat storage was determined in fixed worms using Oil Red O [48, 49]. Briefly, worms were synchronized using hypochlorite treatment and strains were grown on different RNAi plates till L4-YA stage. The worms were then washed and resuspended in 120 µl 1X PBS. To this an equal volume of 2X MRWB buffer (160 mM KCl, 40 mM NaCl, 14 mM Na_2EGTA, PIPES pH 7.4, 1 mM Spermidine, 0.4 mM Spermine, 2% Paraformaldehyde, 0.2% beta-mercaptoethanol) was added and the same was incubated with shaking for 45 minutes. The worms were subjected to three freeze-thaw cycles in dry ice/ethanol bath, pelleted and washed with 1XPBS. Oil Red O was prepared as a stock solution 5mg/ml stock in isopropanol and equilibrated on a rocker shaker for several days. The working stock of Oil Red O was prepared by diluting the equilibrated stock to 60% using water and allowed to stand for 10 min following which it was filtered using a 0.22 µm filter. The Oil Red O stain was added to the fixed worms and the suspension incubated overnight on a shaker at room temperature. Following this, worms were washed twice with 1X PBS and mounted on 2% agarose slides for visualization using a AxioImager M2 microscope (Carl Zeiss, Germany) fitted with Axiocam MRm camera. The intensity of staining was quantified using NIH ImageJ software; statistical analysis was performed using Student's *t* test and plotted in Figure 6C.

ACKNOWLEDGMENTS

We thank all members of the Molecular Aging lab for their help and Dr. S. Mandrup for critical comments. We are grateful to the Department of Biotechnology (DBT), Government of India for a generous infrastructure grant for establishment of the NII NGS core facility. Some strains were provided by the CGC, which is funded by NIH Office of Research Infrastructure Programs (P40 OD010440).

Authors' contribution

AM conceived the project. AM and NK designed experiments as well as wrote the manuscript. NK performed all ChIP-seq and RNA-seq experiments. NK analysed NGS data along with VJ. UJ raised the anti-DAF-16 antibody. NK, AS and SV performed phenotypic analysis.

GRANT SUPPORT

This project is partly funded by the Ramalingaswami fellowship to AM (BT/HRD/35/02/12/2008), DBT Grant No. BT/PR13720/BAB/10/779/2010, ICMR Grant No. 54/3/CFP/GER/2011-NCD-II and core funding from National Institute of Immunology. AS and SV are supported by CSIR and UGC research fellowships, respectively.

CONFLICTS OF INTEREST

The authors declare no conflict of interest.

REFERENCES

1. Kenyon CJ. The genetics of ageing. Nature. 2010; 464:504-512.
2. Antebi A. Genetics of aging in Caenorhabditis elegans. PLoS Genet. 2007; 3:1565-1571.
3. Wolff S and Dillin A. The trifecta of aging in Caenorhabditis elegans. Exp Gerontol. 2006; 41:894-903.
4. Mukhopadhyay A, Oh SW and Tissenbaum HA. Worming pathways to and from DAF-16/FOXO. Exp Gerontol. 2006; 41:928-934.
5. Schuster E, McElwee JJ, Tullet JM, Doonan R, Matthijssens F, Reece-Hoyes JS, Hope IA, Vanfleteren JR, Thornton

JM and Gems D. DamID in C. elegans reveals longevity-associated targets of DAF-16/FoxO. Mol Syst Biol. 2010; 6:399.

6. Riedel C, Dowen R, Lourenco G, Kirienko N, Heimbucher T, West J, Bowman S, Kingston R, Dillin A, Asara J and Ruvkun G. DAF-16 employs the chromatin remodeller SWI/SNF to promote stress resistance and longevity. Nature cell biology. 2013; 15:491.
7. Oh SW, Mukhopadhyay A, Dixit BL, Raha T, Green MR and Tissenbaum HA. Identification of direct DAF-16 targets controlling longevity, metabolism and diapause by chromatin immunoprecipitation. Nat Genet. 2006; 38:251-257.
8. Henderson ST and Johnson TE. daf-16 integrates developmental and environmental inputs to mediate aging in the nematode Caenorhabditis elegans. Curr Biol. 2001; 11:1975-1980.
9. Kwon ES, Narasimhan SD, Yen K and Tissenbaum HA. A new DAF-16 isoform regulates longevity. Nature. 2010; 466:498-502.
10. Lin K, Hsin H, Libina N and Kenyon C. Regulation of the Caenorhabditis elegans longevity protein DAF-16 by insulin/IGF-1 and germline signaling. Nat Genet. 2001; 28:139-145.
11. Tepper RG, Ashraf J, Kaletsky R, Kleemann G, Murphy CT and Bussemaker HJ. PQM-1 complements DAF-16 as a key transcriptional regulator of DAF-2-mediated development and longevity. Cell. 2013; 154:676-690.
12. Alic N, Andrews TD, Giannakou ME, Papatheodorou I, Slack C, Hoddinott MP, Cocheme HM, Schuster EF, Thornton JM and Partridge L. Genome-wide dFOXO targets and topology of the transcriptomic response to stress and insulin signalling. Mol Syst Biol. 2011; 7:502.
13. Dennis G, Jr., Sherman BT, Hosack DA, Yang J, Gao W, Lane HC and Lempicki RA. DAVID: Database for Annotation, Visualization, and Integrated Discovery. Genome Biol. 2003; 4:P3.
14. Hsu AL, Murphy CT and Kenyon C. Regulation of aging and age-related disease by DAF-16 and heat-shock factor. Science. 2003; 300:1142-1145.
15. Wolff S, Ma H, Burch D, Maciel GA, Hunter T and Dillin A. SMK-1, an essential regulator of DAF-16-mediated longevity. Cell. 2006; 124:1039-1053.
16. Fisher AL and Lithgow GJ. The nuclear hormone receptor DAF-12 has opposing effects on Caenorhabditis elegans lifespan and regulates genes repressed in multiple long-lived worms. Aging Cell. 2006; 5:127-138.
17. Larsen PL, Albert PS and Riddle DL. Genes that regulate both development and longevity in Caenorhabditis elegans. Genetics. 1995; 139:1567-1583.
18. Thomas-Chollier M, Herrmann C, Defrance M, Sand O, Thieffry D and van Helden J. RSAT peak-motifs: motif analysis in full-size ChIP-seq datasets. Nucleic acids research. 2012; 40:e31.
19. Murphy CT, McCarroll SA, Bargmann CI, Fraser A, Kamath RS, Ahringer J, Li H and Kenyon C. Genes that act downstream of DAF-16 to influence the lifespan of Caenorhabditis elegans. Nature. 2003; 424:277-283.
20. Furuyama T, Kitayama K, Yamashita H and Mori N. Forkhead transcription factor FOXO1 (FKHR)-dependent induction of PDK4 gene expression in skeletal muscle during energy deprivation. Biochem J. 2003; 375:365-371.
21. Antebi A, Yeh WH, Tait D, Hedgecock EM and Riddle DL. daf-12 encodes a nuclear receptor that regulates the dauer diapause and developmental age in C. elegans. Genes Dev. 2000; 14:1512-1527.
22. Motola DL, Cummins CL, Rottiers V, Sharma KK, Li T, Li Y, Suino-Powell K, Xu HE, Auchus RJ, Antebi A and Mangelsdorf DJ. Identification of ligands for DAF-12 that govern dauer formation and reproduction in C. elegans. Cell. 2006; 124:1209-1223.
23. Antebi A. Steroid regulation of C. elegans diapause, developmental timing, and longevity. Curr Top Dev Biol. 2013; 105:181-212.
24. Dowell P, Otto TC, Adi S and Lane MD. Convergence of peroxisome proliferator-activated receptor gamma and Foxo1 signaling pathways. J Biol Chem. 2003; 278:45485-45491.
25. Gang L, Jason R, Coleen TM and Christopher R. EGF signalling activates the ubiquitin proteasome system to modulate C. elegans lifespan. The EMBO journal. 2011; 30:2990-3003.
26. Rongo C. Epidermal growth factor and aging: a signaling molecule reveals a new eye opening function. Aging (Albany NY). 2011; 3:896-905.
27. Salih DA and Brunet A. FoxO transcription factors in the maintenance of cellular homeostasis during aging. Curr Opin Cell Biol. 2008; 20:126-136.
28. Furuyama T, Nakazawa T, Nakano I and Mori N. Identification of the differential distribution patterns of mRNAs and consensus binding sequences for mouse DAF-16 homologues. Biochem J. 2000; 349:629-634.
29. McElwee J, Bubb K and Thomas JH. Transcriptional outputs of the Caenorhabditis elegans forkhead protein DAF-16. Aging Cell. 2003; 2:111-121.
30. Kenyon C. The plasticity of aging: insights from long-lived mutants. Cell. 2005; 120:449-460.
31. Kim SK, Lund J, Kiraly M, Duke K, Jiang M, Stuart JM, Eizinger A, Wylie BN and Davidson GS. A gene expression map for Caenorhabditis elegans. Science. 2001; 293:2087-2092.
32. Bluher M, Kahn BB and Kahn CR. Extended longevity in mice lacking the insulin receptor in adipose tissue. Science. 2003; 299:572-574.
33. Libina N, Berman JR and Kenyon C. Tissue-specific activities of C. elegans DAF-16 in the regulation of lifespan. Cell. 2003; 115:489-502.
34. Hwangbo DS, Gershman B, Tu MP, Palmer M and Tatar M.

Drosophila dFOXO controls lifespan and regulates insulin signalling in brain and fat body. Nature. 2004; 429:562-566.

35. Eijkelenboom A, Mokry M, de Wit E, Smits LM, Polderman PE, van Triest MH, van Boxtel R, Schulze A, de Laat W, Cuppen E and Burgering BM. Genome-wide analysis of FOXO3 mediated transcription regulation through RNA polymerase II profiling. Mol Syst Biol. 2013; 9:638.
36. Schmittgen TD and Livak KJ. Analyzing real-time PCR data by the comparative C(T) method. Nature protocols. 2008; 3:1101-1108.
37. Zhang Y, Liu T, Meyer CA, Eeckhoute J, Johnson DS, Bernstein BE, Nusbaum C, Myers RM, Brown M, Li W and Liu XS. Model-based analysis of ChIP-Seq (MACS). Genome Biol. 2008; 9:R137.
38. Salmon-Divon M, Dvinge H, Tammoja K and Bertone P. PeakAnalyzer: genome-wide annotation of chromatin binding and modification loci. BMC Bioinformatics. 2010; 11:415.
39. Goecks J, Nekrutenko A, Taylor J and Galaxy T. Galaxy: a comprehensive approach for supporting accessible, reproducible, and transparent computational research in the life sciences. Genome Biol. 2010; 11:R86.
40. Thomas-Chollier M, Defrance M, Medina-Rivera A, Sand O, Herrmann C, Thieffry D and van Helden J. RSAT 2011: regulatory sequence analysis tools. Nucleic acids research. 2011; 39:W86-91.
41. Bailey TL, Boden M, Buske FA, Frith M, Grant CE, Clementi L, Ren J, Li WW and Noble WS. MEME SUITE: tools for motif discovery and searching. Nucleic acids research. 2009; 37:W202-208.
42. Cline MS, Smoot M, Cerami E, Kuchinsky A, Landys N, Workman C, Christmas R, Avila-Campilo I, Creech M, Gross B, Hanspers K, Isserlin R, Kelley R, et al. Integration of biological networks and gene expression data using Cytoscape. Nature protocols. 2007; 2:2366-2382.
43. Mathelier A, Zhao X, Zhang AW, Parcy F, Worsley-Hunt R, Arenillas DJ, Buchman S, Chen CY, Chou A, Ienasescu H, Lim J, Shyr C, Tan G, et al. JASPAR 2014: an extensively expanded and updated open-access database of transcription factor binding profiles. Nucleic acids research. 2014; 42:D142-147.
44. Mortazavi A, Williams BA, McCue K, Schaeffer L and Wold B. Mapping and quantifying mammalian transcriptomes by RNA-Seq. Nat Methods. 2008; 5:621-628.
45. Baggerly KA, Deng L, Morris JS and Aldaz CM. Overdispersed logistic regression for SAGE: modelling multiple groups and covariates. BMC Bioinformatics. 2004; 5:144.
46. Halbritter F, Vaidya HJ and Tomlinson SR. GeneProf: analysis of high-throughput sequencing experiments. Nat Methods. 2012; 9:7-8.
47. Yang JS, Nam HJ, Seo M, Han SK, Choi Y, Nam HG, Lee SJ and Kim S. OASIS: online application for the survival analysis of lifespan assays performed in aging research. PLoS One. 2011; 6:e23525.
48. O'Rourke EJ, Soukas AA, Carr CE and Ruvkun G. C. elegans major fats are stored in vesicles distinct from lysosome-related organelles. Cell Metab. 2009; 10:430-435.
49. Yen K, Le TT, Bansal A, Narasimhan SD, Cheng JX and Tissenbaum HA. A comparative study of fat storage quantitation in nematode Caenorhabditis elegans using label and label-free methods. PLoS One. 2010; 5:e12810.